Meereswissenschaftliche Berichte
MARINE SCIENCE REPORTS

No. 19

GOBEX - Summary Report

Editor:

Eberhard Hagen

Institut für Ostseeforschung
Warnemünde
1996

The GOBEX Secretariat has no responsibility for the content of the contributions included in this volume. Each author is himself responsible for his own chapter. Most contributions are based on preliminary data and have the same form as in the GOBEX - Newsletter. A second volume containing hydrographic data is under preparation.

Only those manuscripts which were received before 1 September 1996 were considered for this volume.

Editor: Eberhard Hagen (GOBEX Secretariat/ IOW)

GOBEX

The Gotland Basin Experiment (1994 - 1995)

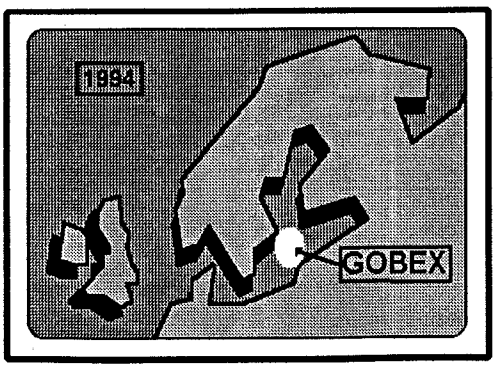

Contents

PREFACE

The Gotland Basin Experiment (GOBEX) was an international, multidisciplinary study of all riparian countries of the Baltic Sea during 1994 - 1995. The planning phase was funded by the European Committee on Ocean and Polar Sciences (ECOPS), which is sponsored by the European Science Foundation (ESF) and the Commission of the European Community (CEC). The GOBEX activities were considered as a preparation for the investigations planned for the MAST-III period (1996 -1999). The German contributions were funded by the "Kultusministerium des Landes Mecklenburg-Vorpommern" under the contract no. 0710, MG 04, 68101-05.

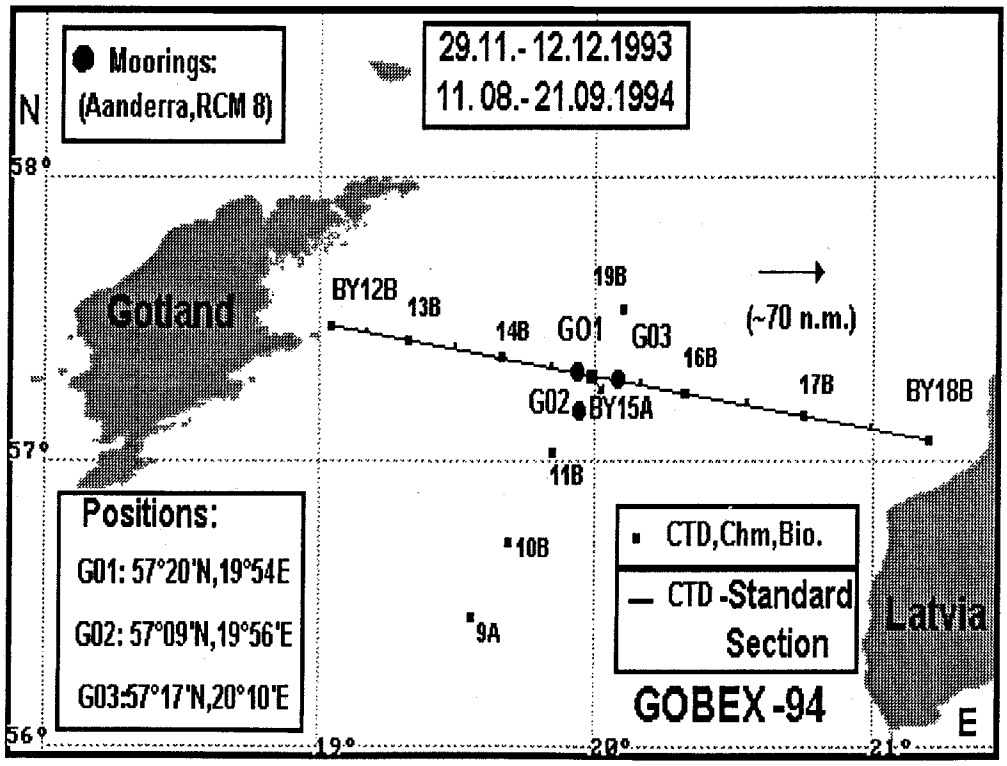

Fig.1 The main area under investigation for GOBEX-94 with positions of the Baltic Year Programme (BY) forming the standard transect between stations BY12B and BY18B; station BY15A is above the Gotland Deep; at each station CTD profiles were repeated by different research vessels during different seasons together with chemical (chm) and biological (bio) measurements in the vicinity of the three current meter moorings at positions GO1, GO2, and GO3.

Several workshops elucidated the main objectives for joint efforts. All scheduled field studies were to be concentrated in the eastern Gotland Basin. It was recommended that the positions of most hydrographic stations should coincide with those of the Baltic Year (BY) programme, which was carried out in 1969 - 1970. The GOBEX-area under investigation is shown in Fig.1. The location of the two hydrographic standard transects is indicated as well as positions of three current meter moorings (GO1, GO2, GO3). The principal aim of the project was a better understanding of the water exchange processes between coastal areas and the Eastern Gotland Basin and their consequences for the ecosystem of the "Baltic Proper".These efforts included, inter alia, the quantification of various past and present fluxes between different no-living and living compartments, different ecological zonation and food webs. All this required the coordination of all national research activities.

Four working groups were formed:

- Meso-scale dynamics
- Benthic processes
- Data management - hydrography/geology
- History of the Baltic Proper

They concentrated their efforts on the following topics:

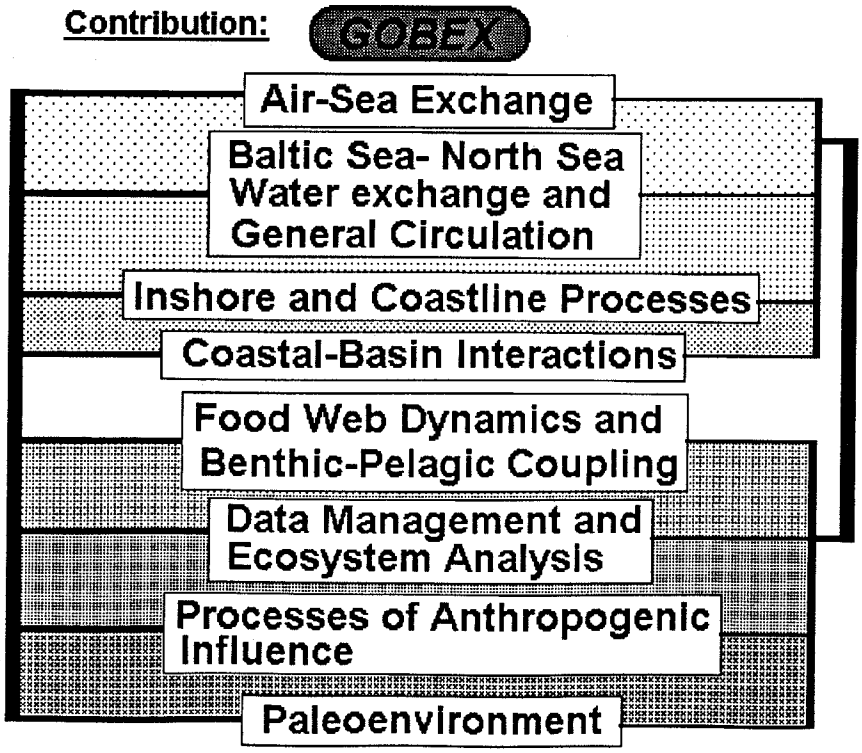

Such an approach involves all marine disciplines and comprises different temporal and spatial scales. For example, sedimentation processes of basin-scale nature are influenced by anomalies in deep water circulation, associated water- mass transformation, and related mixing and exchange processes, all of which are based on different physical mechanisms. A better understanding of these processes is needed for the development of an integrated model describing these relationships in a proper way. The GOBEX programme only provided a first step.

The management of the national hydrographic data was co-ordinated by the ICES in Copenhagen/ Denmark. Figure 2 depicts the time table of all cruise activities. Time windows of moored current measurements are included. Their logistics were co-ordinated by the Institute for Baltic Sea Research Warnemuende (IOW)/Germany.

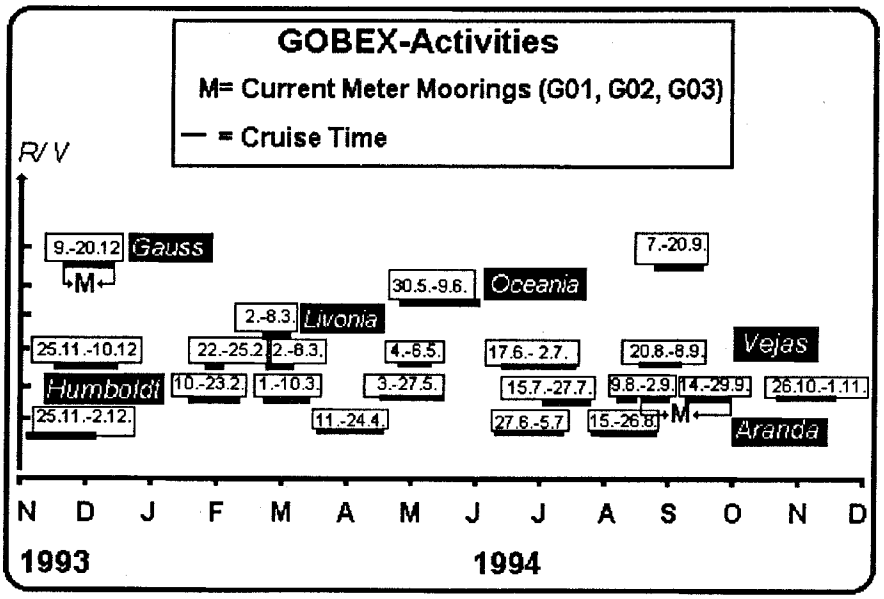

Fig. 2 Time table summarizing all cruise activities of participating research vessels (R/V) and moored current measurements (M) at positions GO1, GO2, and GO3

Relevant news were monthly/ bi-monthly distributed by the GOBEX-Newsletter. This provided a fast presentation of preliminary results and helped in the co-ordination of cruise logistics, data exchange, device calibration procedures, guest researchers, and etc. This summary report contains contributions, which were published in different issues of the Newsletter. Several original papers are included in order to provide the GOBEX-community with a compact overview of the outcomes. Because field measurements play a crucial role for all marine disciplines, we hope our summary is useful for all interested colleagues. At present, some of our GOBEX activities continue in the European project 'Baltic Sea System Study' (BASYS) during the period covering three years (1996 - 1999).

Thanks are due to all contributors and we especially like to acknowledge all crews, officers, and captains of participating research vessels.

Contribution to Geomorphology of the Gotland Depression

Zivile Gelumbauskaite and Algimantas Grigelis
Department of Baltic Marine Geology, Institute of Geology
Sevcenkos 13, 2600 Vilnius, Lithuania

Introduction

Evaluation and prediction of each geosystem, as well as of the present state of an ecosystem, can be done only by means of a comprehensive study of all the parts of the system. This short report has the goal to show how the plasticity and origin of the recent relief in the Gotland Depression has influenced present lithohydrodynamical processes. The data for these analyses have been collected in joint Lithuanian-Swedish expeditions in 1993 - 1994.

The Baltic Sea is a basin of an intracontinental platform type. The Gotland depression, like the entire area of the Baltic Proper, has been formed under conditions of interactions among crustal/isostatic/eustatic movements, and glacial accumulational-denudational processes. Its development is thought to be related to that of the morphostructure/morphosculpture of the Baltic Shield and the Baltic Syneclise, starting in the Mesozoic and ending in the Holocene.

Pre-Quaternary Morphostructure

At present, the Gotland depression lies in the field of the Silurian-Devonian peneplain dissected during the Pre-Quaternary. In the southwestern part, the basin borders upon the zone of tectonic fractures, in the east, it is limited by the Klaipeda-Liepaja structural uplift composed of the Upper Devonian Plavinas-Pamusis Complex and by the Ventspils-Saaremaa Step of the Middle Devonian Burtnieki-Narva Complex. In the north, it is isolated from the Faro Basin by the Jaani-Jaagarahu glint of the Lower Silurian. Its western slope borders upon the Leba-Gotland Plateau of the Lower-Upper Silurian.

The basin itself is clearly divided into the southern and the northern parts and separated by a double swell of banks. The northern one is known as the Klints Bank, whereas the southern one is named the South Klints Bank and described here for the first time. The

plasticity of palaeorelief of these morphostructures in the Gotland depression is directly reflected in the recent relief. This confirmed the fact that glacial accumulation occurred differently and it was controlled by the pre-Quaternary surface which had been formed already.

Thickness of the Quaternary

Distribution of Quaternary thicknesses and composition is unevenly in the area studied. The material collected during 1993 - 1994 expeditions shows the influence of the pre-Quaternary surface roughness on movement of glacier bodies and on formation of palaeo-basins. Analysing seismic profiles, signs of activity typical of the Caledonian and the Hercynian disjunctive structures are detected in the neotectonic period, i. e. vertical tectonic movements have been found to take part in glacial exaggeration/denudation and accumulation processes.

The Quaternary thicknesses in the southern part of the depression range from 5 to 20 - 25 m. The SW end-parts of the Eastern and Western Troughs at the depths of 140 - 165 m are covered by a 10 - 15 m thick layer of the Quaternary deposits; further down, this layer becomes thicker (to 20 - 25 m) at the depths of 165 - 180 m. The infilling of the incisions is quite complicated. They are mainly filled up with morainic and fluvioglacial Pleistocene matter. However, the data of 1994 show that some of the buried incisions seem to be filled up with pre-Quaternary alluvium, too.

The northern part of the depression is more complicated. The Upper Silurian structural/-denudational remnant of the Klints Bank at the depth of 120 m is covered with the Quaternary deposits, 50 - 60 m thick, whereas the eastern slope of the Gotland Deep at the depth of 130 m has Quaternary thicknesses, exceeding 90 m. These layers are considered to consist of glacial/ fluvioglacial deposits, and, for the first time, they are attributed to the Pandivere recession phase marked on the Geomorphological Map of the Baltic Sea and its coasts in 1990.

Total Quaternary thickness in the GOBEX profile 9409G reaches 40 m. The Holocene deposits at the floor of the Gotland Deep make up 10 m, whereas Late-Glacial clays are 21 m thick, and Pleistocene till occurs in a 10 m thick layer. At the geological site 118 (1993; 19°59,9'E: 57°18,8'N, water depth=232.8 m), the pollen analysis has shown the boundary between Upper and Middle Subatlantic [SA3 & SA2], correspondingly to be at the depth of 0.54 cm.

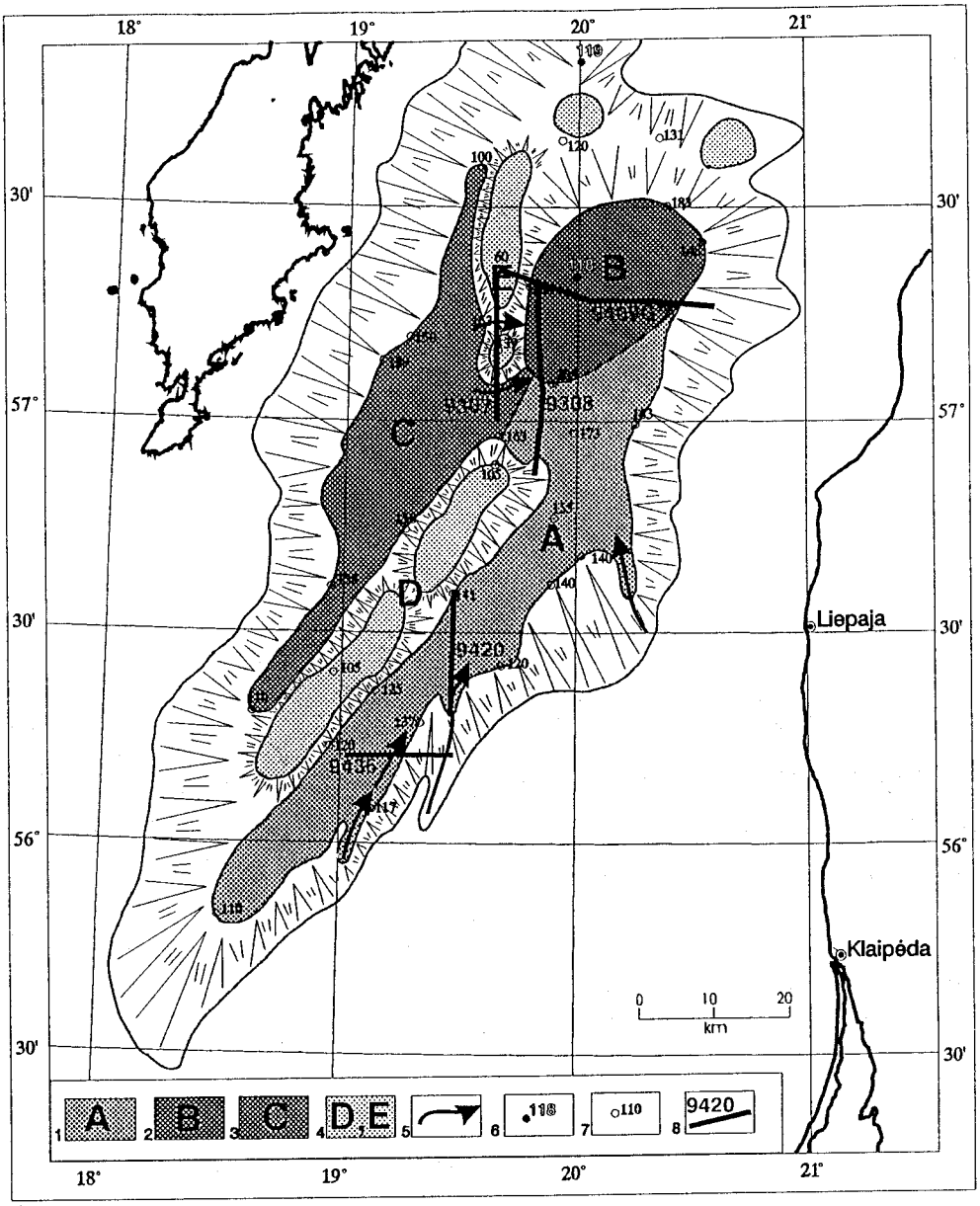

Fig. 1 Morphology of the Gotland Depression according to Gelumbauskaite and Grigelis (1995):

1 - Eastern Gotland Depression;

2 - Gotland Deep;

3 - Western Gotland Depression;

4 - South Klints Bank (D), Klints Bank (E);

5 - general current patterns;

6 - sampling site;

7 - depth of the sea floor (m).

8 - seismic recording and echosounding profiles.

Bottom Relief

The measurements of depth and records of bottom relief plasticity have been done by echosounders SKIPPER 607 and FURUNO 881 MK II. Applying AUTOCAD 11/SURFER 15U software, the bathymetric map of the Baltic Proper was compiled on the scale of (1 : 200 000) in the UTM-34 coordinate system with a 4 m step of isobaths. The data obtained are used for compiling a new morphological scheme of the Gotland Depression in Fig. 1 with all the macroform details, although this was known previously, but morphologically unstudied and not well described. The scheme shows that the Gotland Depression is distinctly divided into the southern and northern parts which both of which are separated by the Klints Bank and the South Klints Bank into the eastern and western parts.

The southern part of the Gotland Depression is prolonged, its floor is inclined and stretching from SW to NE from 110 m to 170 m. The Eastern Depression is separated from the Western one by the South Klints Bank. Eastern and western slopes of the southern depression are at the depths from 70 to 120 - 140 m. The eastern slope is rather steep and stepwise with Upper-Middle Devonian rock glints having no Quaternary cover in some places of the Pre-Quaternary surface; the glints are easily detected in the recent relief. The western slope is less inclined, the Upper-Lower Silurian glints are distinctly seen at its northern part in the recent relief.

Echosounding and seismic profiles reflect a close relationship between the pre-Quaternary palaeorelief of the southern depression and the recent relief. The signs of the palaeo-incision network fixed in seismic profiles are revealed in echosoundings as the arteries of recent currents directed along the eastern slope of the depression. Such signs of the arteries fixed in some profile fragments are detected in the Western Depression as well. A large prolonged graben-shaped incision found in the pre-Quaternary surface is expressed in the recent relief by the zones of active gas seepage. The plateau of the South Klints Bank is at the depth of 110 - 105 m with a lowering to 120 m in its central part. The slopes are rather plane and occur at the depths from 110 - 120 to 140 m.

The northern part of the Gotland Depression differs greatly from the southern one. The northern Gotland deep with a maximum depth fixed at 242 m is a kettle-like depression inclined from SW to NE at the depths of 205 - 242 - 180 m. The fault zone reflected in the pre-Quaternary surface separates the northern part of the depression from the southern one by distinct cliffs and makes up a rise in the relief of about 10 m.

There are four steps on the slopes of the Gotland Deep (profile 9409G). They are especially distinct on its eastern slope: Step 1 at 233.3 - 182.4 m, Step 2 at 182.4 - 150.2 m, Step 3 at 150.2 - 108.0 m and Step 4 at 108.0 - 72.5 m. The western slope is of a similar structure. Steps 1 and 2 correspond to the Silurian glints which are not covered by the Quaternary deposits in some places. Steps 3 and 4 correspond to recessive marginal formations related to the Pandivere recession phase.

The core data from the site 118 show that during the last millennium 540 mm of pelitic deposits settled down in the Gotland Deep. At the same time, only 25 mm have settled on the saddle separating the Gotland and the Faro Depressions in the northern Part of the Basin, according to pollen data from the core of geological site 119 (1993; 20°00,88'E: 57°50,96'N, water depth = 135.3 m). The data mentioned above show that lithodynamical processes are highly complicated in the Gotland Deep. Recent sedimentation occurs not everywhere, since it seems to be related to active hydrodynamics of near-bottom water masses.

The morphology of the northern end of the West Gotland Depression separated by the Klints and the South Klints Banks is the same as that in the southern part; only its central part with depths varying in (140 - 179 - 171) m is inclined from the west to the east and resembles to its northern neighbour. Its connection with the latter one is obviously fixed on the seismic profiles. Signs of the recent near-bottom currents are detected at the southern end of the Klints Bank at the depths of 172 and 153 m. The development of the Gotland Depression can be divided into following time stages:

1) Mesozoic-Palaeogene 1st degree morphostructures,
2) Neogene 2nd and 3d degree morphostructures,
3) Pleistocene glacial morphostructures,
4) Holocene Baltic Sea formation.

Reference

GELUMBAUSKAITE, Z., GRIGELIS, A., 1995: The morphology and development of the Gotland Depression. In: Proceedings of the Conference 'Past, Present and Future of the Baltic Sea'. Stockholm University (in press).

Signals of inflows to the Gotland Basin in the sedimentary record Preliminary results

Christian Christiansen[1] and Helmar Kunzendorf[2]

[1] Department of Earth Sciences, University of Aarhus, Ny Munkegade Build. 520, DK-8000 Aarhus C. [2] Risø National Laboratory, Department of Environmental Science and Technology, Postboks 49, DK-4900

Introduction

During August 1994 the IOW carried out two expeditions with r/v "A. v. Humboldt" into the GOBEX area. Among the purposes of the second leg were studies of

1) flux rates into and out of the depositional system,
2) studies of benthic processes, and
3) studies of environmental records and their diagenetic overprint.

Here we report on preliminary findings on the multicore 20001-5 taken on station 799 (57° 18.33'N, 20° 03.00'E; water depth 243 m). Our data suggests that the 1951 and 1971 strong inflows to the Gotland Basin show up in the sedimentary record.

Methods

Low-level Gamma-spectrometric measurements of ^{210}Pb, ^{137}Cs, and ^{226}Ra were carried out using a reverse-electrode coaxial Ge-detector (10 % rel. efficiency) with energy resolution values of 640 eV (at 5.9 keV) and 1.7 keV (at 1332 keV). Subtracting ^{210}Pb supported, i. e. an amount equivalent to the ^{226}Ra activity, the unsupported activity $^{210}Pb_{unsup}$ is used to estimate linear sedimentation rates for the cores using the constant initial concentration (CIC) model of interpretation. The historical profile was constructed using petrophysical core data and the constant rate of supply (CSR) model for ^{210}PB. Sediment density, porosity, and concentrations of elements were determined using standard laboratory methods.

Results

Dating

Fig. 1a shows results of the ^{210}Pb datings performed on the core. The interpretation of the radiometric profiles from the GOBEX cruise is generally favoured by very high activities, usually a factor of 2 to 5 higher than in the Kattegat area. Using the CIC model for interpretation the sedimentation rate has varied between 0.8 mm y^{-1} and 2.9 mm y^{-1} during the period of time covered by the ^{210}Pb method. The results imply that eventual signals of the 1971 inflow should be found at the 70 mm level and that eventual signals from the 1951 inflow should be found at the 100 mm level in the core. The accumulation rates (using the CRS model) ranging from 106 to 738 g m^{-2} y^{-1}.

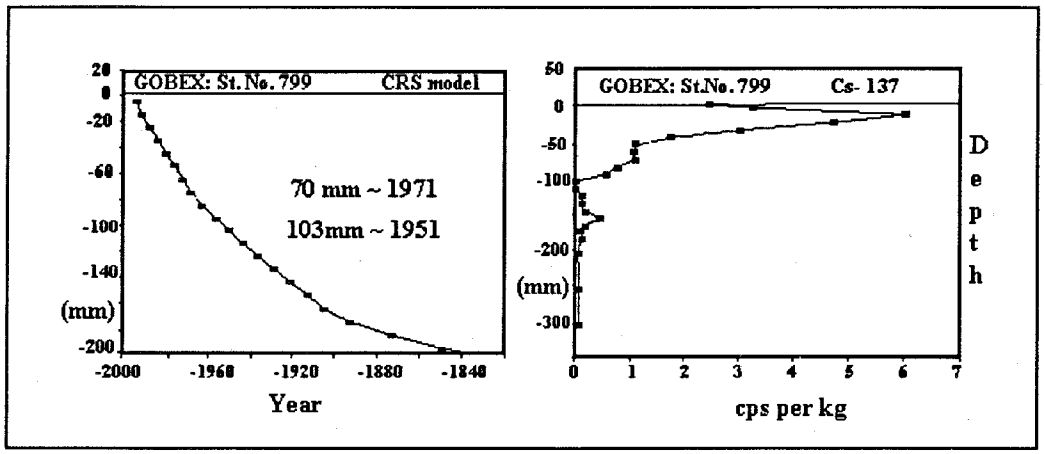

Fig. 1 Dating results from the core:
a) Down-core age/ depth relations.
b) Profile with depth of ^{137}Cs activity.

The Chernobyl accident in 1987 is clearly reflected in the depth profile of ^{137}Cs and there is also an indication of elevated activities due to nuclear bomb testing (sixties, depth $\approx$ 80 mm). The Chernobyl peak is observed at a level dated to the late 1980'ies by the ^{210}Pb method. This suggests that the ^{210}Pb dating are reliable.

Changes with time

The depth profile of bulk density (Fig. 2a) shows a semi-cycling behaviour. There are sharp increases in the relative low densities followed by intervals (periods) of gradual decrease.

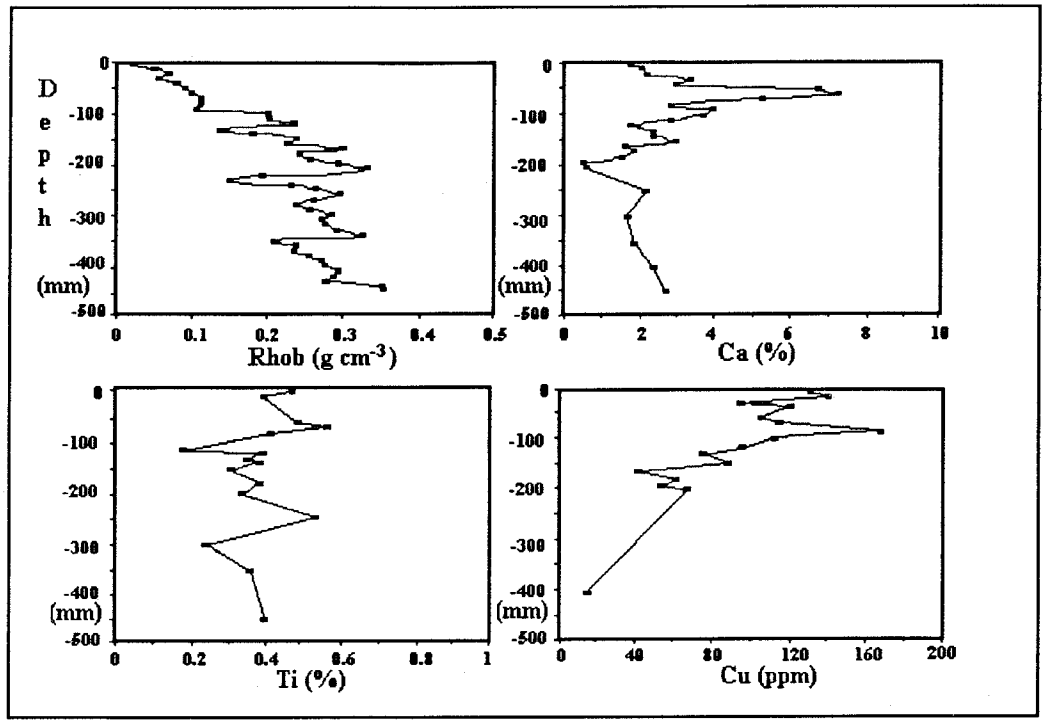

Fig. 2 Down-core variations in sediment density and content of Ca, Ti and Cu.

One possible explanation for this behaviour, at this time, may be that strong near-bottom turbulence during inflows results in higher sediment density, which is followed by stagnant (quiet) periods of sedimentation of more organic rich sediments. Note from Fig. 2a, that density has decreased since the strong 1971 inflow (70 mm level). There clear peaks in the down-core concentrations of both Ca and possible Ti in Fig. 2. The strongest peaks are at the 70 mm level in the beginning of the 1970'ies. A smaller peak is also observed for Ca in the 100 mm level (1951). A recent study in the Kattegat (Christiansen et al., in press, 1994 a) showed very similar results, in that significant changes in concentrations of a number of elements (including Ca and Ti) took place in the beginning of the 1970'ies. Bernard and van Grieken (1989) and Christiansen et al., in press, (1994 b) have found that the North Sea may act as a source for Ca and Ti in Kattegat sediments. Post-depositional dissolution of Ca in periods without inflow may explain the smaller Ca peak at the 100 mm level. There is also a clear decrease in Ca following the 1971 inflow.

The concentrations of Cu show a general increase, which may reflect anthropogenetic impact. There is, however, also a clear peak at the 100 mm level in the core, which suggests import of Cu during inflow situations. Opposite to this, our data show a general increase and more smooth profile of Zn concentrations. This may indicate local sources

for the Zn accumulation.

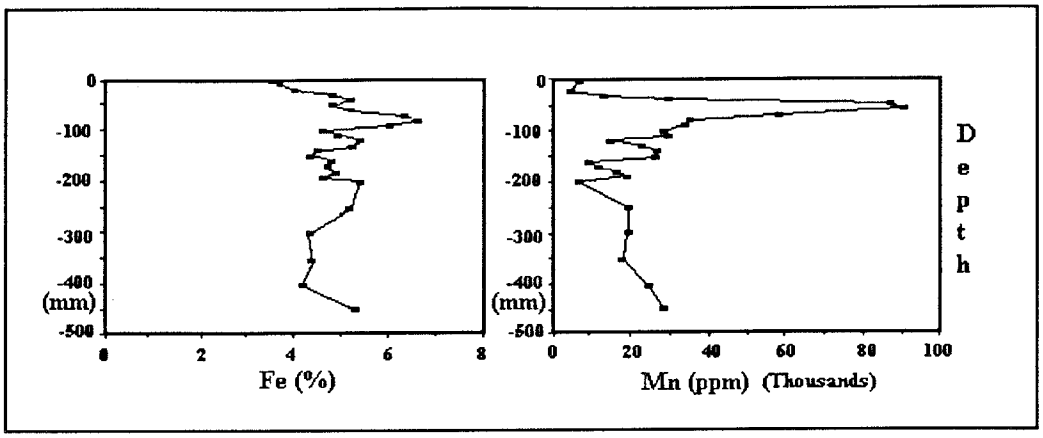

Fig. 3 Down-core variations in Fe and Mn

There are also significant peaks in the concentrations of Fe and Mn at the 70 mm level. These peaks suggest that inflows not only may be observed in concentrations of imported elements. A strong pycnocline and high oxygen consumptions following more saline bottom water inflow may also result in diagenetic overprints on the sedimentary record, which apparently may be used as inflow signals.

Conclusions

We find these preliminary results encouraging in that they suggest that paleoinflows may be detectable in the sedimentary record and probably be distinguished from changes due to redox variations. More work on such signals partly on GOBEX cores and partly in connection with future MAST-3 research in the Baltic may confirm the present interpretations and help to understand the development through time of the Baltic Sea.

Acknowledgements

We thank the IOW for the invitation to take part in the August 1994 expedition.

References

BRÜGMANN, L.

BERNARD, P. C., VAN GRIEKEN, R. E., 1989: Geochemistry of suspended matter from the Baltic Sea. 1. Results of individual particle characterization by automated electron microprobe. Marine Chemistry, **26**, 155 - 177.

CHRISTIANSEN, C., KUNZENDORF, H., OTTO, C., SENSTIUS, J., 1993: Recent and subrecent sedimentary conditions in the southern part of the North Sea - Baltic Sea transition. Boreas, **22**, 357 - 366.

CHRISTIANSEN, C., KUNZENDORF, H., LAIMA, M. J. C., LUND-HANSEN, L. C., PEDERSEN, A. M., 1994a: Recent changes in environmental conditions in the southwestern Kattegat. NGU Bulletin (in press).

CHRISTIANSEN, C., KUNZENDORF, H., TYCHSEN, H. R., 1994b: $CaCO_3$ in sediments of the North Sea - Baltic Sea transition: Signals of high salinity? Prace Pánstwowego Instytutu Geologicznego (in press).

Fe and S in sediment from 3 stations from the GOBEX area
Preliminary results

Henning Matthiesen
Department of Chemistry, University of Aarhus
Langelandsgade 140, DK-8000 Aarhus C, Denmark

Introduction

During August 1994 the IOW carried out an expedition in the GOBEX area with R/V "A. v. Humboldt". Among the purposes were studies of fluxrates into and out of the depositional system. Here are presented some results from porewater-analysis on cores no.

20000-7 (station 798, 57°15.17'N 20°33.64'E, 112 m)
20004-1 (station 802, 57°18.28'N 20°13.66'E, 236 m)
20008-4 (station 806, 57°27.60'N 21°09.60'E, 68 m).

The aim of the present study is to identify the chemical parameters in porewater connected to the mobilisation of phosphate from the sediment. The data suggest a clear connection to iron and sulphate.

Methods

Cores from the different stations were cut into slices in a glovebox (Ar-atmosphere), porewater was separated by centrifugation and the supernatant was filtered (0,45 μm). H_2S was measured on board the ship using the Spectroquant®-kit from Merck. Soluble iron and ortho-phosphate were both measured spectrophotometrically using TPTZ, COLLINS et al. (1959), and phosphomolybdate-complex, KOROLEFF (1983), respectively. The samples were conserved with acid to avoid oxidation of the iron during storage and analysis. Reversed-phase ion-pair chromatography was used for the analysis of sulphate and chloride according to PERRON and GANT.

Results

Fig. 1 shows results of the sulphate, iron and phosphate analyses from the 3 sampling-

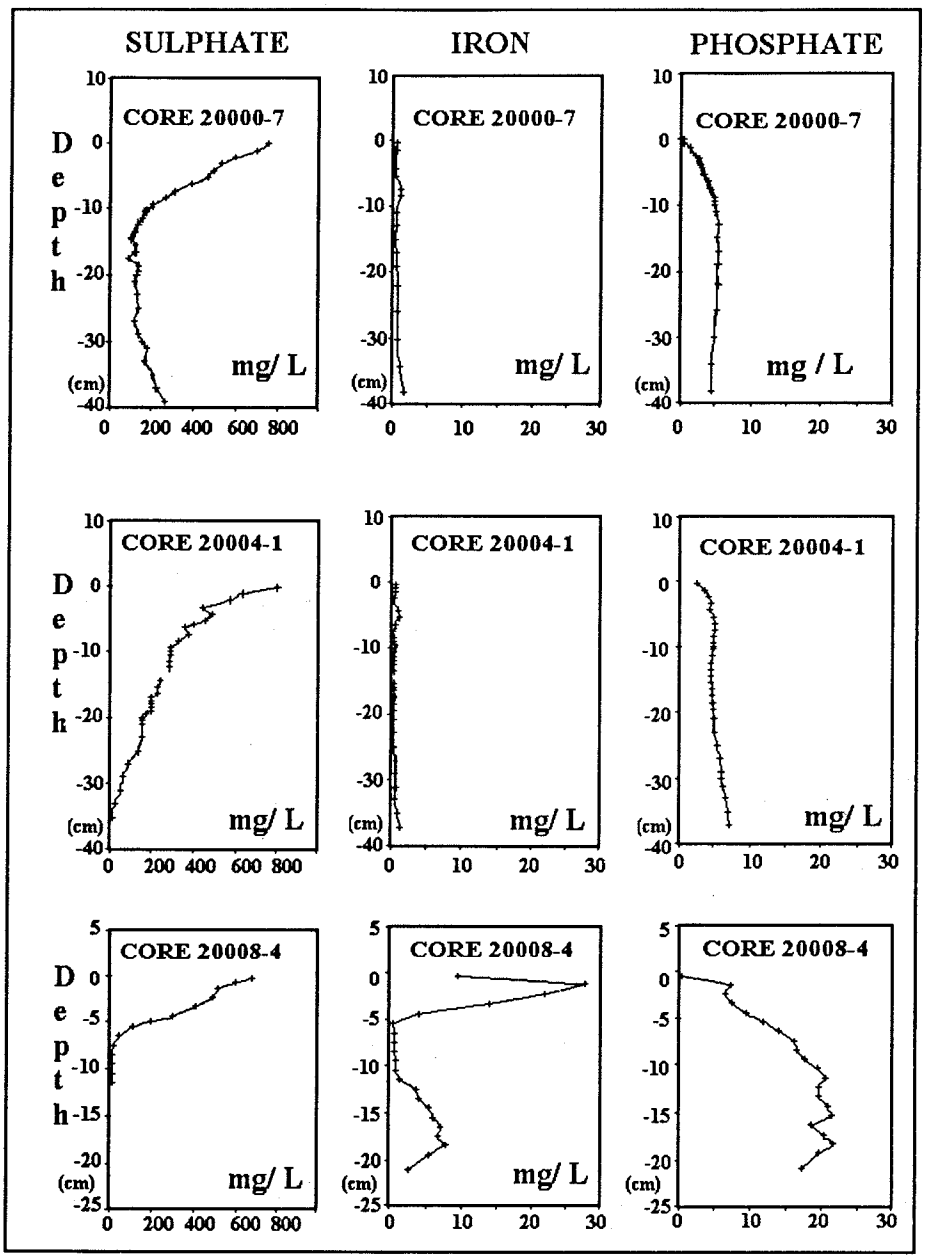

Fig.1 Concentrations of dissolved sulphate, iron, and ortho-phosphate at three stations

stations. The measurement of sulphide is quite uncertain, because sulphide can be lost as H_2S (g) or by oxidation during the analysis.

To minimize this problem, the analyses were performed on board the ship (within a few hours). The results are given in figure 2. Notice that only relative measurements are given (measured extinction x dilution) - conversion to concentration-values are not practicable because no calibration-curve is available at present. The values for chloride were constant

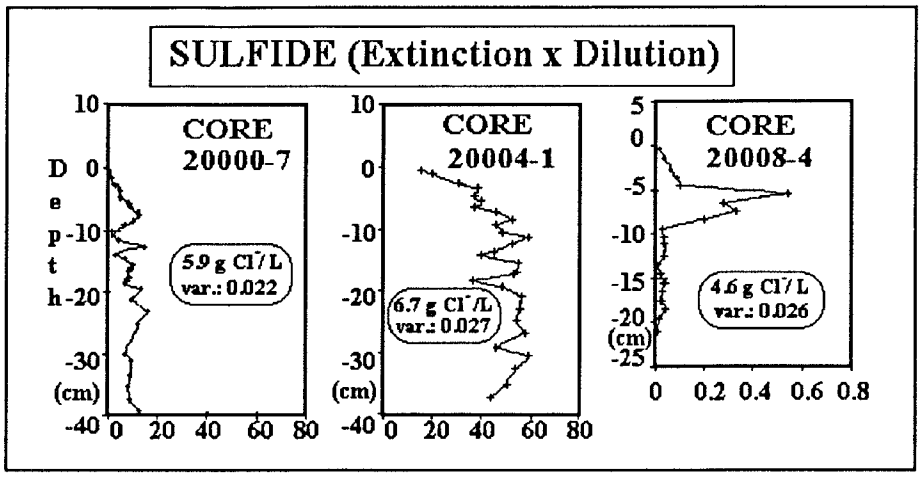

Fig. 2 Distribution of sulphide in the 3 cores. Notice the different extinction-scale in core 20008-4

throughout a core. Their level was:

Core:	20000-7	5.9 g Cl^- / L (var. 0.022)
	20004-1	6.7 g Cl^- / L (var. 0.027)
	20008-4	4.6 g Cl^- / L (var. 0.026).

These values are also given in Fig. 2.

Discussion

Fig. 1 shows some connections between the profiles of dissolved sulphate, iron and phosphate. Starting with core 20008, a large peak of dissolved iron [Fe (II)] is observed in the upper 5 cm. This is probably due to iron-reduction, where Fe (III) from different solid forms is used to oxidize e. g. organic matter. Micro-organisms can also use sulphate as an oxidant with sulphide as the resultant species. This is indicated by the decrease in sulphate concentration (down to 8 cm) and by the peak in sulphide-concentration at 6 cm shown in Fig. 2. In the same layers the phosphate-concentration is increasing. At least two explanations can be given for this:

1) Organic matter contains P. When the organic material is decomposed by oxidation with iron and sulphate, the phosphate is mobilised.

2) Phosphate can bind to the surface of some iron (III) oxides. When the iron is reduced, phosphate is released from the surface.

The same trends can be seen at the two other cores, but the concentration-levels are different. There is less iron, less phosphate and more sulphide. The concentrations of sulphate are about the same, only do the profiles look quite different. There is a connection between dissolved iron and sulphide presumably due to the iron-sulphide solubility. Thus it evident, that when the sulphide raise, the amount of free Fe (II) is kept low and vice versa. This is also seen at the iron and sulphide profiles of core 20008-4.

The differences between the three cores can be connected to several factors:

- different amounts of organic matter,
- different redox-conditions,
- different age etc.

More data is needed to make reliable explanations of the observed phenomena.

Finally it is observed at all three sulphate-profiles, that there is a stagnation of the sulphate-reduction at the concentration-level of 500 mg SO_4^{2-}/ L. This could be a temporal phenomena caused by different salinities in connection with strong inflows of salt water. However, a corresponding change is not seen for the chloride. Dating of the cores will help answering the question.

At cores 20004 and 20008 the stagnation is coincident with a peak in the iron-profile and an inflection on the phosphate-curve. Therefore, the stagnation can also be due to processes within the sediment (e. g. competition between sulphate- and iron-reducing bacteria). However, a theory can not be made without knowing something about the amounts of organic material available, the amounts of reactive Fe (III) and the presence of other oxidants (e. g. manganese).

Conclusion

The profiles of dissolved sulphate, iron, phosphate and sulphide has been demonstrated to be clearly site-dependent. Still the three investigated cores appear to have some features in common. For instance the mobilisation of phosphate seems to be connected to the sulphate and iron profiles at all three sites. To explain these phenomena in detail more data is however needed. Entities like organic C content, total Fe, total Mn, dissolved Mn and others will all help modelling the chemical processes in the sediment.

Acknowledgements

I thank the IOW for the possibility to join the August expedition.

References

COLLINS, P. F., DIEHL, H., SMITH, G. F., 1959: 2, 4, 6-Tripyridyl-s-triazine as a reagent for iron. Determination of iron in limestone, silicates, and refractories. Anal. Chem., 31, 1959, 1862 - 1867.

KOROLEFF, F., 1983: Determination of nutrients. In: Grasshof, K., Erhardt, M., Kremling, K. (eds), Methods of seawater analysis. Verlag Chemie.

PERRON, P. A., GANT, J. R.: Advances in anion analysis: Reversed-phase ion-pair chromatography with indirect photometric detection. Perkin-Elmer Corporation, Norwalk, CT 06856.

The Subsurface Circulation in the Gotland Deep

Ekkehard Mittelstaedt

Bundesamt für Seeschiffahrt und Hydrographie, Hamburg
P. B. 30 12 20, D-20305 Hamburg , Germany

According to observations of the Baltic Sea Research Institute in Warnemuende (IOW), the vigorous inflow of saline subsurface water in January 1993 had reached the Gotland Basin at depths after 3 months, in April. Using this information, we investigated the circulation within the lower layer of the GOBEX region. We hoped that the inflow would possibly intensify the lower layer of the local currents and, thus, would emphasize the topographic influence upon the deep flow.

At the beginning of the "GAUSS"-cruise No. 233, three current meter strings, each with three current meters within the lower layer, were deployed at the GOBEX mooring positions G1, G2, and G3 on 29 November, 1993.

Loc.	Depth	Lat.	Long.	Level 1	Level 2	Level 3
G1	220 m	57°19'N	19°53'E	106 m	165 m	215 m
G3	230 m	57°10'N	19°56'E	126 m	183 m	225 m
G3	220 m	57°19'N	20°09'E	116 m	173 m	215 m

Tab. 1 Mooring positions, water depths and observational depths

Two weeks later they were recovered again, immediately after two short orthogonal CTD-sections. Figure 1 displays temperature and salinity across the Gotland Deep along the proposed section from NW to SE (see Fig. 2).

The salinity of the lower layer in December was evidently higher than before the inflow in January (NEHRING, pers.comm.) and also higher than in August 1993 (FEISTEL, pers. comm.).

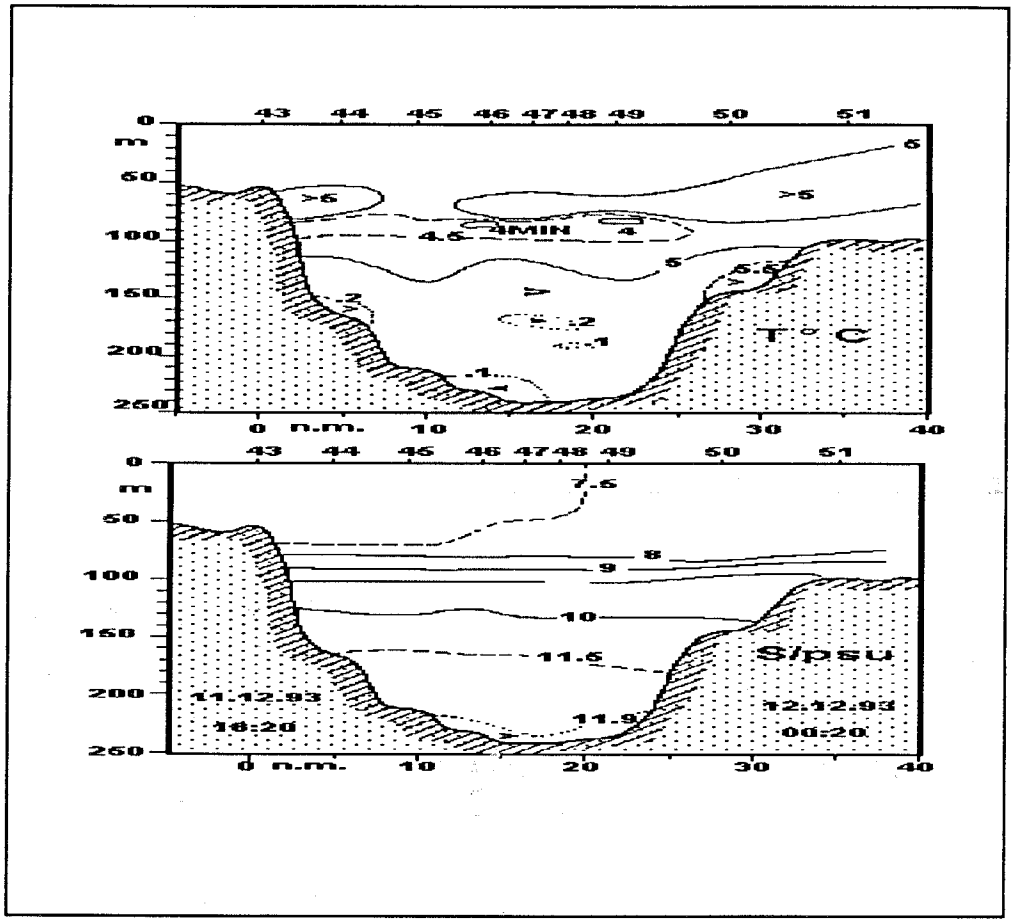

Fig. 1 Temperature and salinity on 11/12 December 1993 across the Gotland Deep along a section running from NW to SE (R/V "GAUSS-cruise No. 233)

After two weeks of operation, the current meters, especially those, which were within 5 m above the bottom, had a black coat at the rotors and the pressure cases. The surface of the rubber cap of the acoustic releases 2 to 3 m above the bottom were roughened, probably due to chemical reactions with H_2S.

The current data of Tab.2 suggest a counter-clockwise mean circulation at depth during the short observation period with vector speeds between 2 and 7 cm/s. The directional behaviour of the mean flow confirms similar results by HOLLAN (1973), cf DIETRICH and SCHOTT (1974), which- to our knowledge- are the only published information on measured currents in the Gotland Deep, so far.

Current statistics on our data on hand reveal highest directional stability S (70 to 90 %) at position G1. At G3 S is 50 to 60 %. The lowest stability (30 to 40 %) happened to occur at G2.

Position/Level	1		2		3	
G1	6	191°	7	202°	4	191°
G2	no data		2	150°	2	73°
G3	3	24°	3	335°	4	317°

Tab. 2 Rounded mean values (vector speeds, cm/s, and direction) of currents

The number of variances are roughly within the same range (20 to 40 cm^2/s^2) at all three moorings. Regarding the maximum scalar speeds 5m above bottom, the records show values between 16 cm/s (G3) and 25 cm/s (G2). 12% of the data recorded 5 m above the bottom exhibit current speeds of 12 to 15 cm/s at all moorings.

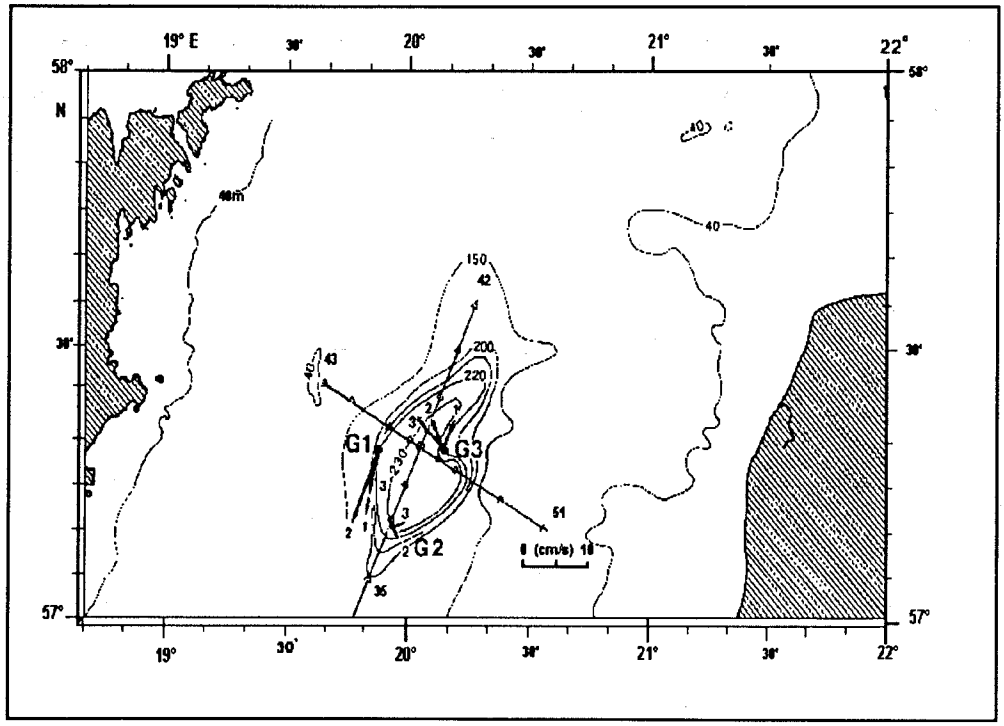

Fig. 2 A hydrographic survey of the Gotland Deep in late fall 1993 ("GAUSS"-cruise No. 233)

- Mooring positions G1, G2, G3, with mean flow vectors (averages over two weeks, from 29 Nov. to 12 Dec.,1993) and recording depths 1,2,3 (see first table),
- Location of two CTD-sections occupied on 12/12 Dec. 1993,

- Schematic depth lines (m)

References

DIETRICH, G., F. SCHOTT; 1974: Wasserhaushalt und Strömungen. In: L. Magaard und G. Rheinheimer (editors); Meereskunde der Ostsee, Springer Verlag, 33 - 41.

Editors Note:

When comparing the deep water circulation (cyclonic rotation sense) presented in Fig. 2 with corresponding measurements (180 m depth, 17 days), which were carried out by HOLLAN (1973) 20 years ago, we may conclude that a cyclonic near bottom circulation permanently dominates in the H_2S regime of the Gotland Deep. Its generation mechanism is still an open question, but it seems that such a response can be explained by vorticity conservation above a cañyon-like bottom topography. Can we expect a seasonal signal within this circulation? There are some hints for meso-scale eddy-like motions which could be bottom intensified. What is their forcing mechanism?

Gotland Waters at Position BY15A, 1970 - 1993

R. Feistel and E. Hagen

Institut für Ostseeforschung Warnemünde (IOW)
P. B. 30 11 61, D-18112 Rostock, Germany

The water in the East Gotland Deep is a proper indicator for climatic changes concerning the Baltic Proper. An extended discussion of various parameters till 1989 was given by NEHRING (1990), MATTHÄUS (1990), and NEHRING and MATTHÄUS (1991). Below 50 m depth, the typical mixed layer depth, annual signals are rather weak. Beneath 150 m, the water is confined to the basin-scale.

Physically, mainly two processes are observed. Water in the basin is aging, indicated by processes of the vertical turbulent exchange, smoothing out salinity and temperature gradients and, this way, gradients in the stratification. If winterly storms have necessary direction and duration, waters from the North Sea with high salinity and oxygen content may sporadically propagate into deeper layers of the Gotland Basin, forming new bottom water and lifting up the existing water column. Usually, such events occur within an interannual time-scale in between 3 - 7 years.

The last two decades of observations, which were carried out during the HELCOM-monitoring programme at least four times per year at the station BY15A in the central part of the Gotland Basin, demonstrate a high temporal variability. Probably due to a generally modified atmospheric situation over central Europe, from 1976 to 1992 almost no deep water renewal took place. As a consequence, the salinity dropped to historically extreme minimum values, dissolved oxygen content became exhausted, and hydrogen sulphide (H_2S) accumulated systematically.

The well documented inflow event of January 1993, which is under discussion by GOBEX, stopped this trend, salinity increased again, and H_2S has practically disappeared. However, the present state of hydrographic conditions in the Gotland Deep is still far from normality, as which the average situation before 1980 is considered. The position of the Baltic Year station BY15A is shown in Fig. 1.

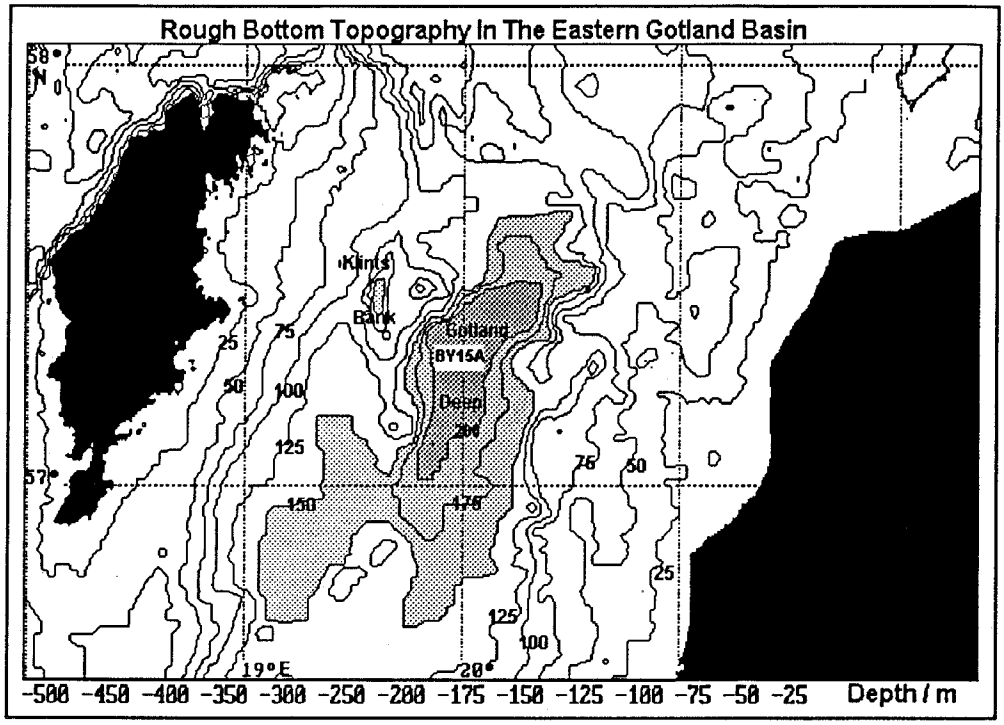

Fig.1 Rough bottom topography in the Gotland Basin with the location of position BY15A (57°20' N, 20°03' E) at 240 m depth (areas deeper than 150 m and 200 m are stippled)

The temporal behaviour in temperature (T) and salinity (S) is shown in Fig. 2. In layers between about 30 - 70 m depth, a cold water mass ($T < 4$ °C) occurs from 1970 - 1989. It seems to be that its layer thickness increased in time. This fact is well expressed by the deepening of the lower 4 °C-isotherm until 1989. During this year this isotherm intersects the sea surface. Obviously, the subsurface cold water vanishes in the period 1990 - 1993. We may conclude that the regeneration of such waters is mainly determined by the winter-time convection and their disappearance is possibly due to mild winter conditions. After 1980, there is a trend with an increasing layer thickness in between isohalines selected. The vertical gradient became smoother and smoother. This way a hint is given for decreasing stratification conditions until winter 1993. Comparing the present state with, say, 1979, the whole water column is 1 PSU less salty.

As temperature gradients are a measure for the thermal distance from equilibrium, gradients in the chemical potential measure the distance from the salinity equilibrium. Both act as irreversible thermodynamic forces.

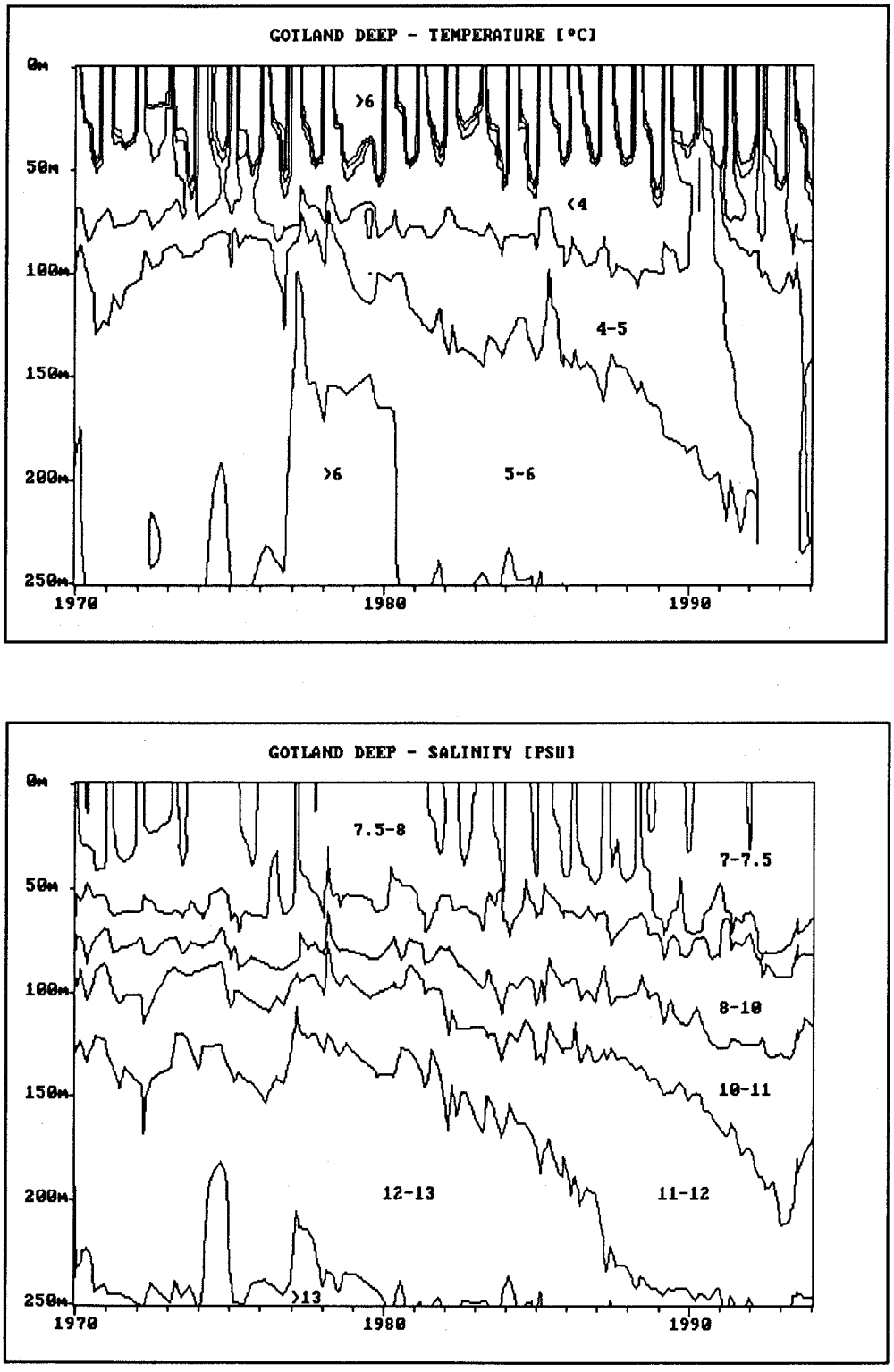

Fig. 2 Time series of the vertical temperature (T/°C) and salinity (S/PSU) distribution at the position BY15A in the eastern Gotland Basin, 1970 - 1993.

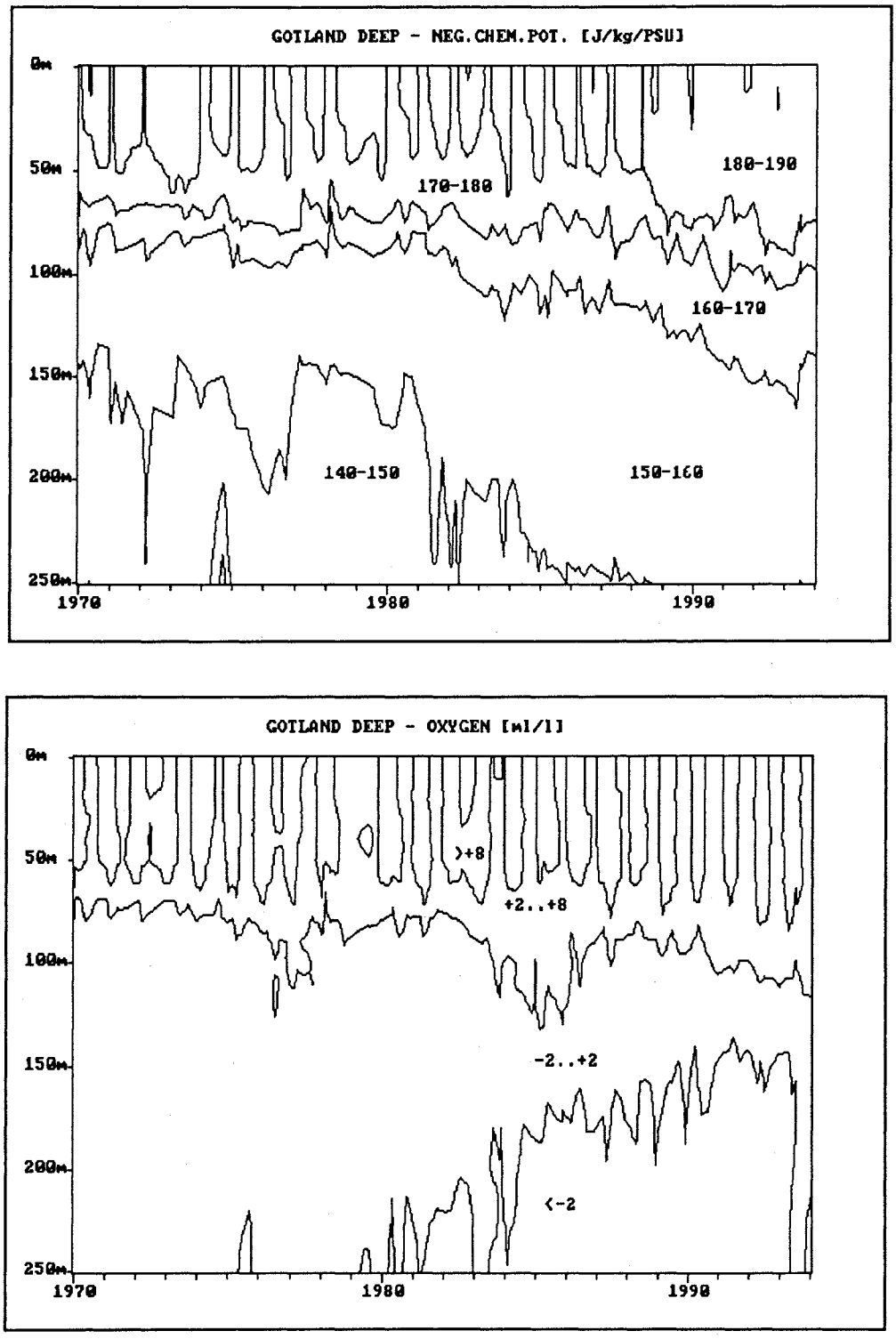

Fig. 3 Time series as in Fig. 2 but for negative values of the chemical potential μ (J/kg/PSU) and dissolved oxygen O_2 (ml/ l; $O_2 < 0 \rightarrow H_2S$)

The chemical potential (μ) became recently available for computation from CTD data and is plotted together with dissolved oxygen (O_2) in Fig. 3 for completeness. Negative oxygen values stand for H_2S. In deep layers (open Atlantic Ocean), μ is almost a linear function of the depth and deviations are only observed in layers with intense vertical mixing processes (FEISTEL AND HAGEN 1994). In the Baltic Proper we note drastic changes of this parameter in the 70 - 80 m top layer after 1989. This observation coincides with the disappearing subsurface cold water at about 60 m depth. However, there is a linear trend with increasing oxygen values in the seasonal peak depth of the 8 ml/l- isoline during the whole observation period. It seems to be that during the mild winter 1991 - 92, (NEHRING et al. 1993), the slight winter-time convection is, due to the poor vertical stability over the entire water column, sufficient for the complete oxygen-ventilation in the 70 m top layer.

From 1980 to 1992 the upper H_2S level rose nearly linearly. Obviously, this trend was stopped by the spreading of deep waters under the influence of the inflow event in January 1993. Plotted vertical profiles of O_2 confirm in Fig. 4 that the accumulation period of H_2S, in layers below about 150 m depth, was associated with decreasing oxygen gradients in the halocline (80 - 120 m depth).

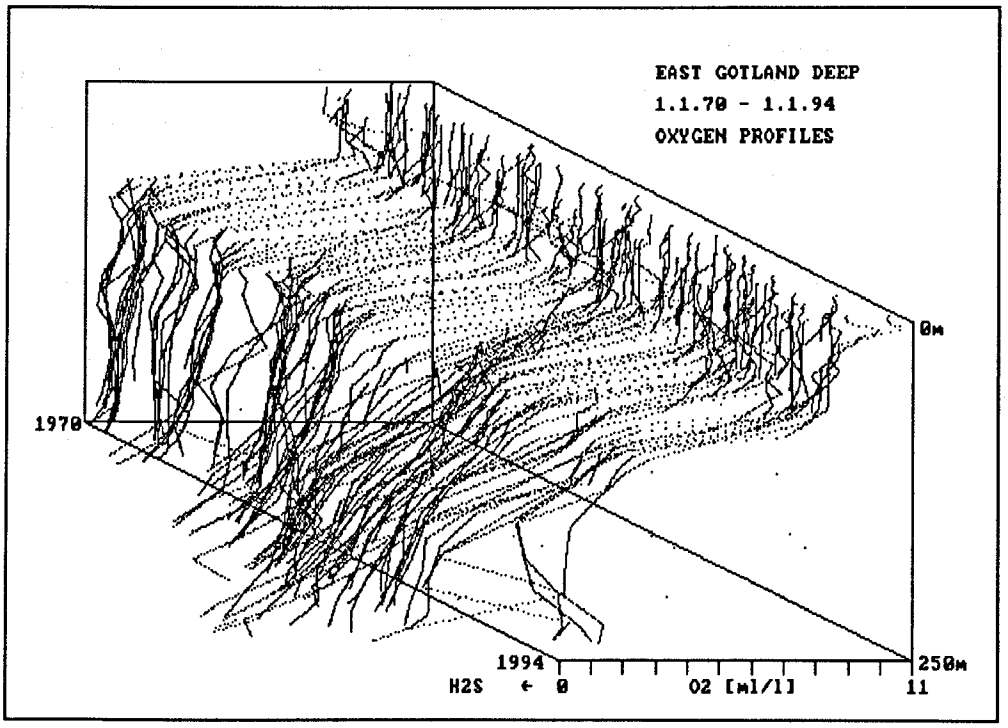

Fig. 4 Vertical profiles of dissolved oxygen (ml/l) shifted in time

References

FEISTEL, R., E. HAGEN, 1994: Thermodynamic quantities in oceanography. In: The Oceans Physical-Chemical Dynamics and Human Impact. Edited by S. K. Majumdar, E. W. Miller, G. S. Forbes, R. F. Schmalz, A. A. Panah, The Pennsylvania Academy of Science, 1 - 16.

MATTHÄUS, W., 1990: Langzeittrends und Veränderungen ozeanologischer Parameter während der gegenwärtigen Stagnationsperiode im Tiefenwasser der zentralen Ostsee. Fischerei-Forschung, **28**, H.3, 25 - 34.

NEHRING, D., 1990: Die hydrographisch-chemischen Bedingungen in der westlichen und zentralen Ostsee von 1979 bis 1988 - ein Vergleich. Meereswissenschaftliche Berichte Nr. 2, IfM Warnemünde, 1 - 45.

NEHRING, D., W. MATTHÄUS, 1991: Current trends in hydrographic and chemical parameters and eutrophication in the Baltic Sea. Internat. Revue der gesamten Hydrobiologie, **76**, 297 - 316.

NEHRING, D., MATTHÄUS, W., LASS, H. U., 1993: Die hydrographisch-chemischen Bedingungen in der westlichen und zentralen Ostsee im Jahre 1992. Dt. Hydrogr. Z. 45, 281 - 312.

Present changes of the hydrographical and hydrochemical situation in the Gotland Deep

G. Nausch and W. Matthäus

Institut für Ostseeforschung Warnemünde (IOW)
PB: 30 11 61, D-18112 Rostock, Germany

Measurements in the eastern Gotland Basin during a monitoring cruise at the end of March 1994 reflected a new inflow event through the Slupsk Furrow. As a result of this inflow, oxygen containing water was found in the bottom layer between 200 m and 239 m of the Gotland Deep with values up to 3.1 cm^3/ dm^3. This oxygen containing water was located below a thin zone with low hydrogen sulphide concentrations (< 0.1 mg/ dm^3 in 175 m depth). The salinity (S) near the bottom (232 m) had increased to S=11.99 (PSU) compared with S=11.54 (PSU) in November 1993. Thus, the salinity is higher than after the inflow in last year when S=11.70 (PSU) were measured in May 1994. Nearly all stations in the basin were free of hydrogen sulphide indicating the inflow event. Only in the Farö Deep the bottom layer was anoxic containing about H_2S = 0.3 mg/ dm^3. The improvement of the situation could be followed during the fourth monitoring cruise in the middle of May 1994. Salinity increased to S=12.39 (PSU) in the near bottom layer of the Gotland Deep (237 m; Fig. 1).

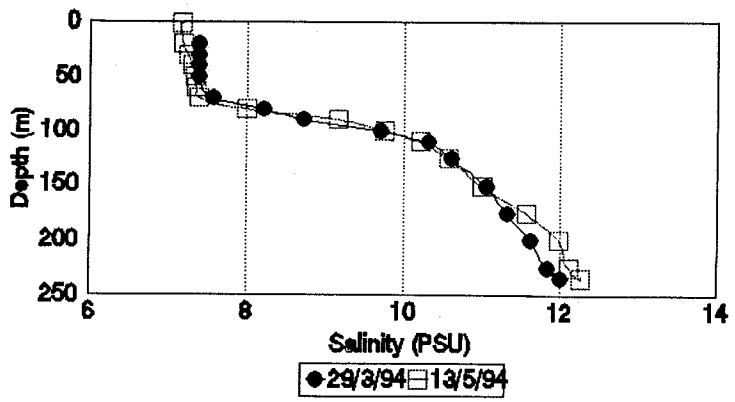

Fig.1 Vertical structure of the salinity in the Gotland Deep; March and May, 1994.

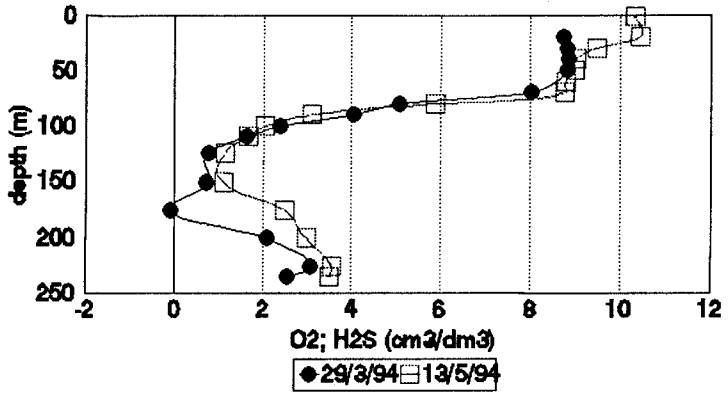

Fig. 2 As in Fig.1 but for dissolved oxygen

The oxygen concentration reached values in the range ($3.0 \leq O_2 \leq 3.7$) cm^3/ dm^3 between 200 m and the bottom, Fig. 2.

Such high concentrations were never recorded since the 30's. Hydrogen sulphide disappeared almost completely in the Gotland and Farö Deeps during the first half of May. Thus, at present, the whole central Baltic deep water is well oxygenated outside of an intermediate layer in the Gotland Deep and the deep waters of the Farö Deep.

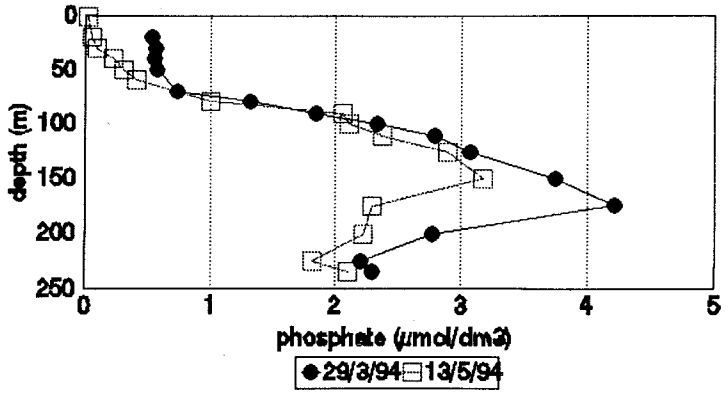

Fig. 3 Corresponding profiles of phosphate

The reason for the observed changes are smaller inflows of both saline water through the Sound and water with S < 17 PSU across the Darss Sill during December 1993 and March 1994 which, however, did not obtain the magnitude of major events. Because of the relatively high salinity and oxygen content in the Bornholm Basin deep water in autumn 1993 and winter 1994, due to the major inflow event in January 1993, the smaller inflows passed directly to the eastern Gotland Basin and caused the observed effects.

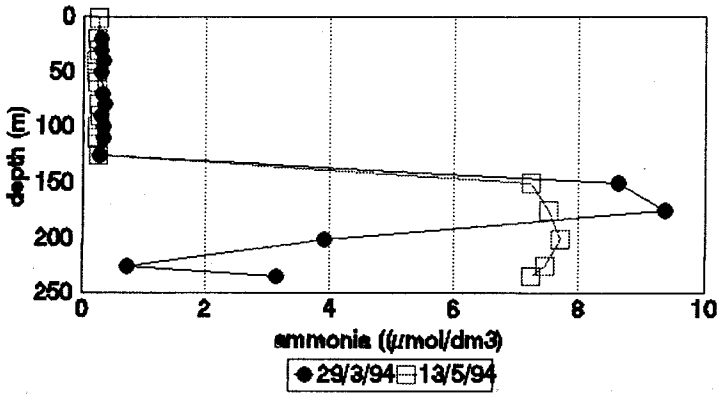

Fig.4 Profile of ammonia

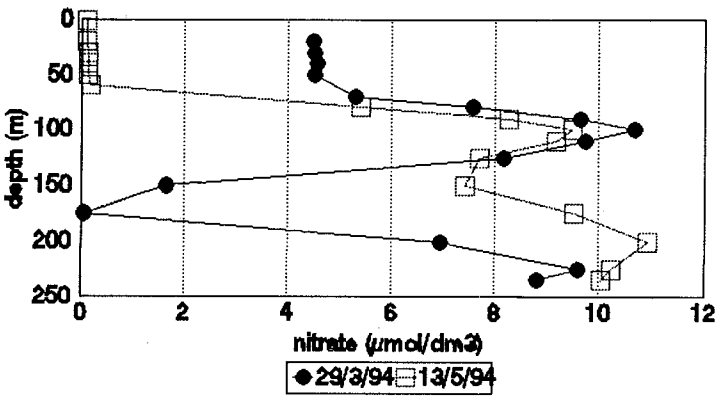

Fig.5 Profile of nitrate

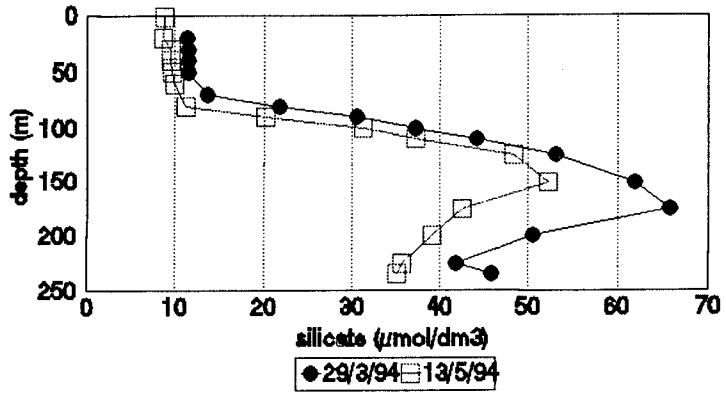

Fig. 6 Plots of silicate

Again, inversions in the oxygen/ hydrogen sulphide distributions in March 1994 were reflected by the nutrient distributions. The intermediate anoxic layer was characterized by high ammonia (7 - 8 μmol/ dm^3) and phosphate concentrations (3.4 - 4 μmol/ dm^3) whereas nitrate was below the detection limit. The oxic bottom water contains remarkable lower concentrations of ammonia (0.9 - 3.0 μmol/ dm^3) and phosphate (2.0 - 2.6 μmol/ dm^3) and a certain amount of nitrate (7.0 - 9.6 μmol/ dm^3).

The further penetration of oxygen rich water into the Gotland Deep brought a continuation of the changes in the nutrient situation. The results are lower phosphate and silicate concentrations in the whole water body below the halocline in May 1994 compared with March 1994 (Fig. 3, 6) due to chemical reactions and dilution effects.

The sufficient amount of oxygen is reflected in the increase of the oxidized inorganic nitrogen compound nitrate (Fig. 5) due to mainly microbial processes. Astonishing is the high amount of ammonia in the deep waters during May 1994 (Fig. 4).

The observations in May 1994 showed that water bodies with relatively high concentrations in salinity and oxygen are located at the bottom of the Slupsk furrow (salinity up to S=15/ PSU; oxygen up to 4.7 cm^3/ dm^3) and in the southern part of the eastern Gotland Basin [(11≤ S≤ 13)/ PSU; oxygen: 5 cm^3/ dm^3]. These water bodies propagate further to north into the direction of both the Gotland and Farö Deep.

Lenses of relative saline deep water in the eastern Gotland Basin?

E. Hagen and R. Feistel

Institut für Ostseeforschung Warnemünde (IOW)
P. B. 30 11 61, D-18112 Rostock, Germany

Within the GOBEX activities, the IOW carried out an expedition with R/V "A. v. Humboldt" during 14 - 29 September, 1994. Its main objective was the study of the exchange of deep water from the Bornholm Basin through the Stolper Furrow into the Gotland Basin (and vice versa). The station map with corresponding sections is shown in Fig. 1.

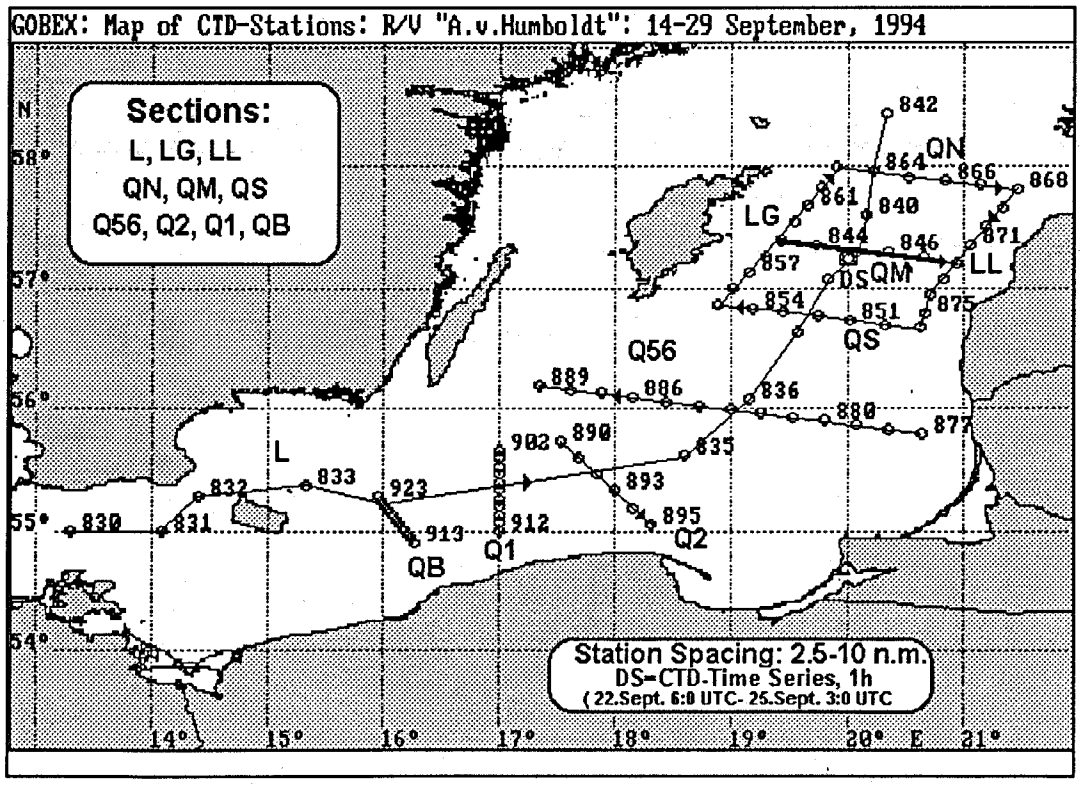

Fig.1 Station map for hydrographic measurements carried out by R/V "A. v. Humboldt" in September, 1994; the notation of transects is involved as well as the position of time series (DS) in the Gotland Deep

Inter alia, hydrographic measurements were carried out using the CTD probe OM-87 of the IOW along the GOBEX-standard section connecting the Baltic Year (BY) station BY13B in the West (Gotland) with BY18B in the East (Latvia); bold line in Fig. 1. The central station of this transect is represented by station BY15A above the Gotland Deep. Here, we may ask how representative is the course of any isoline along such a hydrographic transect? For this short note, we selected plots of the potential density because the temperature and salinity have, at least sometimes, an opposite influence on local stratification conditions. Furthermore the stratification selects the spatial scale of baroclinic motions, which is usually expressed by the internal radius of deformation in the order of several kilometres. Spatial differences in the stratification generate internal pressure gradients, which are associated with baroclinic motions. For the deep circulation in the Gotland Basin, the internal pressure gradients and their response on irregularities in the bottom topography should play an important role. The vertical distribution of the potential density, which is calculated by the potential temperature with the reference level at the sea surface (0 Bar), is plotted in Fig. 2.

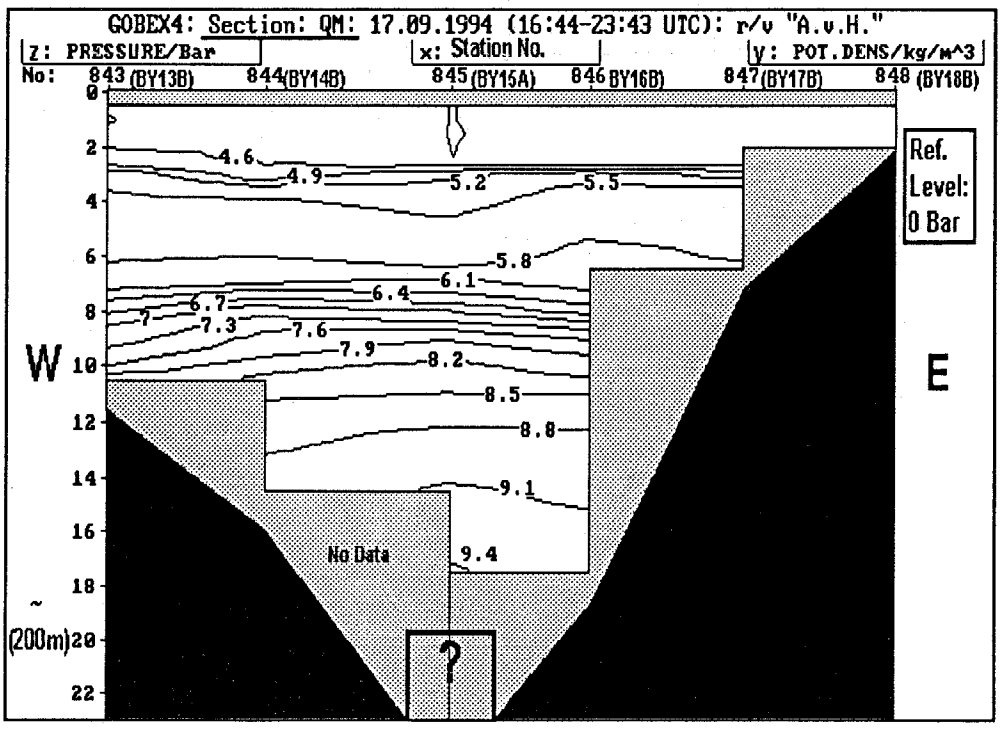

Fig. 2 Potential density structures along the transect (QM) shown in Fig. 1

The actual thermocline produces a pycnocline at the pressure level of about 3 Bar (≈ 30 m depth) while the "permanent" halocline is responsible for the main pycnocline between 7 Bar (≈ 70 m) and 10 Bar (≈ 100 m).

In a previous note, we discussed interannual changes in temperature, salinity, and chemical potential at this position. However, "short time" fluctuations, within the time-scale of hours to several days, are an unsolved problem not only with respect to the interpretation of hydrographic sections (aliasing), but also for the understanding of circulation patterns in the deep basin.

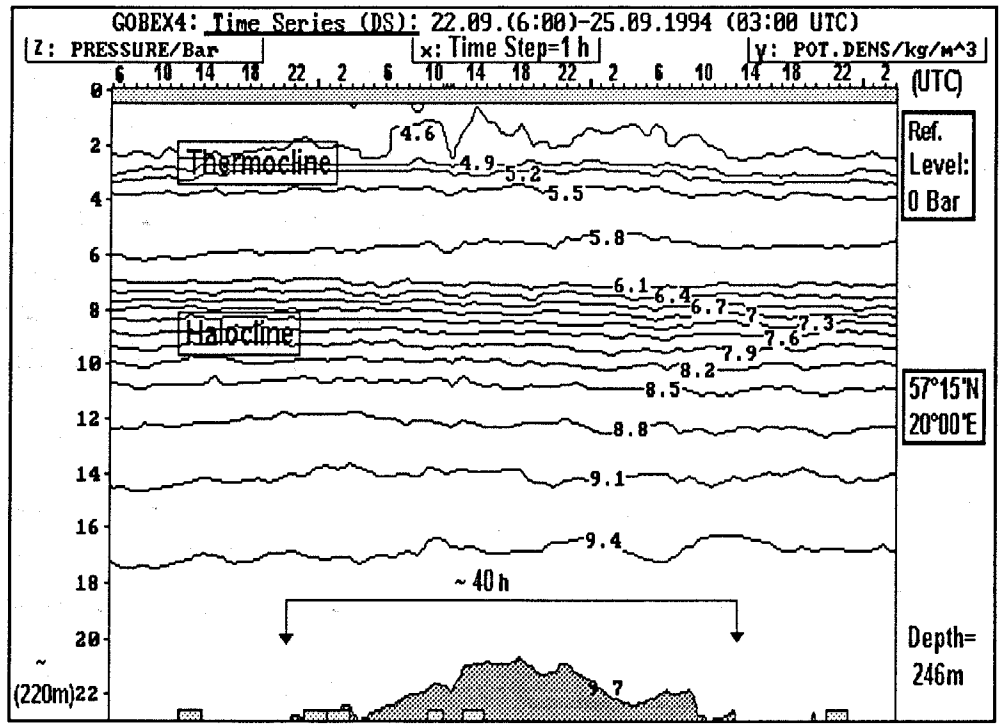

Fig.3 Plotted time series of the potential density (PD) with the time step Dt = 1 h at the position of station (DS) above the Gotland Deep; the intrusion of denser water (PD > 9,7 kg/m³) occurs in layers deeper than 200 m for about 40 hours.

In order to overcome this shortcoming, we measured 70 vertical CTD profiles with time steps of one hour (22 [06:00 UTC]- 25 September [03:00 UTC], 1994) at the position DS (57°15'N, 20°00'E). Due to this sampling strategy, only variations with periods longer than two hours are resolved. The station position (DS) lies in the immediate vicinity of

station BY15A. Using our GPS navigation, the exact position was the starting point for each profile.

The resulting time series are plotted for the potential density in Fig. 3. Obviously, wind-mixing and convection processes generate relative strong fluctuations within the upper 20 m-layer. In deeper layers the straight course of isolines justifies the interpretation of vertical plots along "quasi-synoptic" sections, especially with respect to the "core-depth" of pycnoclines enclosed. On the other hand, we note an increasing vertical displacement of isopycnals in layers located beneath the main pycnocline. As expected, baroclinic eddy-like features and/or internal waves should be more relevant for the deep basin circulation than in the subsurface layer where the wind forced motions dominate.

The most interesting result of these measurements is the intrusion of relative saline rich waters (S > 12.2 PSU) within the near bottom layer. The isopycnal surface of 9.7 kg/m^3 clearly shows a dome-like shape by its upward displacement for about 40 hours. Its relative maximum lies about 30 m above the horizon of 230 m (23 Bar). That dome-like shape suggests a cyclonic rotation sense for geostrophic currents, which are trapped in the deep basin. This event reduced the concentration of dissolved oxygen by a factor of about two down to values around 1.5 ml/l although the thermic regime was not significantly changed.

In a previous contribution of this issue, Mittelstaedt reported a counter-clockwise mean circulation with mean vector speeds between 2 and 7 cm/s from two weeks' current measurements in November 1993. Regarding the maximum scalar speeds at 5 m above the bottom, these records showed peak values between 16 and 25 cm/s. At the same positions (G1, G2, G3), averaged velocities were measured between 2 - 5 cm/s within the near bottom layer over six weeks (August-September, 1994). Again, sporadic events were recorded with peak values between 16 and 20 cm/s at levels 5 m above the sea bed. Altogether, the current meter records are still under investigation. *Here, we only wish to give a hint for the existence of temporal changes in the baroclinic mass field within a time-scale of a few days in the deepest layers of the Gotland Basin.* Of course, we can speculate about eddy-like features trapping waters from the last inflow of saline rich waters. Such phenomena may have some similarities with the "meddies" detected in the Mediterranean outflow area of the northern Atlantic. On the other hand, these observations may be caused by low frequency waves. One possible candidate could be the process of topographically trapped Rossby waves. In any case, such deep intrusions could have some impact on the temporal and spatial conditions for sedimentation and deposition.

Observation of Meso-Scale Eddy-Like Structures and Thermohaline Intrusions in the Gotland Basin after the 1993 Major Baltic Inflow

V. M. Zhurbas
P. P. Shirshov Institute of Oceanology, Russian Academy of Sciences, Moscow, Russia

V. T. Paka
Atlantic Branch of P.P.Shirshov Institute of Oceanology, Russian Academy of Sciences, Kaliningrad, Russia

Abstract

"Tow-yo" CTD measurements are analysed to examine the meso-scale and fine-scale response of mass-field properties in the Gotland Basin to the recent major Baltic inflow. A cyclonic eddy, which is undetectable at the sea surface, is found in the permanent halocline. This cyclonic feature is estimated to be strongly nonlinear and considerably contributes to the transport of salty water. The halocline is characterized by intense thermohaline intrusions. A well-defined frontal zone is associated with that intrusive region. The frontal zone propagates from the northern part of the Stolpe Channel into the direction of the Gotland Deep with a speed of about 2 cm/s. A substantial horizontal intermittency of intrusion intensity related to meso-scale eddy-like structures is observed behind this frontal zone. In context of major Baltic inflows, meso-scale eddies carrying inflowing waters and thermohaline intrusions are shown to be responsible for the deep water ventilation..

Introduction

The water exchange between the North Sea and the Baltic Sea is greatly restricted by a narrow and shallow transition area consisting of the Kattegat and the Belt Sea. Circulation and horizontal mixing of the deep water in the Baltic Sea are strictly controlled by the bottom topography. The Baltic Proper consists of a sequence of basins (Arkona-, Bornholm-, Gotland-Basin), which are separated by sills but linked by channels. Depths of both the sills and the basins increase from the transition area to the Gotland Sea, where the maximum depth is greater than 250 metres. Due to the permanent halocline, the strong density stratification prevents deep water from the vertical exchange. This mechanism supports periods of stagnation, which are, among other things, characterized by increasing phosphate and nitrate concentrations, decreasing salinity and oxygen

concentrations, and sometimes by considerable hydrogen sulphide concentrations, MATTHÄUS (1993). During a "normal" inflow the inflowing water mixes with ambient waters and becomes lighter than the old bottom water. The density of such mixture is insufficient to displace the old bottom water in deep basins of the Central Baltic. The interruption of stagnation periods and a ventilation of the deep water only occurs when strong inflows of highly saline and oxygenated water intrude from the North Sea. Such events, which are also called "Major Baltic Inflows", are typical, but relatively rare phenomena.

The meteorological precondition for the major Baltic inflows is an anomalous atmospheric circulation with southerly winds over the NE Atlantic. It causes enhanced transfer of highly saline water from the open ocean to the North European shelf , DICKSON (1973). The major inflows occur between the end of August and the end of April with a mean frequency of about one event a year, cf. MATTHÄUS and FRANCK (1992) and MATTHÄUS (1993). These events are quite irregular, and the longest period without any major event lasted almost 10 years (1983 - 1993).

The recent major inflow took place in January, 1993, attracting close attention of oceanographers from the Baltic countries; cf. DAHLIN et al. (1993), GRELOWSKI and WOJEWODZKI (1993), HÅKANSSON et al. (1993), MATTHÄUS (1993); MATTHÄUS et al. (1993); OZMIDOV (1993), and PAKA (1996). This event followed 16 years of stagnation, since some inflow events were concluded of minor importance between 1976 and 1983. Compared with all identified events in the past, the 1993 major inflow was classified as a moderate one with limited effects in the deep central Baltic basins, MATTHÄUS (1993).

The immediate meteorological cause for the 1993 major inflow was a very strong west weather situation between 6 and 25 January in the transition area. In this period, three hurricanes occurred and passed through on 14, 22, 24 January, when extreme squalls of 45, 39, and 34 m/s from 250° - 260° were recorded at the meteorological station Arkona at Rügen Island, MATTHÄUS et al. (1993). The inflow of highly saline water through the Sound across the Drogden Sill (7 m depth), and through the Great Belt across the Darss Sill (18 m depth) into the Arkona Basin started on January 6 and January 13 respectively, and finished on January 26 - 28. According to MATTHÄUS et al. (1993), further propagation of highly saline water into the Baltic Proper can be described as follows:

The inflowing water was accumulated in the Arkona Basin for a week. The 15 PSU isohaline was first lifted from 38 m depth to 10 m, and then lowered until mid-February

to the depth of 30 - 35 m. This indicates a flushing time of about 2 - 3 weeks for the Arkona Basin . The associated inflow of saline water partly mixed the surface water and then flowed back into the transition area. Another part mixed shallow water remaining in the basin. The leavings flowed through the Bornholm Channel (45 m depth at the sill) into the Bornholm Basin and replaced the old bottom water. As a result, salinity in the bottom layer increased from about 15 to 20 PSU between January and March 1993. The main body of highly saline water, which entered the Baltic Sea in January, 1993, was stored in the Bornholm Basin. The old, deep Bornholm water of lower salinity and some part of the new mixed water were lifted together above the sill depth of 60 m and overflowed the Stolpe Furrow.

Water masses with characteristic TS-properties of the Bornholm Intermediate Water were observed in the Stolpe Channel from March to May. Maximum salinity of this water changed within a week. Therefore, we may speculate that the outflow from the Bornholm Basin was rather intermittent. A turnover of highly saline water from the Bornholm Basin through the Stolpe Channel into the Eastern Gotland Basin started in the first days of March. In the beginning of April, first indications of the bottom water renewal were observed in the Gotland Deep at the Baltic Year (BY) station BY15 at the position 57°20' N, 20°00' E. At this station, salinity below 225 m increased from 11.0 PSU on March 15 to 11.7 PSU on June 4, cf. DAHLIN et al. (1993).

The scenario of salt water propagation in the Baltic Proper described above results from CTD measurements at hydrographic stations, which formed a line between the deepest locations connecting the Darss Sill and the Gotland Deep. The station spacing changed between 10 and 30 km. Such sparse spacing of stations is not sufficient to resolve involved baroclinic motion structures properly. Concerning meso-scale mass-field patterns, one can expect to discover several specific mechanisms of salt water propagation and mixing and to improve the understanding of deep water ventilation.

CTD measurements suitable to study the meso-scale variability were carried out in the Stolpe Channel and the Eastern Gotland Basin in March-April, 1993, during the cruise no. 29 of R/V "Professor Shtockman", OZMIDOV (1993). Here, we will use this data base to examine both the meso-scale and fine-scale response of motion dynamics to the recent major inflow in the largest and deepest basin of the Baltic Proper.

Data

The CTD measurements were carried out in the Stolpe Furrow and in the Eastern Gotland Basin from March 30 to April 18, 1993, just after the first observational evidence for the bottom water renewal in the Gotland Deep. All observations were taken with a Mark III NBIS-CTD profiler. To achieve high horizontal resolution, the CTD profiling was carried out using a winch-driven "tow-yo" vehicle. To prevent destruction of the probe when touching the ground, the vehicle was equipped with a 7 m long heavy chain which met the sea bed allowing the probe to keep small but safe enough distance from it, cf. PAKA (1996). Almost 2000 CTD profiles spaced apart by 300 - 500 m have been obtained from the thermocline surface to the sea bed. A map of the CTD measurements in the Eastern Gotland Basin is shown in Fig. 1. The experiment had two stages.

During the first stage, from March 30 to April 2, a detailed "tow-yo" CTD survey consisting six legs was carried out in the eastern part of the Gotland Basin. In Fig. 1, the survey area is delineated by a dashed box. During the second stage (16 to 18 April) sampling was done along both transects (A - B) and (C - D). In addition to the transects, a few separate CTD stations were made during the second stage, from the station BY15 toward the South almost along the deepest connection. These stations are also shown in Fig. 1. In this paper, the data of the longest transect, (A - B) from April 17 - 18, will be analysed in detail. Its length was 157 km comprising 411 stations. So, the mean distance between successive CTD profiles was 383 m. The (A - B) transect started in the NE periphery of the Gotland Deep (point B: 57°29' N, 20°30' E), passed to the SSW as long as (56°41' N, 19°39' E), and than deviated to the SWW, ending at point A (56°29' N, 18°52' E). In all following figures, the transect starts at point (A) and ends at point (B).

Intermediate Cyclonic Eddy

Figure 2 shows the potential density (σ_Θ) versus pressure and section-distance for the halocline layer (50 - 170 dbar) along the (A - B) transect. The most outstanding feature in Fig. 2 is a "convergence" of isopycnals inside the halocline at the distance of 48 - 55 km, which may be interpreted as a meso-scale eddy-like feature covering the whole halocline layer. In addition, there are also involved cases of local "divergences" of isopycnals, namely at distances of 116 - 129 km and 138 - 150 km. Such structures may be produced by anticyclonally rotating lenses, which are embedded in the halocline.

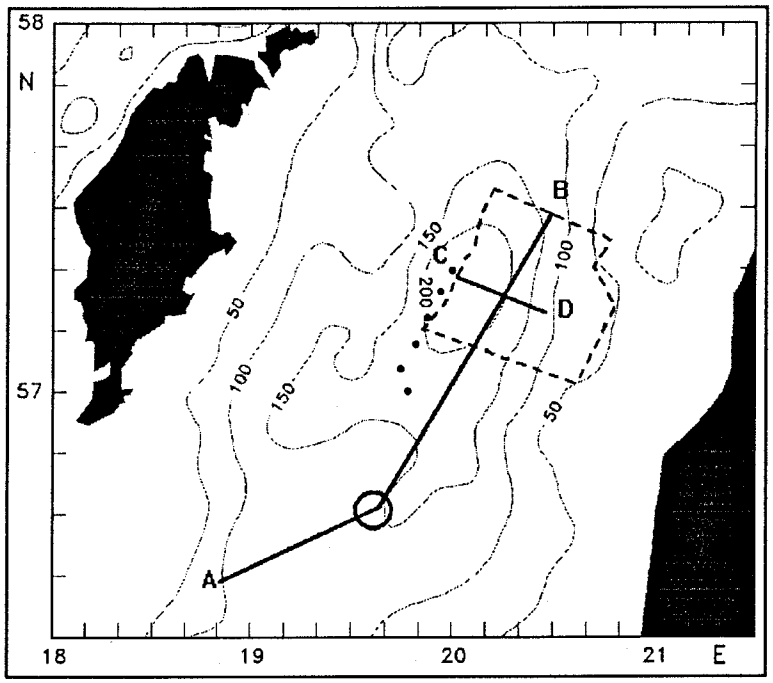

Fig. 1 The area under investigation in the Gotland Basin during March-April, 1993; the box (dashed line) with the area of the CTD survey from the first stage of the experiment (March 30 until April 2); the bold lines (A - B, C - D) describe the hydrographic transects; single dots indicate CTD stations of the second stage (April 16 - 18) of the experiment; the open circle denotes the location of the detected cyclone; the bathymetric contours are given in metres.

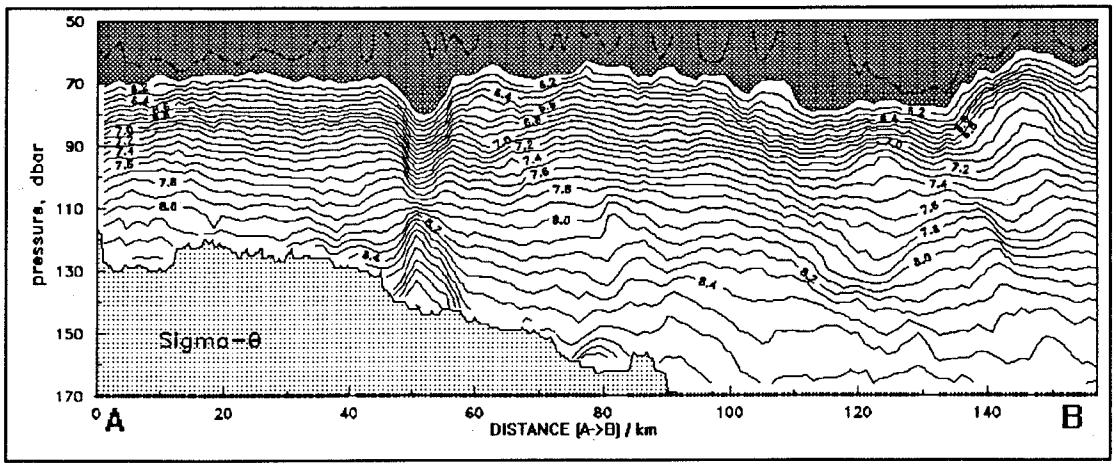

Fig. 2 Potential density (σ_θ [kg/m^3]) relative to the sea surface vs. pressure (dbar) along the section-distance (km); well mixed upper layers are hatched while the bottom topography is stippled.

To be sure that the feature detected at the distance of (48 - 55) km is really a meso-scale cyclone rather than, for example, a topographically steered tongue of intrusion, we need additional transects, which should be directed normal to (A - B). Unfortunately, we had no possibility to make such sections. Consequently, the following discussion should be considered as an "eddy hypothesis", which likely provides a self-consistent description. However, such hypothesis can stimulate further field studies planned for this area in the next future.

We shall consider dynamic properties of the hypothetical cyclone in more detail. This is a interesting exercise, because such eddies can contribute to the salt water transfer and deep water ventilation in the Baltic Sea.

$$F_g(p,x) = (\frac{1}{f}) \int_{p}^{p_o} [\frac{1}{\rho(p,x)} - \frac{1}{\rho(p,\infty)}] dp \qquad (1)$$

Using the density ρ (p, x) versus hydrostatic pressure (p) and distance (x), the empirical geostrophic flow function $F_g(p,x)$ has been computed according to (1), where ρ (p, $\propto$) is the background density versus pressure away from the cyclone and p_o= 140 dbar is the reference pressure level for no geostrophic motion.The across transect component of the geostrophic velocity (u_g) is written as the x-derivative of the flow function; $u_g = \partial F_g/\partial x$.

Fig. 3 shows the geostrophic flow function computed for a fragment of the (A - B) transect, which includes the central part of the cyclone and its northern periphery, where the pressure at the sea bed is no less than 140 dbar. This function has an intermediate minimum at p ~ 107 dbar where the core of the cyclone is located while $F_g(p,x)$ increases to a close-to-zero noise level over the halocline away from that feature. Thus, we may conclude that the cyclone is located within the halocline, being dynamically undetectable on the sea surface.

To estimate characteristics of the cyclone (its size and velocity of rotation), according to ZHURBAS et al. (1992), the empirical geostrophic flow function F_g(p = 107 dbar, x) has been approximated by an analytical function $F'_g(p,x)$, namely the Gaussian Curve, where A, x_o, R are parameters to be determined. Using the least square technique (non-linear regression), the following values were obtained:

A = -1116 m²/s, x_o= 51.15 km, R = 2.94 km.

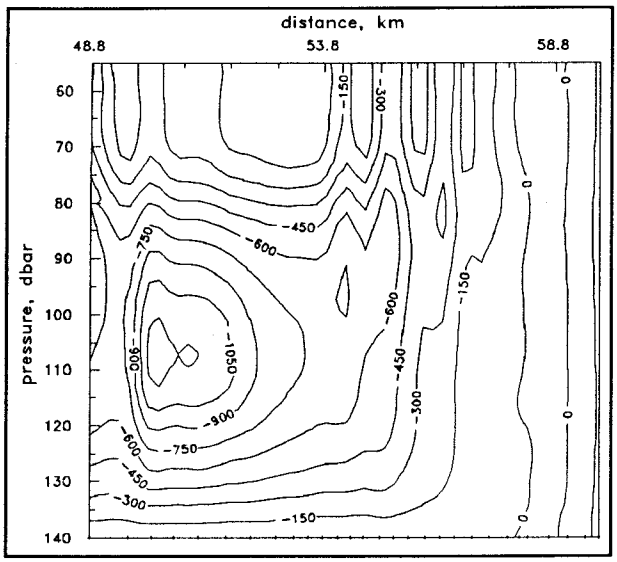

Fig. 3 Geostrophic flow function $F_g(p,x)$ vs. pressure (p) and the distance (x) cutting-out a fragment of the transect (A-B), which includes the cyclone core at about 107 dbar.

$$F_g(x) \equiv F_g(p,x)|_{p=107dbar} = A \exp - \frac{(x-x_o)^2}{2R^2} \quad (2)$$

Since only a single transect across the cyclone is available, distances between the transect and the cyclone's centre are unknown. One should estimate what kind of errors is introduced into parameters of the cyclone by this uncertainty. If the cyclonic eddy-like feature is axisymmetric and its flow function is described by the two-dimensional Gaussian Curve, we obtain equations (2.1 and 2.2) with respect to the y-axis aligned normal to the direction of the transect (x-axis).

$$F'_g(x,y) = A' \exp[- \frac{(x-x'_o)^2 - (y-y'_o)^2}{2R'^2}] \quad (2.1)$$

$$F'_g(x,y) = A' \exp - [\frac{(x-x'_o)^2 + (y-y_o)^2}{2R'^2}] \quad (2.2)$$

Here, x'_o, y_o, R', A' are "real" parameters of the flow function along the *x*-axis at the distance of $(y_1 - y_o)$ from the eddy's centre. We will come to (2) instead of (2.1) or (2.2) with following relationships between "real" and "measured" parameters:

$$x = x'_o, \qquad R = R', \qquad A = A' \exp\left[-(y_1 - y_o)^2 / (2R'^2)\right] < A'$$

Thus, having a single transect, the right value of the eddy's size (R) and underestimated values of the eddy's intensity (A) will be obtained. Otherwise, if the flow function is equal to a non-zero constant inside an axisymmetric eddy, turning into zero outside it, a single transect will give the right value of the eddy's intensity but underestimated values of its size. The first case, with a Gauss-like flow function, seems to correspond more closely to reality. Consequently, we expect that we have the right value of the cyclone's size, while the cyclone's intensity and, as a consequence, its frequency of rotation could be underestimated. According to (2), geostrophic estimates of azimuthal velocity and frequency of cyclone's rotation are

$$u_g(r) \equiv \frac{\partial F_g}{\partial r} = -\frac{Ar}{R^2}\exp-\left[\frac{r^2}{2R^2}\right], \quad \omega_g \equiv \frac{\partial u_g}{\partial r}\Big|_{r=0} = -\frac{A}{R^2} \qquad (3)$$

where $r = (x - x_o)$ is the radius of that feature. With the above values of (A) and (R), the second of the formulae (3) yields $\omega_\gamma = 1.29 * 10^{-4}\ s^{-1}$, which is comparable with the value of Coriolis frequency $f = 2\ \Omega \sin(\phi) = 1.22* 10^{-4}\ s^{-1}$. Here, $\Omega = 0.727*10^{-4}\ s^{-1}$ is the frequency of the Earth rotation and $\phi = 56.7^\circ$ is the latitude. Since (ω_g) and (f) are of the same order of magnitude, a centripetal acceleration (u^2/r) of the azimuthal velocity (u) must be taken into account. Thus, instead of a simple geostrophic balance, the cyclone can be described by the balance between the Coriolis acceleration, the baroclinic pressure gradient, and the centripetal acceleration:

$$-\left[\frac{u^2}{r}\right] = -f\,u_g + fu \qquad (4)$$

By solving the quadratic equation (4) for u, we obtain

$$u(r) = -(\frac{f\,r}{2})[1-(1+\frac{4\,u_g}{f\,r})^{1/2}]$$

(5).

Equation (5) yields the following expression for the frequency of eddy rotation:

$$\omega \equiv \frac{\partial u}{\partial r}\Big|_{r=0} = -\frac{f}{2}[1-(1+\frac{4\ \omega_g}{f})^{1/2}]$$

(6)

By substituting the above values of (ω_ε) and (f) into (6), we calculate $\omega = 0.785*10^{-4}$ s^{-1} = 1.29*(f/2). Due to the centripetal acceleration, the frequency of the rotation (ω) decreases by a factor of 1.64 in comparison to the value, which results from the simple geostrophic balance. Nevertheless, it remains greater than (f/2), the upper limit for a frequency of anticyclonic rotation. Our observations confirm the well known statement that cyclones are more energetic than anticyclones in both the atmosphere and the ocean. As for the maximum azimuthal velocity (u_{max}) in our cyclone, the geostrophic value, $u_{g,max}$= 23 cm/s at r = 2,94 km, decreases to the value of u_{max} = 16 cm/s at r = 3.33 km when the centripetal acceleration is taken into account. It should be noted that, having been calculated from single transect data, the above values of (ω) and (u_{max}) probably lie on the low side.

The thermohaline structure of the cyclone is shown in Fig. 4. Isotherms are plotted on isopycnal surfaces vs. the distance from point (A). The upper layer of the halocline coincides with values $\sigma_\otimes < 6{,}4$ kg/m³. Here, the isopycnic temperature is nearly constant. In contrast, in deeper layers covering the density range ($6.4 < \sigma_\otimes < 8.4$) kg/m³, the temperature is (0.2 - 0.3) K lower in the centre of this cyclone than in its surroundings. However, in the very deep layer, which is adjusted to the sea bed, both density and salinity are greater inside the cyclone than their respective peak values in ambient waters. This cyclonic feature traps heterogeneous water in intermediate and deep layers of the halocline, while it is reduced to a solitone-wave-like feature in the isopycnals, which is characzerized by not having thermohaline anomalies in the upper layers.

To illustrate the transfer of salty water by the cyclone, Fig. 5 displays the same fragment of the (A - B) transect with respect to salinity. Maximum salinity in the cyclone is greater than 11.5 PSU. It should be recalled that the maximum salinity in the bottom layer of the Gotland Deep was 11.0 PSU in the middle of March, 1993, and increased to 11.7 PSU by June due to the Major Baltic Inflow in January 1993, DAHLIN et al. (1993). Thus, the cyclone is proved to transfer salty water originating from the recent major inflow, so contributing to the deep water renewal in the Eastern Gotland Basin.

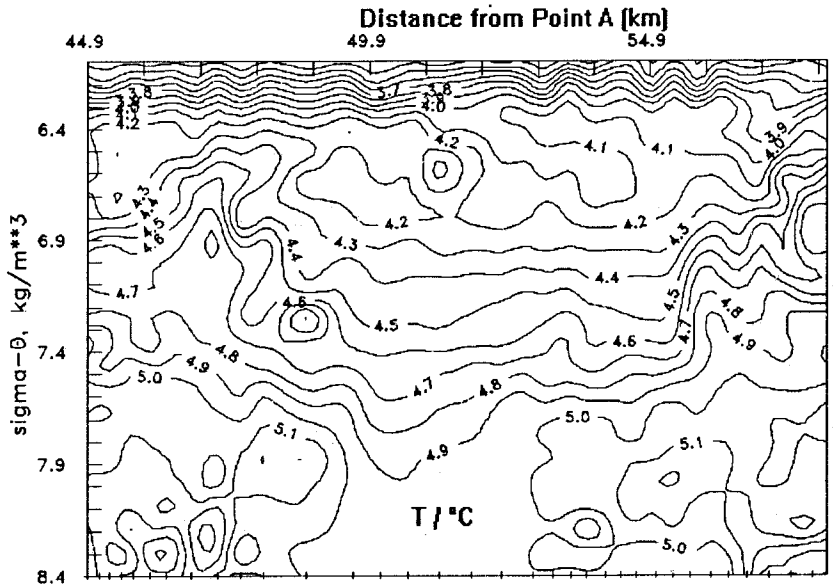

Fig. 4 Isopycnic distribution of the temperature (T/°C)

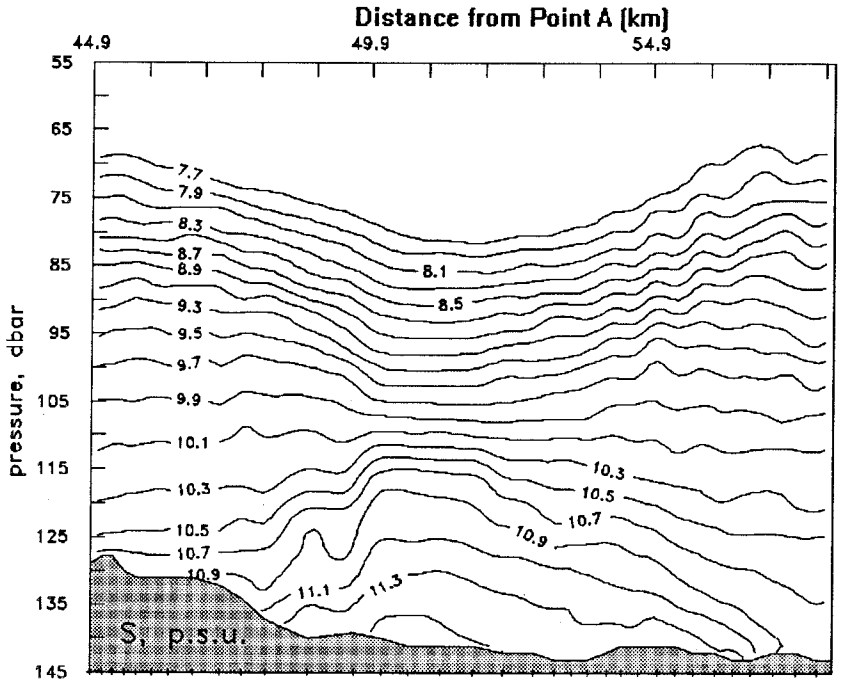

Fig. 5 Salinity (S/PSU) section trough the cyclonic feature

The TS-diagram of the cyclone centre is shown by a dashed line in Fig. 6b. Its curve lies between those from the Gotland Deep and the Stolpe Channel. However, pronounced intrusions only occur in measurements, which were carried out between the cyclone centre and the Gotland Deep. Therefore, the cyclone contains the least transformed Bornholm water, which overflowed into the Gotland Basin after the recent major inflow.

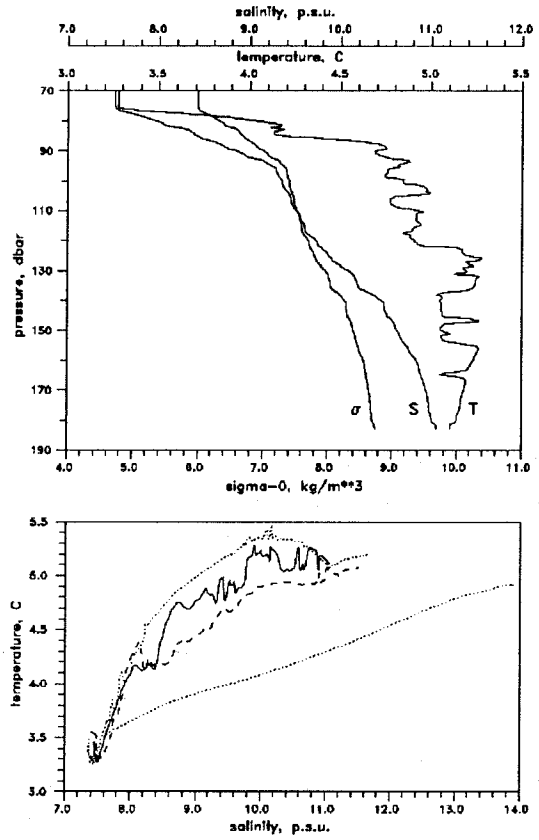

Fig. 6 a: Vertical profiles of temperature (T), salinity (S), and potential density ($\sigma_\otimes$) demonstrating thermal intrusions in the halocline at the distance of 125.9 kmfrom the point (A).

b: TS-diagrams from the profiles shown in Fig. 6a (solid), from the Gotland Deep (station BY15, upper dotted), from the Stolpe Channel (lower dotted), and from the cyclonic eddy-like feature (dashed).

Thermohaline Intrusions

The thermohaline fine-structure at the (A - B) and (C - D) transects was characterized by abundant intrusions. An example of vertical profile defines thermal intrusions from the (A - B) transect in Fig. 6a. Such intrusions are clearly visible due to vertical inversions of the temperature (T) with a magnitude of up to (0.2 - 0.3) K. There are no similar inversions in the corresponding profiles of S(p) and $\sigma_\otimes$(p). This fact suggests that the vertical density profile is mainly determined by the salinity profile and related intrusion-anomalies in (T) do not affect the resulting stratification drastically. Here, the mean

density ratio, $<R_\rho> = (\alpha\partial<T>/\partial z)/(\beta\partial<S>/\partial z)$ yields $|<R_\rho>| < 0.04$. Mean values are given with brackets while the coefficient of thermal expansion is $\alpha = -(1/\rho_o)\partial\rho/\partial T)$ and that of the haline contraction is $\beta = (1/\rho_o)\partial\rho/\partial S$. The depth is given by (z) while $\rho_o = 10^3$ kg/m^3 is the reference water density.

To examine the origin of intrusions, one can use TS-analysis. For that example shown in Fig. 6a, Fig. 6b indicates the water properties by a TS-plot (solid line) as well as those from stations sampled in the central part of the Gotland Deep (station BY15, upper dotted line), the Stolpe Channel (lower dotted line), and the cyclonic eddy-like feature (dashed line). In Fig. 6b, the isopycnals are omitted because they are almost indistinguishable from vertical lines. The TS-diagram with well defined thermal intrusions (dashed plot) lies between curves, which result from the station BY15 (upper dotted) and from the Stolpe Furrow (lower dotted). Such a configuration confirms the suggestion, that the origin of the thermal intrusions should be related to the spreading of Bornholm Water into the Eastern Gotland Basin. Probably, this was triggered by the recent Major Baltic Inflow which is described in the literature.

The same origin of intrusions is confirmed in the spatial and temporal variability of the intrusion intensity (J). A detailed "tow-yo" CTD survey, which was carried out in the Gotland Deep during the first stage of our experiment, did not display any considerable intrusions. A fortnight later, during the second stage of the experiment, many intense intrusions could be detected within intermediate layers of the south-eastern part of the Gotland Basin as far as 57°18′ N, being limited to the North and West by deep waters without any indications of similar intrusions. We may only speculate that, thereafter, this internal domain of thermal intrusions propagated northward following the topographic slope along the eastern Gotland Basin and advancing more than 12 nautical miles a fortnight. These values yield an averaged travelling velocity of, at least, 2 cm/s.

The propagation of the intrusion domain is front-like in character. To illustrate it, a sequence of temperature profiles from the (A - B) transect between 57°10′ N and 57°20′ N is shown in the upper panel of Fig. 7. Despite the 3-km wide gap in CTD profiling, a sharp front of intrusive layering is clearly visible. When crossing the front, intrusions do not appear in the whole water column. They occur in thinner sublayers with increasing thickness when observed from the outside into the centre of the intrusion domain.

$$J = \sum_{i=1}^{n} \frac{\Delta T_i}{h_i} \qquad [\frac{^{\circ}C}{m}]$$

(7)

The intrusion intensity (J) for a layer between chosen isopycnals is defined as the total inversion temperature difference (ΔT_i) in the i-th sublayer divided by its thickness (h_i) and (n) is the number of sublayers in the entire intrusion layer of thickness (h). Two layers have been selected for such an analysis. The upper layer is between isopycnals of 7.1 - 8.1 kg/m³, and the lower layer is between isopycnals of 8.1 - 8.6 kg/m³. The choice of layers was determined by the following: First, both layers are characterized by well defined intrusions in both (A - B) and (C - D) transects. Second, the mean vertical gradient of temperature in each of the layers does not change sign: In the upper layer the mean temperature increases with the depth, while it decreases in the lower layer with depth. Third, the total water depth is sufficient to identify an upper layer along the whole (A - B) transect. In contrast, at the southern end of the (A - B) transect, the potential density near the sea bed is less than 8.6 kg/m³, and is impossible to allocate the lower layer.

The problem of revealing relationships between the intensity of intrusions and local meso-scale dynamics and kinematic parameters in oceanic frontal zones (parameterization of interleaving) was first stated by ZHURBAS et al. (1988). With respect to the latter problem, two parameters were chosen, namely the parameters of termoclinicity $(T_h)_\rho$ (the mean isopycnic gradient of temperature), and baroclinicity $\Delta = \gamma_\rho N^2/f$, where ($\gamma_\rho$, N, f) are the mean slope of isopycnals to isobars, buoyancy frequency and Coriolis frequency, respectively. The baroclinicity is proportional to the vertical shear in geostrophic flow, $(u_g)_z = \gamma_\rho N^2/f = N\Delta$, and related to the geostrophic Richardson number $Ri_g = N^2/(u_g)_z^2$ as $\Delta = (Ri_g)^{-1/2}$. Using data of CTD measurements in the Gulf Stream, (J) was found to increase with $(T_h)_\rho$ but decrease with (Δ). The decrease of (J) with (Δ) was interpreted on the assumption that double-diffusive intrusions are suppressed (or destroyed) by shear instability in a stratified flow. However, different conditions are reported from similar measurements carried out in the Subarctic Frontal Zone of the West Pacific Ocean by KUZMINA et al. (1994). Here, a new regime could be detected with both increasing (J) and increasing (Δ). According to the model of KUZMINA and RODIONOV (1992), this last regime was explained as a result of generation of intrusions due to the baroclinic instability. In addition to parameters of thermoclinicity and baroclinicity, we shall also

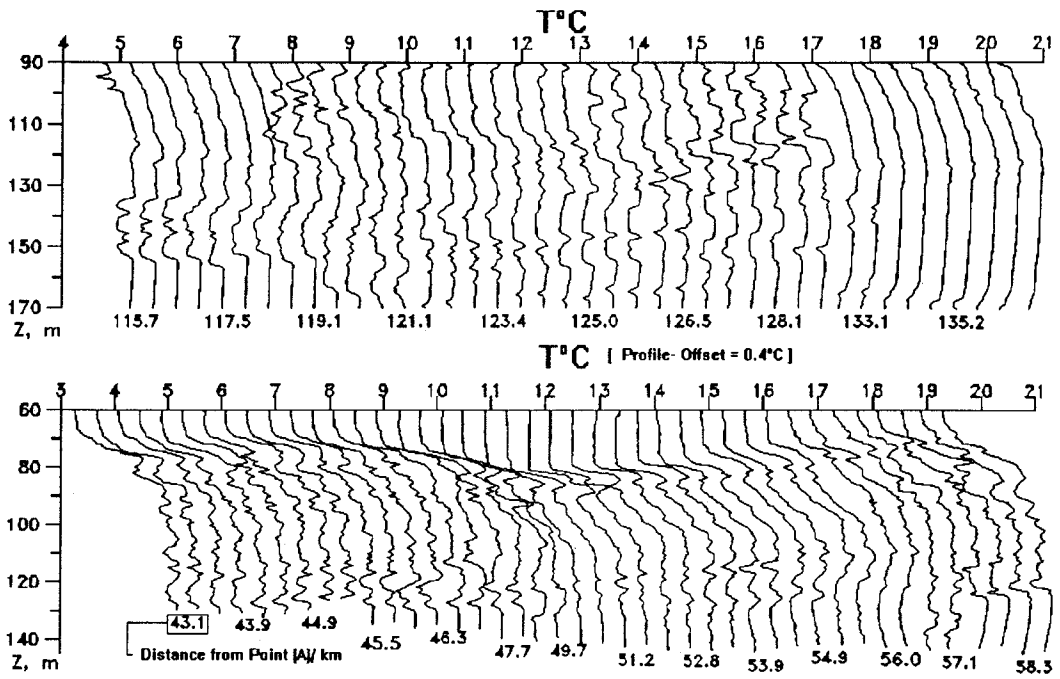

Fig. 7 Sequence of vertical profiles of the temperature (T°C) from fragments of the (A-B) transect between 57°10′ N and 57°20′ N, which includes the lateral front-like boundary of the intrusive region (upper panel), and the cyclonic eddy-like feature (lower panel) between 56°39' N and 56°44' N.

(Numbers under the profiles provide distances (km) from the point (A); the temperature scale is correct on the very left side; successive profiles involve the offset of 0.4 K .)

In the lower panel of Fig. 7, there is another sequence of temperature profiles from the (A - B) transect, between 56°39′ N and 56°44′ N, which includes the cyclonic eddy. Intrusions in the cyclone core are substantially suppressed with respect to those of the surroundings. Horizontal coherence of intrusions, is of the order of 1 km (Fig. 7). It is also evident from Fig. 7, that the intrusion intensity behind the front is horizontally intermittent with a typical scale of the order of 10 km. Probably, this intermittency is associated with the spatial variability of some meso-scale hydrological parameters. To evaluate qualitatively the development of intrusions by temperature profiles, a simple measure of intrusion intensity, introduced by ZHURBAS et al. (1987), is used.

consider the planetary component of the potential vorticity $V = f(\rho_z/\rho_o)$, where (ρ_z) is the mean vertical gradient of density while (ρ_o) is the constant reference density. The reason for introducing this parameter is as follows: If intrusions move as the ideal fluid, the potential vorticity, defined as

$$V = (\omega_z + f)\frac{\rho_z}{\rho_o} \tag{8}$$

where (ω_z) is the vertical component of relative vorticity and should be constant for material particles. Furthermore, if we suppose that $|\omega_z/f| << 1$, the planetary component of potential vorticity (V), will be unchanged, too. Of course, the intrusive motion is hardly described by the ideal fluid theory, and our considerations are rather arbitrary. However, they suggest that intrusions do move preferably in the direction of minimum changes in (V), and sites of extreme values of (V) are unfavourable for intrusive layering. Since (f) is near-constant for meso-scales, the conservation of (V) means conservation of (ρ_z).

Figure 8 shows the intensity of intrusions (J), mean values of temperature (T) and pressure (P), as well as the potential vorticity (V) for upper (solid line) and lower layers (dotted line) versus the distance along the (A - B) transect. The change in (J) with the distance exhibits well-defined intermittency. There is a front of intrusive layering at the distance of 130 - 133 km, and intrusions are practically absent North of the front in both layers. This is the same frontal zone as depicted in the upper panel of Fig. 7.

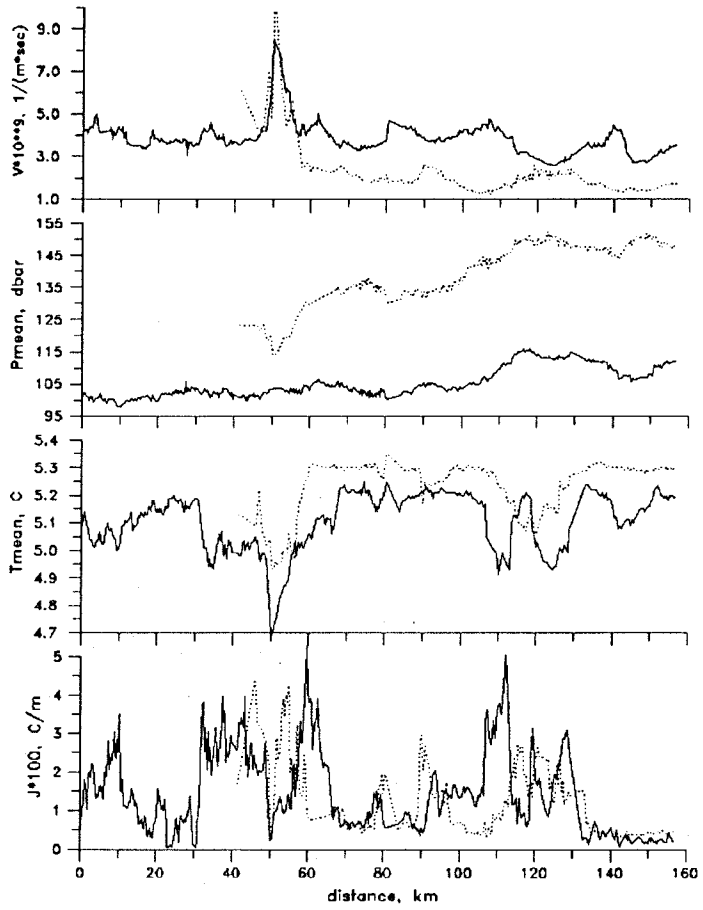

Fig. 8 Intrusion intensity (J), mean values of temperature (Tmean), mean pressure (Pmean), and planetary component of potential vorticity (V), in the upper (solid) and lower (dotted) isopycnal layers versus the distance along the (A - B) transect.

Comparing changes of (J) in upper and lower layers one can visually identify several coherent structures of high intrusion intensity in both layers. However, these structures are transformed to such extent that the correlation coefficient for series of (J) for the upper and lower layers takes rather the low value of 0.26. As for relations between the intensity of intrusions and selected meso-scale parameters, Fig. 8 clearly reveals only two features. First, (J) is low for (T_{mean}) over some limit, namely for $T_{mean} > 5.10°C$ in the upper layer, and for $T_{mean} > 5.25°C$ in the lower layer. Second, at the distance of about 50 km there is a sharp absolute maximum of (V) in both layers which corresponds to the absolute minimum of (T_{mean}) and low values of (J). It is worth mention that the distance of 50 km is just the location of the above described cyclone.

To analyse relations between the intrusion intensity and meso-scale parameters in more

detail, diagrams of (T_{mean} , J), ($|\gamma_\rho|$, J), (V, J) have been plotted for both layers in Fig. 9. When estimating the slope of isopycnals to isobars, $\gamma_\rho = (dP_{mean}/dx)/(g\rho_o)$, to eliminate some noise in (P_{mean}) due to errors of hydrostatic pressure measurements, the series of P_{mean} (x) were passed through low-pass filter with a smoothing scale of about 2.5 km, and the derivative (dP_{mean}/dx) was approximated by finite differences with the same scale. None of the diagrams shows a well defined relation between the intrusion intensity and other meso-scale parameters. Nevertheless, despite of the scatter of points, some regular trends do exist on (T_{mean} , J) and (V, J) diagrams. Namely, high values of (J) are concentrated at moderate values of (T_{mean}) and (V), while the vicinities of peak values of (T_{mean}) and (V) are characterized by low values of (J) in both layers. The occurrence of high values of (J) with medium values of (T_{mean}) is consistent with the general notion of layered intrusions: Extreme values of (T_{mean}) correspond to the transformed Bornholm and Gotland Water, while more moderate values result from an intrusive stirring of both water-masses. The similar scatter diagram between (J) and (V) suggests an interesting new aspect. Of course, being poorly defined, this statistical relationship has to be considered only as a preliminary one, and more data is needed to prove it in the next future. To explain the V-dependence of (J), we shall re-examine the spatial variability of the potential density in the (A-B) transect shown in Fig. 2.

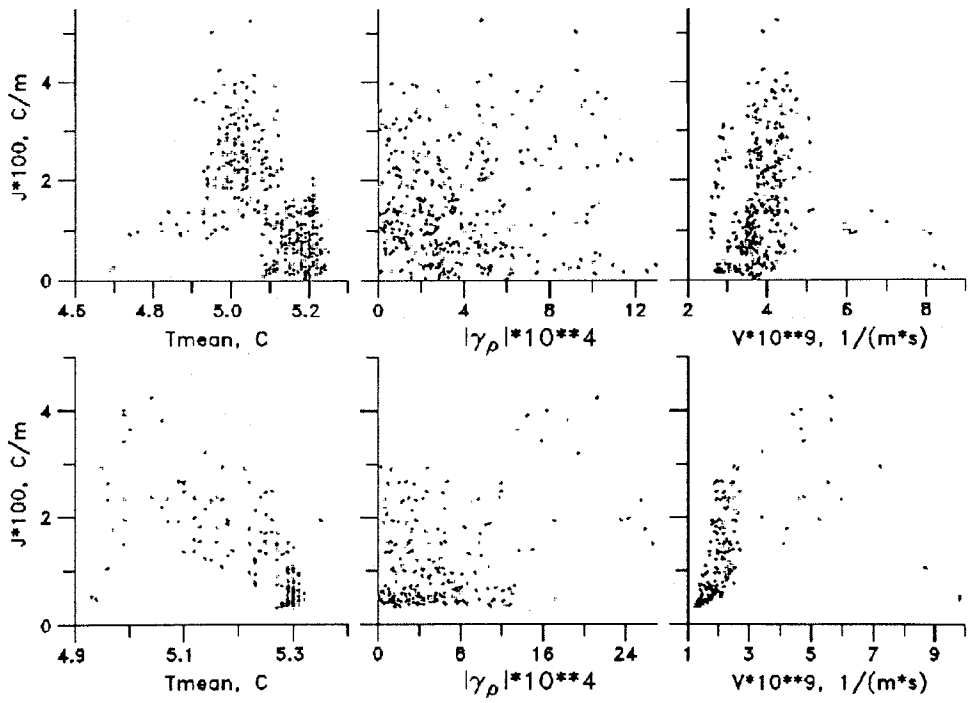

Fig. 9 Scatter diagrams of (T_{mean} , J), ($|\gamma_\rho|$, J), and (V, J) for the upper (upper panel) and lower layers (lower panel) of the (A - B) transect.

Meso-scale eddy-like structures correspond to extrema in (V): Generally, (V) indicates a maximum in cyclones but a minimum in anticyclones. When comparing Figs. 2 and 8 (lowest panel) one can conclude that a core of each eddy is characterized by low intrusion intensity, no matter whether it is the cyclone or one of the anticyclones.

Observed V-dependence of (J) can be explained qualitatively, assuming that the inflowing water is mainly transferred by meso-scale eddies-cyclones and/or anticyclones. In the eddies' cores, which are filled up with the least transformed inflowing water, (V) is extremal, preventing the development of intrusions. The intensity of intrusions is enhanced in areas, which are 10 - 20 km wide. These zones are observed in the vicinity of eddy-like features. This suggests that intrusions are detached from them and produce an exchange between eddies and their surroundings. In this way one can explain several main features, which are associated with changes in the intrusion intensity along the (A - B) transect. For instance, peak values of (J) occur in the zone between distances of (30 - 40) km and (60 - 65) km with a relative minimum at the distance of 50 km. This minimum zone coincides with the location of the cyclonic eddy. A sequence of relative maxima and minima can be detected between the section distance of 90 km and 135 km. This is the region of influence of several anticyclonic eddies. The above pattern of spatial variability of intrusion intensity in the cyclone or in one of the anticyclones, which could be observed in the Baltic halocline, is common for oceanic meso-scale eddies, whether they are Mediterranean Salt Lenses in the North Atlantic Ocean, ARMI et al. (1989), or rings in the Subarctic Frontal Zone of the western Pacific Ocean, ZHURBAS and SAGDIEV (1992).

Summary

CTD profiling of high horizontal resolution, which had been carried out in March-April, 1993, in the Eastern Gotland Basin, allowed the examination of the meso-scale and fine-scale response of largest and deepest basins of the Baltic Proper to the recent major inflow of the salty North Sea Water.

The most remarkable feature is a strongly nonlinear cyclonic eddy, undetectable on the sea surface, which has been revealed in the halocline. The cyclone is proved to transfer salty water originating from the recent Baltic inflow. The cyclone is likely to be generated by a non-stationary, pulsed supply of the Bornholm Water into the Gotland Basin, and subsequent geostrophic adjustment of the inflowing portion of water, in which the initial density stratification is stronger than that of the surroundings. In contrast to anticyclonic lenses that have been observed earlier during the stagnation period in the Gotland Deep

by LIPS et al. (1992), our cyclonic eddy-like feature seems to be an interesting finding.

A profuse intrusive layering with numerous temperature inversions has been revealed in the permanent halocline. This feature is a familiar one, but the important findings are:

1) A well-defined frontal zone separated the intrusive region from ambient waters and propagated north from the Stolpe Channel into the direction of the Gotland Deep with about 2 cm/s or more.

2) There was a spatial intermittency of intrusion intensity behind the frontal zone.

To explain this intermittency, relations between the intrusion intensity and meso-scale dynamics and kinematic parameters have been analysed. A preliminary (linear) dependence of the intrusion intensity upon mean potential vorticity for isopycnal layers under consideration could be detected by simple scatter diagrams. This relationship implies some linkage between intrusions and meso-scale eddies, which transport salty water after the inflow.

The frontal zone of intrusive layering arrived at the Gotland Deep (57°18′ N) on April 17, or two-three weeks after the first indications of the bottom water renewal had been recorded. We assume that there are, at least, two mechanisms of deep water ventilation caused by Major Baltic Inflows. In the case of gradual supply of salty waters, they propagate along the sloping sea bed as a near-bottom gravitational current, filling up the deepest layer of the Gotland Basin. Salinity of these new waters is greater than 11 PSU, and they are clearly seen on the TS-curve of station BY15 (Fig. 6b) due to a sharp minimum of temperature at 11 PSU. The inflowing dense bottom water is responsible for the renewal of the deepest layer of the basin, presumably below 200 m in the case of the recent major inflow. Meanwhile, the water column up to the depth of 100 m has been ventilated, as the oxygen concentration increased considerably in the whole layer by June, 1993, cf. DAHLIN et al. (1993). Thus, another mechanism of deep water ventilation must to exist. We assume that these are meso-scale eddies, generated in the halocline in the case of time-intermitted supply of salty water. There is some observational evidence that such eddy-like features are laterally eroded by intrusions, ventilating the upper layer of stagnant water.

Acknowledgments

This study was partly funded by Grants No 95-05-14342 and 95-05-15440a from the Russian Foundation for Basic Research and by the INTAS Grant 93-0525.

References

ARMI, L., D. HERBERT N. OAKEY, J. PRICE, P. RICHARDSON, T. ROSSBY, B. RUDDICK, 1989: Two years in the life of a Mediterranean Salt Lens. J. Phys. Oceanogr., **19**, 354 - 370.

DAHLIN, H., S. FONSELIUS, B. SJÖBERG, 1993: The changes of the hydrographic conditions in the Baltic Proper due to inflow to the Baltic Sea. ICES Statutory Meeting 1993, C.M.1993/C:58, Session V.

DICKSON, R. R., 1973: The prediction of major Baltic inflows. Dt. Hydrogr. Z., **26**, 97 - 105.

GRELOWSKI, A., T. WOJEWÓDZKI, 1993: Distribution of highly saline waters observed in April 1993 - after the inflow into the southern Baltic. ICES Statutory Meeting 1993, C.M.1993/C:28, Sess.V.

HÅKANSSON, B. G., B. BROMAN, H. DAHLIN, 1993: The flow of the water and salt in the Sound during the Baltic major inflow event. ICES Statutory Meeting 1993, C.M. 1993/C:57, Sess.V.

KUZMINA, N. P., V. M. ZHURBAS, A. M. SAGDIEV, 1994: Dependence of fine-structure intensity upon mean hydrological parameters at the Subarctic Frontal Zone of the Pacific. Oceanology, **34**, 201 - 205.

KUZMINA, N. P., V. P. RODIONOV, 1992: About the influence of baroclinicity upon generation of thermohaline intrusions in frontal zones of the ocean. Izvestiya Akad. Nauk SSSR, Atmospheric and Oceanic Physics, **28**, 1077 - 1088.

LIPS, U., T. KÕUTS, YU. ELKEN, 1992: On winter-time evolution of stratification, meso- and small-scale structures in the Gotland Deep during enhanced stagnation. 18th Conference of the Baltic Oceanographers, St. Petersburg, Russia, 23 - 27 November,

1992, Proceedings, Vol. 2, 39.

MATTHÄUS, W., 1993: Major inflows of highly saline water into the Baltic sea - a review. ICES Statutory Meeting 1993, C.M.1993/C:52, Sess.V.

MATTHÄUS, W., H. FRANCK, 1992: Characteristics of major Baltic inflows - a statistical analysis. Cont. Shelf Res., **12**, 1375 - 1400.

MATTHÄUS, W., H. U. LASS, R. TIESEL, 1993: The major Baltic inflow in January 1993. ICES Statutory Meeting 1993, C.M.1993/C:51, Sess.V.

OZMIDOV, R. V., 1993: Peculiarities of mixing processes in the Baltic Sea. (29th cruise of R/V Professor Shtokman). Oceanology, **33**, 788 - 791.

PAKA, V. T., 1996: Thermohaline structure in the Stolpe Furrow of the Baltic Sea in the spring 1993. Oceanology, in press.

ZHURBAS, V. M., N. P. KUZMINA, I. D. LOZOVATSKII, 1988: The role of baroclinicity in intrusive layering in the ocean. Oceanology (Engl. Ed.), **28**, 34 - 36.

ZHURBAS, V. M., T. KÔUTS, J. J. LAANEMETS, U. K. LIPS, A. M. SAGDIEV, YU. ELKEN, 1992: Spatial distribution of fine-structure intensity in a Mediterranean salt lens. Oceanology (Engl. Ed.), **32**, 273 - 278.

ZHURBAS, V. M., A. M. SAGDIEV, 1992: Fine-structure of the Subarctic Frontal Zone in the Western Pacific. In: Data of Oceanological Studies, **4**. Structure of hydrophysical fields in the Subarctic Frontal Zone of the Pacific. Catalogue, P. P. Shirshov Inst. Oceanol., Moscow, 22 - 24.

Appendix

Concerning a cyclonic feature, which was detected in superficial layers of the southern Gotland Basin, our interpretation of measurements is not very convincing due to the sparse data base. Only one hydrographic transect was available intersecting that phenomenon. After this paper had been submitted to the editorial board, we analyzed some additional data and got further evidence for the cyclone and associated anomalies in the meso-scale mass-field.

Hydrographic data result from measurements carried out by R/V 'Professor Shtockman' during the same cruise. A station map is shown in Fig. A1. Bold dots (1 - 10) indicate CTD stations with a station spacing of 15 n.m.. The stations form the transect, which nearly follows the line of deepest water depths between the Stolpe Channel and the Gotland Deep. We obtained data from two stages. The first one started 31 March and ended 5 April, 1993, while the second one repeated the samplings during 15 - 16 April, 1993. For comparison, this map also indicates the (A - B) transect shown in Fig. 1 of the previous paper with the location of that eddy-like feature (open circle).

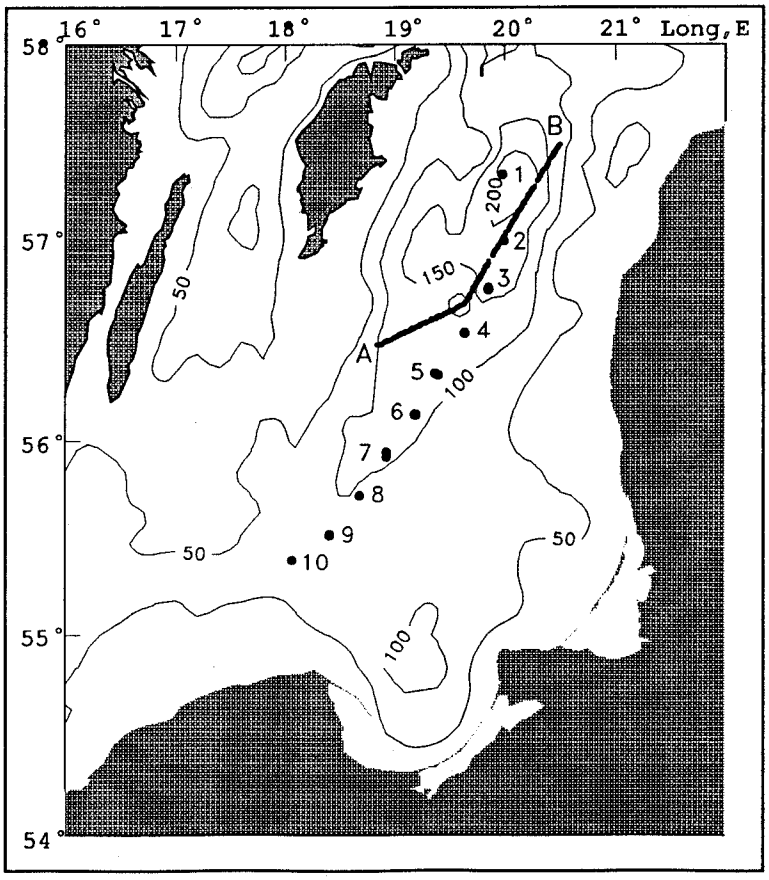

Fig. A1
Station map of supplementary measurements carried out in the Gotland Basin (cruise no. 29 of R/V 'Professor Shtockman') during March - April 1993.

Vertical profiles of salinity are plotted from selected stations in Fig. A2. To avoid clustering of resulting profiles, only data of some stations are considered. Profile 10 results from the first stage, the profiles 1 and 5 result from both stages while all other profiles are based on measurements of the second stage. Corresponding T-S diagrams are drawn in Fig. A3. Both plots suggest that the inflowing salty water occupied -more or less- the bottom layer at all stations shown in Fig.A1, except station no. 7. As it was mentioned above, the salinity of the near-bottom layer was lower than 11 PSU in the Gotland Basin by the middle of March, 1993. Thereafter the inflow of saline water masses started during January 1993.

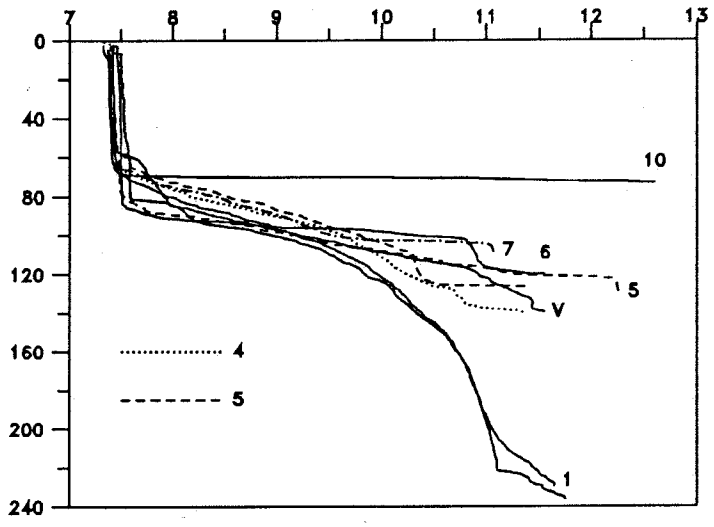

Fig. A2 Vertical profiles (dbar) of salinity (PSU) from selected stations following the deepest line in water depths as shown in Fig. A1; V denotes the 'eddy-profile' obtained at transect (A - B) during the first stage; stations no. 4 and 5 lie in the vicinity (second stage)

The station no.1 locates in the central part of the Gotland Deep and its position coincides with the well-known Baltic Year Station BY15A. Here, the renewed water has been observed since March 31. The deep/ saline inflow water (S = 11.74 PSU) was vertically separated from the fresher/old water by a strong salinity (density) gradient centred at the pressure level of about 220 dbar. By April 16, the halocline indicated an upward displacement of about 20 m to the pressure level of 200 dbar. Mixing processes vertically smoothed associated gradients and the peak value of salinity decreased by about 0.1 PSU.

In the transition area between the Stolpe Channel and the Gotland Basin (station no. 10), the salinity was greater than 12.5 PSU within the near-bottom layer. The T-S plots, which result from both 'border stations' (no. 10, Stolpe Channel's transition area and no. 1, Gotland Deep), envelop all other curves. Along the line of deepest water depths, the modification of T-S curves widely varied in between the stations as well as between both observational stages.

For example, the T-S curves of stations 5 and 6 (second stage) were much closer to that of the station no. 10 than those of adjacent stations 4 and 7. In addition, the maximum salinity increased from 11.38 PSU (April 5) to 12.26 PSU (April 15) at the station no. 5.

We like to conclude that the spreading of salty water into the Gotland Basin was highly irregular not only in space but also in time. Consequently, vertical and lateral density gradients were locally established/ destroyed and subjected to considerable meso-scale variations in the mass-field.

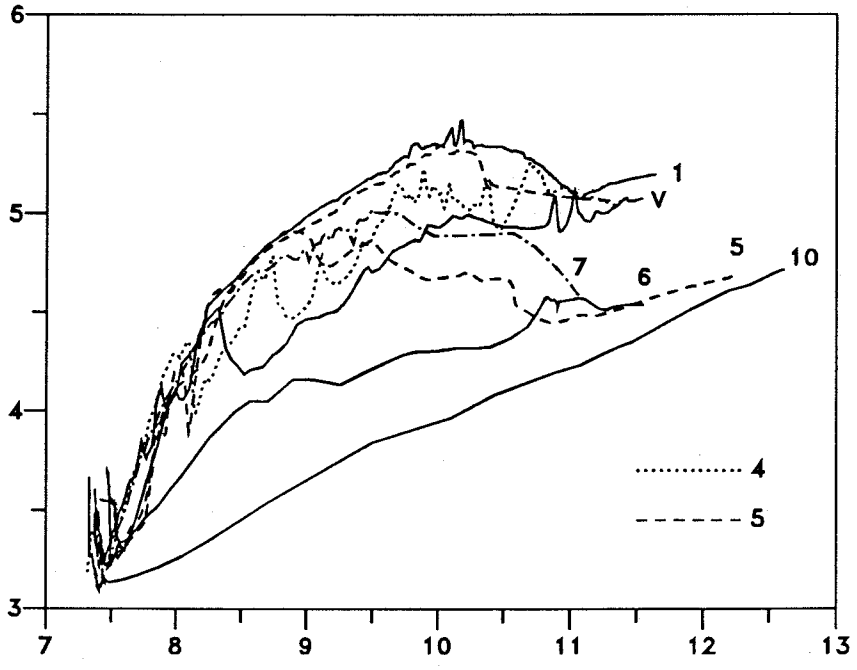

Fig. A3 As in Fig. A2 but for T-S curves; ordinate (T°C), abscissa S (PSU)

At all the stations (except the stations 5 and 6 of the second stage), the upper part of the halocline vertically fluctuated in between a relative thin layer of about 10 m (55 - 65)

dbar. However, at these two stations the top of the halocline shifted by about (15 - 20) m into deeper pressure levels of about (80 - 85) dbar. Such locally and temporally fixed downward displacement results from intensified vertical motions due to eddy-activities on the meso- scale. For instance, there was no any lowering of the upper halocline detected at these stations during the first stage, cf salinity profiles of point 5 in Fig. A2.

Taking into account that the local lowering of the top halocline boundary was accompanied with a local increase of near-bottom values in the salinity/ density, one can speculate that its dynamics are substantially not based on wave-like processes but probably depend from deep intrusions forming different eddies due to baroclinic interaction processes with irregularities in the bottom topography. Corresponding vertical gradients of salinity/ density increased by a factor of about two within the entire halocline in response to such phenomena, which support the spreading of salty water into the near-bottom layer of the halocline. Unfortunately, the insufficient station spacing does not permit to estimate the spatial dimension of that eddy by our additional transect. However, we can consider its data as a, more or less, appropriate supplement to transect (A - B).

The T-S curve and the vertical profile S (p), which are obtained from the eddy-station , are indicated by bold lines (V) in Fig. A (2, 3) while the station position is shown by an open circle in Fig. A1. This position was separated about 20 n.m. from that of station no. 5 in the north where a similar cyclonic-like anomaly had been observed on April 15, or 58 hours earlier. Between the cyclone detected at the (A - B) transect and the station no. 5 (second stage) there was no cyclone-like anomaly observed at station no. 6. Consequently, two aspects can be pointed out:

- the existence of two independent cyclones;
- the single cyclone moving north with the speed of about 18 cm/s.

The T-S curves, which result from the cyclone along the (A - B) transect and from the station no. 5, being similar in the whole but still differ substantially in detail. This difference is unlikely to be explained as a result of mixing processes with a duration of 2.5 days. That means the first aspect seems to be preferable.

First Investigations of the Near Surface Turbulence Structure and Energy Dissipation Caused by Wind Mixing in the Baltic Sea

Adolf Stips

Institute for Remote Sensing Applications,
CEC Joint Research Centre, 21020 Ispra, Italy

Introduction

In order to investigate the small-scale structure of the near surface turbulence a special uprising micro-structure profiler, which includes a remotely controlled underwater winch, was developed. The aim of these first measurements under sea conditions was to develop a deployment technology and to demonstrate the general functionality as well as to acquire first data sets of marine near surface turbulence in shallow water environments. For this purpose, we got the possibility to participate the March 1995 GOBEX expedition of the Institute for Baltic Sea Research Warnemünde with R/V "Professor Albrecht Penck" (P. A. P.) and carried out several time series of different duration at different positions.

The main aim of these investigations is to enhance our knowledge and understanding of the near surface fluxes and mixing processes, which are caused by different meteorological forcing mechanisms as given, for instance, by wind forcing and heating/cooling processes. Especially the dependence of the energy dissipation rate from the wind stress will be examined. In the literature, comparable measurements mostly tend to confirm a "law of the wall" behaviour, in which the energy dissipation inversely decays with the depth. However, several exceptions are also reported. We may distinguish micro-structure measurements of cases with and without breaking waves, SOLOVIEV et al. (1987). For no breaking waves, most of the known experiments confirmed the logarithmic velocity profile. Such profile was, for example, used by JONES and KENNEY (1977) to proof the validity of "the law of the wall". We refer to CHEUNG and STREET (1988) for a brief review. However, KITAIGORODSKI et al. (1983), THORPE (1984), GARGETT (1989), and AGRAWAL et al. (1992) found a wave enhanced zone with effective energy dissipation reaching down to an approximate depth of about 20 % of the surface wave-length (or 10 times the rms surface wave height), which seems to have a decay with a power law of about -3 to -4. These values are substantially "faster" than the first-power decay, which is predicted by

the "law of the wall". Using conventional turbulence closure schemes, CRAIG and BANNER (1994) also predicted such an enhanced turbulence regime in near surface layers due to the gravity waves.

Methods

For the measurements we used the uprising micro-structure profiler EDP (Enhanced Dissipation Profiler), a joint development of ME Meerestechnik-Elektronik GmbH and the Institute for Remote Sensing Applications. Additional support was provided by the EUREKA/EUROMAR project MICSOS (EU1246). To avoid any falsification from the wake of the ship, the portable underwater winch was deployed about 150 m away from the anchor station of the ship. A short technical description of the EDP system is given below. Measurements were performed as time series of 10 h to 19 h duration each. The frequency of subsequent profiles varied between one cast every 5 minutes to one cast every 20 minutes. Standard meteorological parameters have been measured with the meteorological station on board, roughly 8 m above the sea surface. Using the CTD probe "OM87", every one hour a CTD cast was additionally conducted. During our measurements, hourly mean values of the wind speed varied from 3 m/s up to 12 m/s. The nautical sea state was most of the time fetch limited and varied between 2 and 5 at all stations, except of the station "rueg".

Technical Description Enhanced Dissipation Profiler (EDP):

The complete EDP system has now 3 main components.

1. *Measuring probe:*
   The EDP probe is designed as a quasi free rising (sinking) instrument with micro-structure- and CTD-sensors as well as sensors to control the sinking process of the probe. The rise (fall) rate, typical about 0.5 m/s, can be adjusted by removable weights.

2. *Board unit:*
   The board unit is the central data registration-, control- and operating unit for the whole system. This unit includes computer capacity for the on-line data evaluation. It consists of a processing computer (PC), the deck unit, interfaces, and a joystick for winch controlling.

3. *Special underwater winch:*
   A designed underwater winch enables, manually controlled, a quasi free rising and positioning of the probe. For use in shallow waters, the EDP probe can be operated automatically.

Main features:

- high resolution micro-structure and high precision CTD sensors
- depth range for operation 100 m
- 8 channels
- 1000 scan/ s
- resolution 16 bit
- baudrate 307 kHz
- stainless steel, titanium materials
- overall length 1.35 m
- diameter 0.15 cm
- weight in air/water about 20/2 kg

Further sensor data are tabulated in Table 1.

Sensors	**range**	**accuracy**	**resolution**	**time constant**
pressure	0 ... 200 dbar(~ m)	+/- 0.1 % fs	0.002 % fs	40 ms
temperature	-2 ... 38 °C	+/- 0.01 °C	0.001 °C	160 ms
conductivity	0 ... 60 mS/cm	+/- 0.01 mS/cm	0.001 mS/cm	100 ms
μ-temperature	-2 ... 38 °C	+/- 0.05 °C	0.001 °C	7 ms
μ-conductivity	0 ... 60 mS/cm	+/- 0.1 mS/cm	0.001 mS/cm	7 ms
dissipation	10^{-2}.. 10^{-9} W/kg	not spec.	10^{-9} W/kg	4 ms

Tab.1 Sensor data of the EDP (m = micro-structure)

Micro- Structure Data

Time and co-ordinates of the measurement places are summarized in Table 2. Resulting positions of our anchor stations have been chosen in accordance with the general objectives of the GOBEX experiment and its planned station grid. In other words, these positions could not be selected with respect to requirements and/or the suitability for near surface turbulence measurements. The water depth was determined by the echosounder while recorded wind-speeds only represent a crude estimation.

Station	Position	Time/ GMT	Depth [m]	Wind [m/s]	Md	Casts Time Step
1 : test (001)	test	08.03 14:30	22	7 - 8	R	6 dt =5 min.
2 : b_f	55 04.171 N 14 34.398 E	09.03 12:30 09.03 13.30	38	5 - 6	F	10 dt =5 min.
3 : b_r	55 04.171 N 14 34.398 E	09.03 15:40 09.03 16:20	38	6 - 8	R	6 dt =5 min.
4 : rueg (r1b)	54 40.616 N 13 54.645 E	10.03 16:30 12.03. 06:00	28	5 - 15	R	159 dt=20 min.
5 : r2b	54 40.616 N 13 54.645 E	13.03 21:20 13.03 22:20	28	10 - 12	R	4 dt=20 min.
6 : r3b	54 39.200 N 13 09.685 E	14.03 18.20 14.03 19:30	18	7 - 8	R	8 dt=10 min.
7 : r4b	54 39.200 N 13 09.685 E	15.03 05:50 15.03 08:00	18	13 - 15	R	21 dt =5 min.
8 : r5b	54 39.200 N 13 09.685 E	15.03 15:40 15.03 20:15	18	7 - 8	R	17 dt=20 min.
9 : r6b	54 39.200 N 13 09.685 E	16.03 05:45 16.03 16:10	18	7 - 6	R	82 dt = 5 - 10 min.

Tab.2 Starting and ending time of series, water depth, range of wind velocity, sampling mode (Md: F = falling, R = rising), number of casts with the sampling frequency (dt).

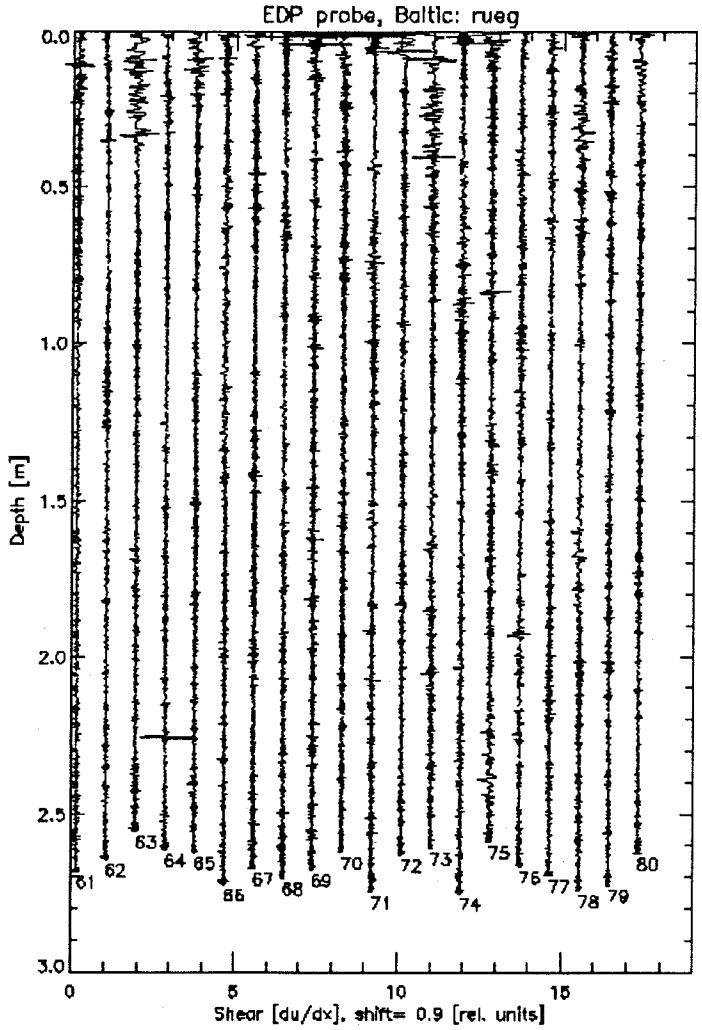

Fig.1 Series of 20 small scale current shear profiles measured at station "rueg" (every 20 minutes one cast), cf. Table 2 for further station data; the average wind speed was 9 m/s, measurements have been performed at March 11th, 1995, in the afternoon from 1 to 8 pm; the cast number is given at bottom of the profile.

Station names have been chosen arbitrarily. Unfortunately, the fast temperature sensor of the EDP probe was broken already at station No. 2 and the substituted sensor not worked

properly. Using the fast conductivity sensor, the exact sea surface hit of all sensors was determined. Resulting uncertainties should be lower than the value of about 1 cm. A second shear sensor, which was properly shielded, recorded any vibrations of the probe.

The joint data set was used to distinguish between signals of the real current shear and those of artificial hits produced by surface waves. The final laboratory calibration of all shear data could not be done until now. Consequently, the shear data and resulting dissipation rates are given either as relative values or as values, which are calibrated preliminarily. All together 313 micro-structure casts have been sampled.

Results

Under the point of view of preliminary observations, we like to discuss surprising outcomings under the aspect of "undisturbed records". In Fig. 1, we plotted a series of twenty small-scale current shear profiles acquired at the anchor station "rueg". The profiling time covers about six hours. During this period (one profile every 20 minutes), the wind velocity was practically constant with the mean value of about 9 m/s. Preliminary calculations of the dissipation rate show no indications for a logarithmic profile vertically. Due to sporadically occurring whitecappings at the sea surface, we assume sporadic events of breaking waves. Therefore, we may speculate that such features create a strong turbulence in very near surface layers. The cast No. 63 provides an example within the uppermost 30 cm layer. However in some other cases, we also found artificial high shear levels, which are probably caused by any probe vibrations due to the hit of sensors by a breaking waves. This conclusion is based on measurements recorded by our reference shear sensor. This way, we could identify contaminated measurements clearly. Examples are provided by casts No. 69 and No. 71 in the uppermost 10 cm.

Our measurements involved a period of relative strong winds with hourly wind speeds ranged from 8 m/s to about 12 m/s. We calculated the overall vertical distribution of the corresponding dissipation rate. Vertical averages, which cover a layer of 1 metre, are drawn in Fig. 2. Obviously, the highest dissipation rates intermittently occur in the uppermost metre and are also restricted to the very near surface layer. The corresponding temperature response is plotted in Fig. 3. The isotherms are practically orientated vertically. As it was expected, such situation confirms a complete thermal mixing of the entire water column. For instance, a surface cooling was recorded during the night from the 11th to the 12th of March. Consequently, the dissipation rate increased, too. Generally, such cooling events force the onset of convection processes vertically.

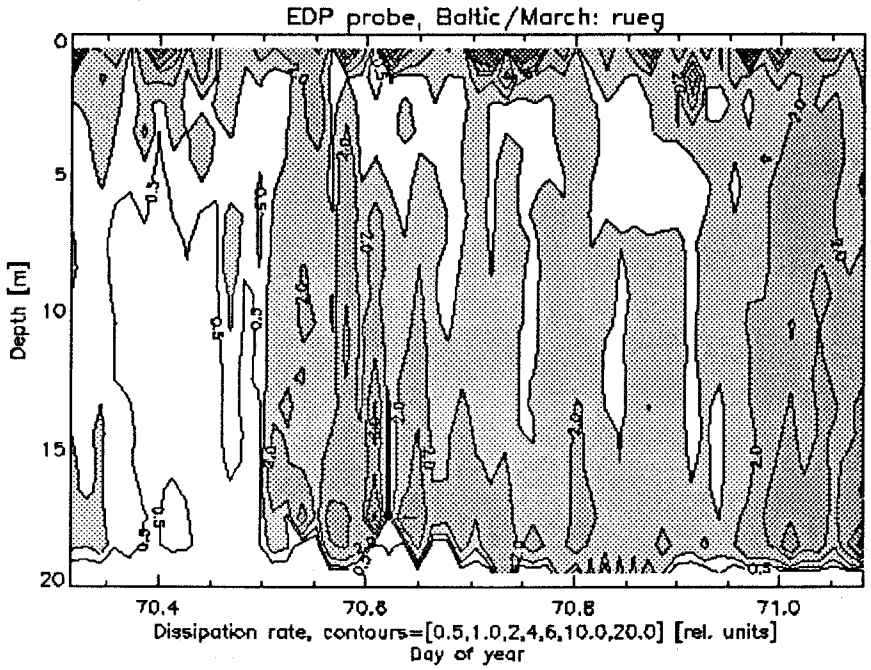

Fig. 2 Vertical distribution of relative dissipation rate (ϵ, in relative units) vs. time (day of the year) at station "rueg"; the sampling period was 19 hours with profiles casted every 20 minutes at March 11th, 1995; the water depth was 28 m.

Unfortunately, suitable records of moored current meters or moored ADCP's are not available and this point remains under speculation.

To elucidate the relationship between the input of kinetic energy from the local wind into near surface layers and vertical exchange processes, we correlated hourly mean values of the wind speed and corresponding dissipation rates, which were averaged over the uppermost 1m- layer. Combining all hourly averages (53 samples from station "rueg") we get the scatter plot shown in Fig. 4, which suggests a pronounced increase of the dissipation rate with increasing wind speed. Such scatter plot could be fitted by some theoretical approaches. For instance, we can use a simplified version of a boundary layer model for turbulent dissipation as proposed by MAC KENZIE et al. (1994):

$$\epsilon(W, z) = (5.82\ \ 10^{-9})^* W^{3}/ z. \qquad (1)$$

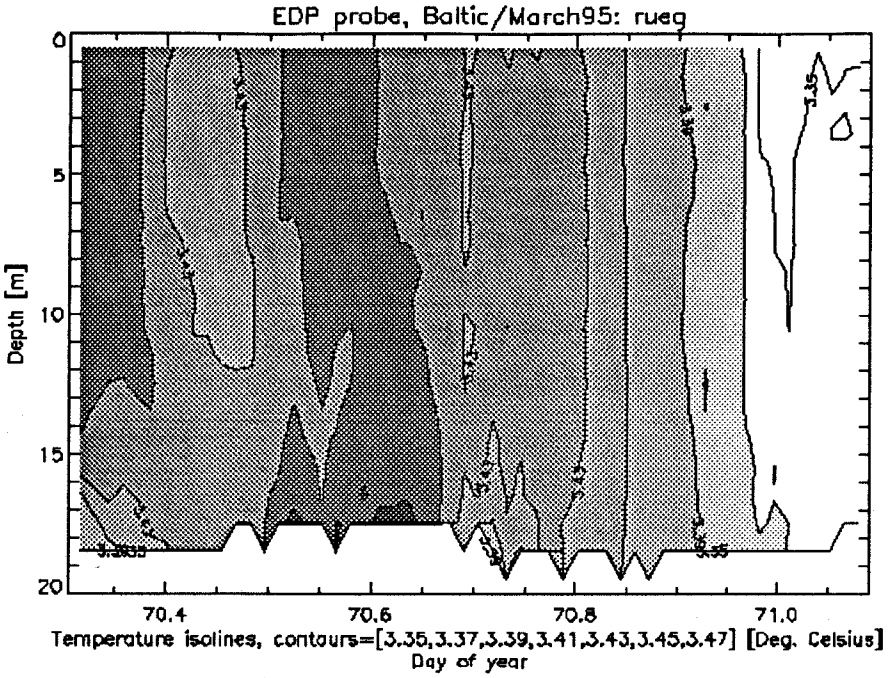

Fig. 3 As in Fig. 2 but for the temperature (°C)

Here, ϵ(W, z) is the dissipation rate of turbulent kinetic energy ($m^2\ s^{-3}$) while (W) is the wind speed ($m\ s^{-1}$) but (z) the depth (m). The resulting curve is plotted as solid line in Fig. 4. Despite of the strong scatter of all data points, the general tendency seems to confirm the theoretically expected relationship between (ϵ) and (W) for a fixed (z). The assumed depth dependence in relation (1) is that of a typical wall layer in the form of $\epsilon(z) \sim (1/z)$. This fact should be represented by a straight line in log-log plots of $\epsilon(z)$ as shown in Fig. 5. All values, which were averaged over period 2 of the anchor station "rueg" and cover about 19 hours in Fig. 5, do not match the theoretical curve exactly. There is a rather logarithmic decrease in the uppermost 3 m-layer. Considering all possible uncertainties of our measurements, the correspondence $\epsilon(z)$ seems to be quite good in the very near surface layer. In addition, we find a relative minimum in $\epsilon(z)$ in layers between 3 m to 10 m depth. In deeper layers, the values again increase down to about 20 m depth but not reach amounts of the top layer. Considering the relative constant but strong wind velocity for the duration of about one day, a homogenous bottom friction layer should be established. This case, a second logarithmic layer occurs in log-log plots for deepest layers above the sea bed (about 28 m water depth).

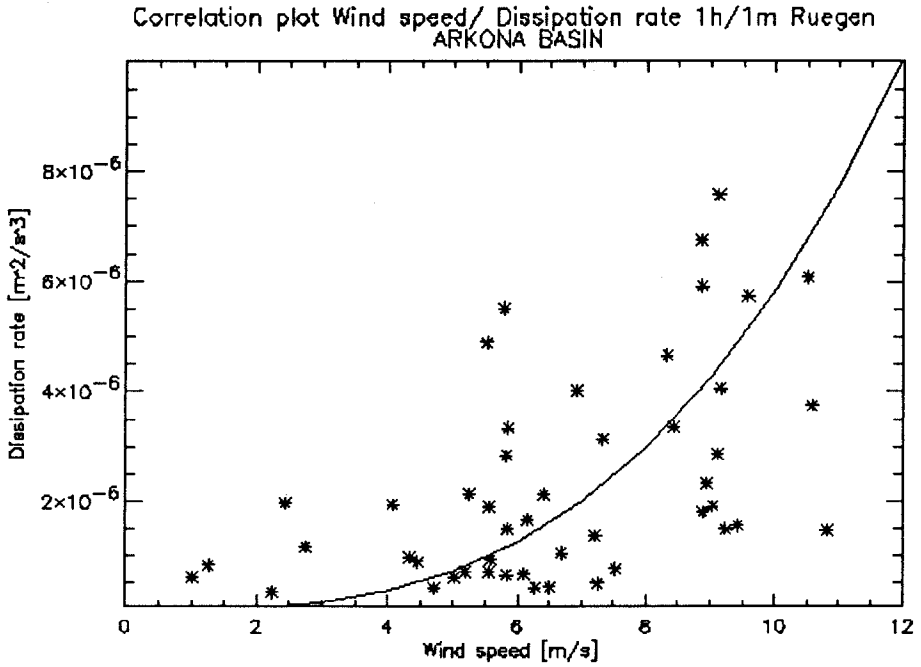

Fig. 4 Scatter plot of hourly averages of the wind speed (W) vs. corresponding values of the dissipation rate (ϵ) integrated over the uppermost 1m-layer; data result from measurements carried out at the station "rueg"; values of formulae (1) are drawn by a solid curve.

The superposition of both logarithmic dissipation regimes would result in an intermediate minimum of $\epsilon(z)$ as it is depicted in Fig. 5.

Conclusions

To our knowledge, uncontaminated (free of vibrational noise) small-scale shear measurements, which are recorded by a quasi-free uprising micro-structure profiler equipped with airfoil type shear sensors, are not available anywhere else. We developed a measuring system and its sufficient deployment technology. Consequently, under wind conditions of up to 7 Bft , controlled measurements of the uncontaminated dissipation rate are possible in shallow waters. Preliminary data reveal that enhanced turbulent dissipation rates sporadically occur within the top layer with depths between 10 cm down to 50 cm. Probably such events are associated with breaking gravity waves at the sea surface. In the deeper layers, however, the occurrence of turbulent bursts is characterised by strong spatial and temporal intermittence.

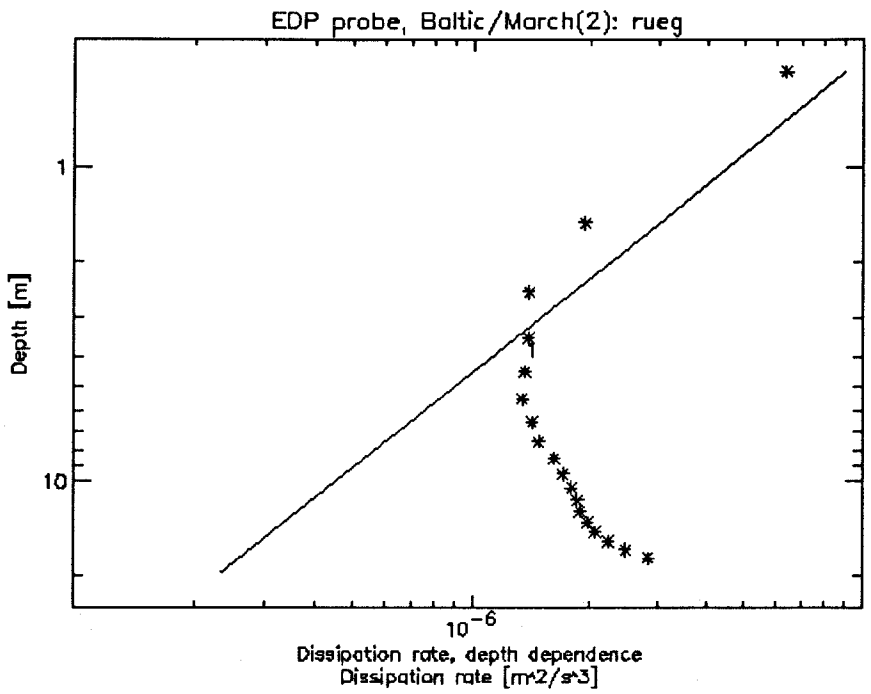

Fig. 5 Log-log plot of $\epsilon(z)$ from measurements during the observatinal period 2 (19 hours at March 11th) at anchor station "rueg"; the average wind speed was $<W> = 9.2$ m/s.

Hourly dissipation rates, which were integrated over the uppermost 1m layer, suggest a weak but pronounced cubic increase with the wind speed, although single values scatter strongly. Such findings confirm most of the known dissipation models, which assume a kinetic energy input for the turbulence production in intermediate layers via gravity waves at the sea surface. Therefore, the associated dissipation rate should be proportional to the cube of the wind velocity. The expected dependence of the "wall layer depth" for cases without breaking surface waves could be confirmed. Assuming a "logarithmic top layer" this process is restricted on depths between about 1 m to 3 m. Postulated enhanced dissipation rates in the surface layer, as obtained empirically by DRENNAN et al. (1992) or theoretically by CRAIG and BANNER (1994), only consider the case of breaking waves by $\epsilon \sim \text{const} * (W^3/z)$. Commonly, the wave-affected layer is marked by large values of (ϵ). Our measurements suggest that the enrichment of (ϵ) only occurs within the uppermost layer (< 50 cm), which is smaller than that value reported by THORPE (1992) and others authors, who assumed a thickness of about 10 times the rms wave amplitude.

Consequently, the approach of formulae (1) is not directly applicable for cases without dominating breaking waves. Nevertheless, our profiles of (ϵ) indicate that this power law could be also valid for the case of single breaking waves but only within the uppermost top layer (1 - 2 m depth). The influence of single breaking waves on $\epsilon(z)$ disappears in long term mean values, which generally confirm the classical wall layer theory. For a sound statistical description of processes associated with near surface turbulence, an extended measurement programme has to be performed under various hydrographical and meteorological conditions. Such field campaign could start in shallow water areas of the Baltic Sea and must involve records of the wave field characteristics including the frequency of breaking waves. In addition, we need measurements from moored current meters and ADCP's in order to document changes in the motion field not only in space but also in time.

Acknowledgement

We thank the IOW and especially Eberhard Hagen for the invitation to take part in the March 1995 expedition. Without the active support of several people these measurements could not have been performed, so we would like to thank Drs. Peter Schlittenhardt, Hartmut Prandke, Rainer Feistel, Christoph Zülicke as well as Dirk van der Linde, Ulisse Devisioni, Uwe Scholz, and the Crew of R/V "Professor Albrecht Penck" for their valuable help. The joint research project between IRSA and ME-GmbH was additionally supported by the EUREKA/EUROMAR project MICSOS (EU 1246).

References

AGRAWAL, Y. C., E. A. TERRAY, M. A. DONELAN, P. A. HWANG, A. J. WILLIAMS, W. DRENNAN, K. KAHMA, S. A. KITAIGORODSKI, 1992: Enhanced dissipation of kinetic energy beneath breaking waves. Nature, **359**, 219 - 220.

CHEUNG, T. K., R. L. STREET, 1988: The turbulent layer in water at an air-water interface. J. Fluid Mechanics, **194**, 133 - 151.

CRAIG, P. D., M. L. BANNER, 1994: Modelling wave-enhanced turbulence in the ocean surface layer. J. Phys. Oceanogr., **24**, 2546 - 2559.

DRENNAN, W. M., K. K. KAHMA, E. A. TERRAY, M. A. DONELAN, S. A. KITAIGORODSKI, 1992: Observations of the enhancement of kinetic energy

dissipation beneath breaking waves. In: Breaking Waves, M. L. Banner and R. H. J. Grimshaw, Eds., Springer, 95 - 101.

GARGETT, A. E., 1989: Ocean Turbulence. Ann. Rev. Fluid Mech.., **21**, 419 - 451.

JONES, I. S. F., B. C. KENNEY, 1977: The scaling of velocity fluctuations in the surface mixed layer. J. Geophys. Res. **82**, 1392 - 1396.

KITAIGORODSKI, S. A., M. A. DONELAN, J. L. LUMLEY, E. A. TERRAY, 1983: Wave turbulence interactions in the upper ocean. Part II: Statistical characteristics of wave and turbulent components of the random velocity field in the marine surface layer. J. Phys. Oceanogr. **13**, 1988 - 1999.

MACKENZIE, R. B., T. J. MILLER, S CYR, W. C. LEGGET, 1994: Evidence for a dome-shaped relationship between turbulence and larval fish ingestion rates. Limnol. Oceanogr., **39** (8), 1790 - 1799.

SOLOVIEV, A. V., N. V. VERSHINSKY, V. A. BEZVERCHNII, 1988: Small-scale turbulence measurements in the thin surface layer of the ocean. Deep Sea Res. **35**, 1859 - 1874.

THORPE, S. A., 1984: On the determination of K_V in the near-surface ocean from acoustic measurements of bubbles. J. Phys. Oceanogr., **14**, 855 - 863.

THORPE, S. A., 1992: Bubble clouds and the dynamics of the upper ocean. Quart. J. Roy. Meteor. Soc., **118**, 1 - 22.

Exchange Coefficients and Dissipation Measurements -A March Case Study-

Ch. Zülicke, Institute for Baltic Sea Research, Warnemünde, Germany
I. Schuffenhauer, Department of Electronics, University of Rostock, Germany
A. Stips, Institute for Remote Sensing Application, Ispra, Italy

Introduction

In the sea, diapycnal fluxes are mainly caused by turbulent processes (microstructure dynamics at the mm-s-scale). Therefore, their understanding and parameterization requires knowledge of the dynamics of oceanic turbulence. In order to investigate such micro-scale structures in the near-surface layer a microstructure profiler was applied, which includes a remotely controlled underwater winch.

The turbulent quantities are guided by the turbulent kinetic energy (TKE)

$$E_{turb} = \rho/2 \; (\; <u'^2> + <v'^2> + <w'^2> \;) \; . \qquad (1)$$

Here, primes denote fluctuations from the mean value and brackets indicate mean values. The dynamics of the TKE can be expressed for the statistically stationary and horizontally homogeneous model case [LANDOLT & BOERNSTEIN (1986) NSV/3b page 169 eq. (48.a). MONIN and OZMIDOV (1982) corrected in their equation (2.16) the formulation (1.52') of KRAUSS (1972). A right-hand coordinate system (x, y, z) is used with velocity components (u, v, w) pointing to the East, North and upwards. Consequently, temporal changes in the TKE can be expressed by

$$\partial E_{turb}/\partial t = -g \; <\rho'w'> \; - \rho \; (\; <u'w'> \; \partial u/\partial z \; + \; <v'w'> \; \partial v/\partial z \;) \; - \rho \; \epsilon \; +$$

$$- \; \partial/\partial z(\; \rho \; <(u'^2+v'^2+w'^2)w'>/2 \; + \; <p'w'> \; - \nu \; \partial E_{turb} \;) \; = \; 0 \qquad (2)$$

Here, (t) denotes the time, (g) the acceleration due to gravity, (ρ) the density, (ν) the kinematic viscosity and the dissipation (ϵ) is given by

$$\epsilon = \nu \; < \; (\partial u'/\partial z)^2 \; + \; (\partial v'/\partial z)^2 \; + \; (\partial w'/\partial z)^2 \; > \; . \qquad (2.1)$$

According to this equation, turbulence is generated by buoyancy (first term) and vertical current shear (second term). The energetic loss is reflected through dissipation in the third term. The flux of TKE (in brackets) is realized through fluctuating transport of TKE and pressure force as well as by viscous diffusion. Near the surface, the wind-generated shear and wave-produced TKE should be mainly balanced by the dissipation. More in the bulk, buoyancy effects become dominant. The ratio of both contributors is expressed through the flux Richardson number (R_f)

$$R_f = -g\langle\rho'w'\rangle \,/\, \rho(\, \langle u'w'\rangle(\partial u/\partial z)+\langle v'w'\rangle(\partial v/\partial z)\,). \qquad (3)$$

Correspondingly, the ratio of the driving forces in terms of density and momentum gradients is introduced with the gradient Richardson number

$$Ri = N^2 \,/\, (\,(\partial u/\partial z)^2+(\partial v/\partial z)^2) \qquad (4)$$

A necessary condition for turbulence is that both values of (R_f) and (Ri) are smaller than the value of about 0.1.

The eddy coefficient for momentum exchange (K_u) is usually defined by

$$\langle u'w'\rangle = -K_u\, \partial u/\partial z. \qquad (5)$$

For the stationary homogeneous case it can, according to GREGG (1987), be expressed via (R_f)

$$K_u = 1/(1-R_f)\, \epsilon/(\,(\partial u/\partial z)^2 + (\partial v/\partial z)^2\,). \qquad (6)$$

The parameterization of the velocity flux with the mean shear underestimates the contributions of short-term energy-rich shear fluctuations. This situation can be improved by using semi-empirical relationships at the appropriate scales, cf. eq. (3.11) in MONIN and OZMIDOV (1987).

The eddy coefficient for diapycnic fluxes (K_ρ), which describes the mixing most adequate, is defined by the density anomaly flux

$$\langle\rho'w'\rangle = -K_\rho\, \partial\rho/\partial z\,. \qquad (7)$$

Following GREGG (1987) and using (Rf) we find :

$$K_\rho = R_f/(1-R_f)\ \epsilon/N^2 = \gamma_{mix}\ \epsilon/N^2. \qquad (8)$$

The shear is replaced by the density flux and the (empirical) mixing intensity (γ_{mix}) is introduced with $\gamma_{mix} = 0.2$ for the critical flux number $R_{fcr} = 0.15$, cf. OSBORN (1980). However, PETERS et al. (1988) recommended

$$K_\rho = MIN[\ \gamma\ \epsilon/N^2\ ,\ \gamma\ \epsilon\ /\ (\partial u/\partial z)^2\ ];\quad \gamma \approx 0.2. \qquad (9)$$

We will follow the latter equation because the evaluation of the quality of the different parameterizations should be done with reference to direct measurements of the vertical fluctuating transports $<w'\rho'>$, which were not available for the present study.
In the following we search for the exchange coefficient (K_ρ) and study its variability within the surface mixed layer. The effective turbulent transport is described by means of the turbulent exchange coefficient (K_ρ) at the meter-hour-scale. Here enter averaged micro-scale parameters such as the dissipation rate (ϵ) and the Brunt-Väisälä frequency (N^2). At the second step of investigation, we attempt to describe the bulk properties of the transport by averaging intervals covering several meters. This way, the depth-averaged transport will be related to the bulk-differences of driving forces.

The data base

The data base was acquired during one of the GOBEX-Expedition's (07.03. - 17.03.1995) of the Institute for Baltic Sea Research Warnemünde (IOW) in cooperation with the Institute for Remote Sensing Application (IRSA)/ Ispra. Table 1 provides measuring position and observational time expressed by the day of the year (DOY)

Station	Position/ Deg	Time/ UTC	Time/ DOY	Depth /m
R6B	54.3980 N 13.09867 E	16.03.95- 05:45 16.03.95- 16:10	75.239583 - 75.673608	18

Tab. 1: R6B station parameters of the cruise GX950307. AVH

This position was located in the North-West of the Rügen island. The ship was anchored

in the wind shadow of the island. During most of the time the wind was blowing from north-north-easterly directions with velocities between 4 and 10 m/ s.

The measurement comprised three different types of data with different sampling strategies:

- the meteorological data (60 samples a hour)
- 4 data sets of Aanderaa current meters (12 samples a hour)
- the dissipation data (4 samples a hour)

For the following investigation, we choose an one-hour / one-meter grid resolution. A microstructure profiler EDP (Enhanced Dissipation Profiler) of ME Meerestechnik-Elektronik GmbH (Trappenkamp, Germany) was available for dissipation measurements. This device is a multi-parameter probe for simultaneous measurements of the intensity of small-scale turbulence (temperature, current shear, pressure). It precisely provides profiles of temperature, conductivity, and pressure, too. We refer to STIPS (this issue) with respect to all device parameters and a detailed technical description.
The meteorological parameters have been measured and handled with a standard device on board of R/V "Prof. A. Penck" (DATADIS -system). The current velocity and direction was registered with four Aanderaa current meters at fixed levels (2.5, 4.5, 5.5, and 10 m water depth) using a shallow water mooring system.

Results

We plotted time-series of the dissipation rate (ϵ) in Fig.1, the Brunt-Väisälä-Frequency (N) in Fig.2, and the turbulent viscosity (K_ρ) in Fig.3. Hourly mean values from the following three layers are determined:

layer	layer depth / m	layer thickness / m
z_{1-2}	4.5 - 5.5	1
z_{2-3}	5.5 - 10.5	5
z_{1-3}	4.5 - 10.5	6

Tab. 2 Layers according to moored current meter depths

The surface layer (0 m - 4.5m) depth was excluded from the considerations, because wind and breaking waves should have the main influence there, cf. STIPS this issue.

Consequently, our attention was mainly directed on the bulk layer (z_{1-3}) covering the water column between z_1 = 4.5 and z_3 = 10.5 m.

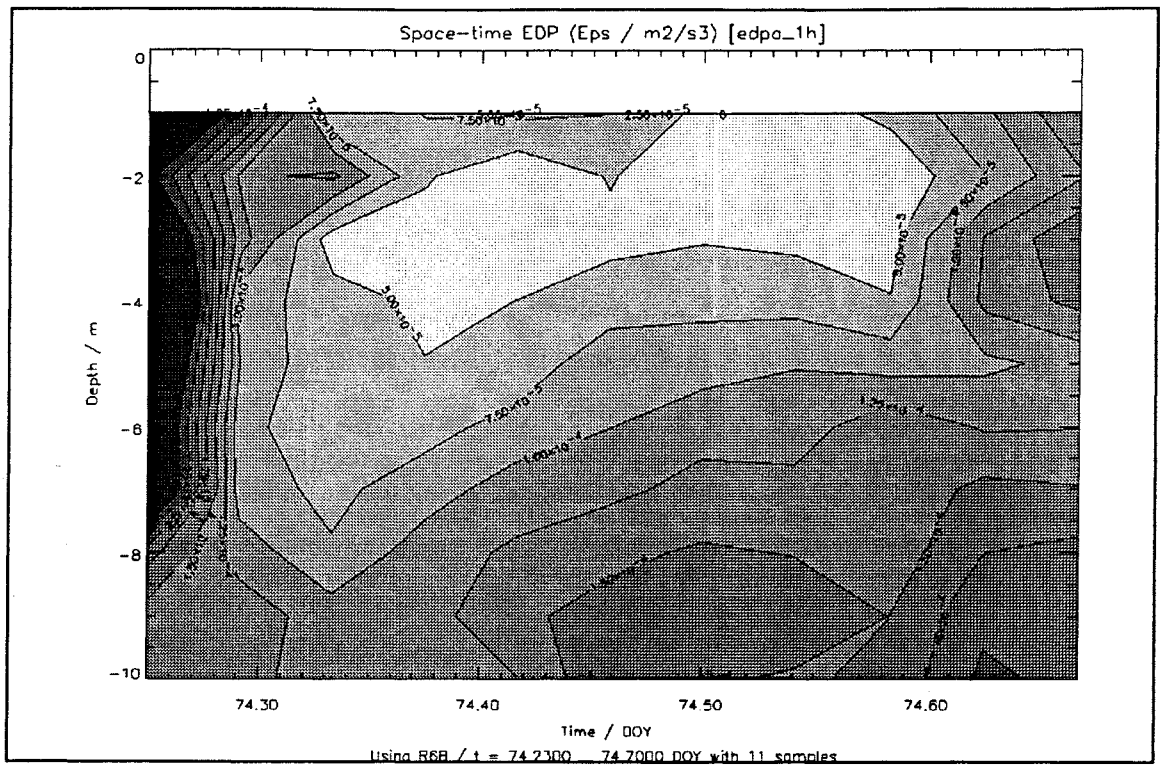

Fig. 1 Contour plot of the dissipation rate (ε) with a line spacing of 2.5 10^{-5} m^2/s^3 [W/kg]; the abscissa follows the time (day of the year, DOY) over the 10 hours; the depth varies between about 1m and 10m.
(Note peak values from the surface down to 8 m during the first hour; two events of increased dissipation develope in time beneath the 8m horizon; another feature occurs in the layer between 2.5m and 4m depth in the last stage.)

Dissipation rate

We start with the time series of the dissipation rate (ε). Resulting mean values are $<\varepsilon>$ = (121 $\pm$ 26) 10^{-6} m^2/s^3 (W/ kg). Single values ranged between (10 - 400) 10^{-6} m^2/s^3. Their variations occurred on the hourly scale and comprised events with spatial scales of several meters. This clearly follows from our Fig. 1 and Fig. 2 of STIPS, this issue. At the beginning of the series there is a turbulent event extending from the sea surface down to about 8 m depth. It is probably imported/ advected from ambient regions although there are no drastic changes in the temperature- salinity characteristic. Consequently, we deleted its value due to two arguments:

1. Formally, the (ε)-value for the first hour is outside of the 2-σ-range [here, (σ) represents the standard deviation].
2. Local relations of (ε) are practically not existing with respect to the current shear and the stratification.

At the end of the series a slightly increased dissipation was detected in the near bottom layer. We state that the total layer (z_{1-3}) should be well representative for the description of the bulk surface layer, which is well mixed. In the following 10 hourly averaged values will be considered only .

10-hourly averages

Mean values/ layer z_{i-j}	u'^2_{ij} / 10^{-03} $1/s^2$	$1/N^2_{ij}$ / 10^{+03} $1/s^2$	$1/Ri_{ij}$	$<\varepsilon>_{ij}$ / 10^{-06} m^2/s^3	$<K_\rho>_{ij}$ / 10^{-03} m^2/s	$K_{\rho ij}$ / 10^{-03} m^2/s
z_{1-2}	1.79 $\pm$ 0.74	0.94 $\pm$ 0.64	1.69 $\pm$ 1.31	83 $\pm$ 21	16.3 $\pm$ 5.6	13.6 $\pm$ 5.2
z_{2-3}	1.46 $\pm$ 0.51	1.33 $\pm$ 0.23	1.91 $\pm$ 0.69	135 $\pm$ 28	55.2 $\pm$ 19.0	35.8 $\pm$ 9.2
z_{1-3}	0.90 $\pm$ 0.42	1.16 $\pm$ 0.14	1.03 $\pm$ 0.48	121 $\pm$ 26	50.0 $\pm$ 15.9	27.4$\pm$ 38.0

Tab. 3 10-hourly mean values and related standard deviations for three depth intervals of Table 2.

Table 3 reveals, with respect to (ε) and (K_ρ), the main influence of the stratification, which is expressed by the term ($1/N^2$). This parameter significantly increases with decreasing water depth .The stratification is 30% smaller in the middle layer (z_{2-3}) than in upper layer (z_{1-2}). The related dissipation rate is 63% larger. The overall value obtained from layer (z_{1-3}) fits into this picture.

Hourly averages

In the following we represent hourly averaged values of the dissipation rate, which cover the water column from $z_1 = 4.5$ m to $z_3 = 10.5$ m.

$$<\varepsilon>_{13} = \int dz/z_{13}\, \varepsilon_z ; \quad z_{13} = z_3 - z_1 \tag{10}$$

Results are related to the hourly bulk estimates of driving forces in terms of the vertical current shear, the Brunt-Väisälä frequency, and the gradient Richardson number

$$(\partial u/\partial z)_{13} = (u3\text{-}u1)/z_{13} \tag{11-1}$$

$$N^2_{13} = g/\rho_{p13}\,(\rho_{p3}\text{-}\rho_{p1})/z_{13} > 1.0\ 10^{-6}\ 1/s^2 \tag{11-2}$$

$$Ri_{13} = N^2_{13} / u'^2_{13} . \tag{11-3}$$

Here, we introduced the potential density (ρ_p) with the reference level at the sea surface. Negative values are excluded within the accuracy of measurements. The regression between $<\varepsilon>_{13}$ and the parameters of (11-1), (11-2), and (11-3) yields coefficients tabulated in Table 4. The number of values is given by (n).

Regression coeff. ρ/ layer (n = 10)	$<\varepsilon>_{13} \sim (\partial u/\partial z)^2_{13}$	$<\varepsilon>_{13} \sim 1/N^2_{13}$	$<\varepsilon>_{13} \sim 1/Ri_{13}$
$z_{1\text{-}3}$	+0.64 ± 0.24	-0.83 ± 0.18	+0.44 ± 0.28

Tab. 4 Regression coefficients between the dissipation rate and the given parameters in layer (z_{13}) ;
(80% significance range (t-Test) reading $\rho = r \pm t(\alpha=0.1,\phi=8)(1\text{-}r^2)^{1/2}/9^{1/2}$))

The variability of the dissipation rate is well explained by the shear fluctuations. The correlation with ($1/N^2$) is not positive, as one would expect. This observation suggests, that the stratification guides the short-term fluctuations as a quasi-stationary background field. Nevertheless, variantions in the dissipation are reasonably described by the Richardson mumber (Ri). Time series of sufficient length are required to sample both short-term fluctuations and longer-term trends in the subsequent field campaigns. It turns out from our measurements, that production of turbulent kinetic energy by the shear is

much larger than the buoyant losses. This is underlined by the value of the surface Richardson flux number,

$$R_f \approx -g\alpha j_0/c_p\rho \; / \; (u_{*0}^2 \, \partial u/\partial z) \; . \qquad (12)$$

In a first approximation, we adopted characteristic atmospheric parameters measured at another expedition, which was carried out in the Baltic Proper during March 1994 (GX940321.PAP). We refer to ZÜLICKE AND HENNIG, this voulme. Making use of standard bulk formulae for the calculation of fluxes, Landolt&Boernstein NSV/3b page 332, we obtain

$j_0 = j_L + j_H + j_{LW} \approx 30.9$ W/m^2	: Surface heat losses (latent and sensible heat, long-wave (thermal) radiation)
$j_{sw} \approx 50.2$ W/m^2	: Surface heat gain (short-wave (solar) radiation)
$j_0 = j_{sw} - j_0 \approx 19.3$ W/m^2	: Net heat flux from atmosphere to ocean
$u_{*0} = 0.013$ m/s	: Surface friction velocity

The following material parameters were used (cf. Landolt&Boernstein NSV/3b page 233) for T=4°C, S=8 PSU, p=0 dbar:

$g = 9.81$ m/s^2	: Gravitational acceleration
$\alpha = 25.8\ 10^{-6}$ 1/K	: Thermal expansion coefficient of sea water
$c_p = 4150$ Ws/kgK	: Heat capacity of sea water
$\rho = 1006.3$ kg/m^3	: Density of sea water
$\nu = 1.578$ 10-6 m^2/s	: Kinematic viscosity ov sea water

Now the current shear must be specified. Within the viscouse skin layer, we assume molecular diffusion of momentum and express the current shear through the surface friction velocity

$$(\partial u/\partial z)_{skin} = u_{*0}^2 \; / \; \nu. \qquad (13)$$

Thus, the skin flux Richardson number is given by

$$R_{fskin} \approx (g\alpha j_0/c_p\rho) \; / \; (u_{*0}^4/\nu) \approx 6.46\ 10^{-8} \; . \qquad (14)$$

We state that the influence of stratification is neglectible in the viscouse skin layer. For the bulk, we still presume constant vertical fluxes of both heat (j_0) and momentum (τ_0) but use the current shear from our measurements recorded between $z_1 = 4.5$ m and $z_3 = 10.5$ m. We obtain

$$(\partial u/\partial z)_{bulk} = 0.03\ 1/s \tag{15}$$

resulting in the bulk flux Richardson number

$$R_{fbulk} \approx (g\alpha j_0/c_p\rho) / (u_{*0}^2\ \partial u/\partial z) \approx 2.31\ 10^{-4}. \tag{16}$$

Thus, in the bulk layer again the shear dominates the turbulent behaviour, but not as drastic as in the skin layer. Note, that even in the bulk the value of the Richardson flux number (Rf) is two orders of magnitude smaller than the critical $R_{fcr} = 0.15$. We would like to interpret our result as a qualitative hint on a relative strong influence of the shear on the scale under consideration. The mixing intensity, based on these measurements, would be

$$\gamma mixbulk = Rf/(1\text{-}Rf) \approx 2.31\ 10^{-4}\ . \tag{17}$$

Thus, the energy is accumulated rather in the momentum then in the density flux.

Exchange coefficient

At first we represent bulk estimates of the turbulent exchange coefficient based on 10-hourly means. Following PETERS et al. (1988), we will use their mixing intensity ($\gamma = 0.2$) and like to interpret relative values only. We alternatively calculate the exchange coefficient (K_ρ) in the limits of shear-driven turbulence to be

$$K_\rho = \gamma\ \epsilon\ /\ (\partial u/\partial z)^2 \approx 2.68\ 10^{-3}\ m^2/s \tag{18}$$

but convectively driven turbulence to be

$$K_\rho = \gamma\ \epsilon/N^2 \approx 2.80\ 10^{-3}\ m^2/s\ . \tag{19}$$

There is no large difference between both estimates of the (K_ρ) resulting from (18) and (19). That means the time-scale for the vertical exchange of both processes should be of

the same magnitude.

Finally, the turbulent exchange coefficient was calculated for every meter depth according to

$$K_{\rho z} = \gamma \, \epsilon_z / N^2{}_z \; ; \qquad \gamma = 0.2. \tag{20}$$

This formula must be treated with some care because it is believed to be valid for strong stratification only. Thus, we definitely excluded small (and negative) values of the stability parameter (N^2), (11-2). The accuracy of the calculations is limited by natural and artificial fluctuations. Its most critical point is the determination of density gradients form routine CTD observations. Note, that the accuracy of 10^{-2} kg/ m^3 would be equivalent to an error of about 50 % in (N^2) for the reference density of 1025 kg/m^3 and +/- 0.1 m at 1.0 m reference depth. In fact, the correct estimate of such quantities remains a drastic challenge in the presently used observational techniques.

We note a relatively inertial behaviour of the stratification (N^2), Fig.2. After the impact of the strong turbulent mixing event, which is detected at 74.3 DOY, the stratification shows a relative minimum. After noon 74.5 DOY, the stratification permanently increases. It seems to be that the depth of the associated pycnocline follows the relative minimum layer of the dissipation rate shown in Fig.1. We excluded some negative values of (N^2), which may be an artefact of the numerical differentiation used.

Both dissipation and stratification are reflected in (K_ρ) plotted in Fig. 3. After very high mixing at the beginning, where the action of dissipation is modulated by stratification into two centres placed at 3 m and at 7 m depth, a relaxation takes place. A period of very small stratification is revealed in Fig.2 for the near bottom layer during (74.45 - 74.55) DOY. This period is obviously accompanied by increased dissipation.

The total mean value (11 hours) is found to be

$$K_\rho = (50.0 \pm 15.9) \; 10^{-3} \; m^2/s.$$

This value is about four orders of magnitude larger than that of the kinematic viscosity, which is estimated to be $\nu = K_m = 1.6 \; 10^{-6} \; m^2/s$. The resulting difference to the bulk estimate could be explained by energy-rich fluctuations occuring on the high frequeny scale. In our time series, the coefficient (K_ρ) appears to be highly variable. Its value

depends from the state of stratification and dissipation.

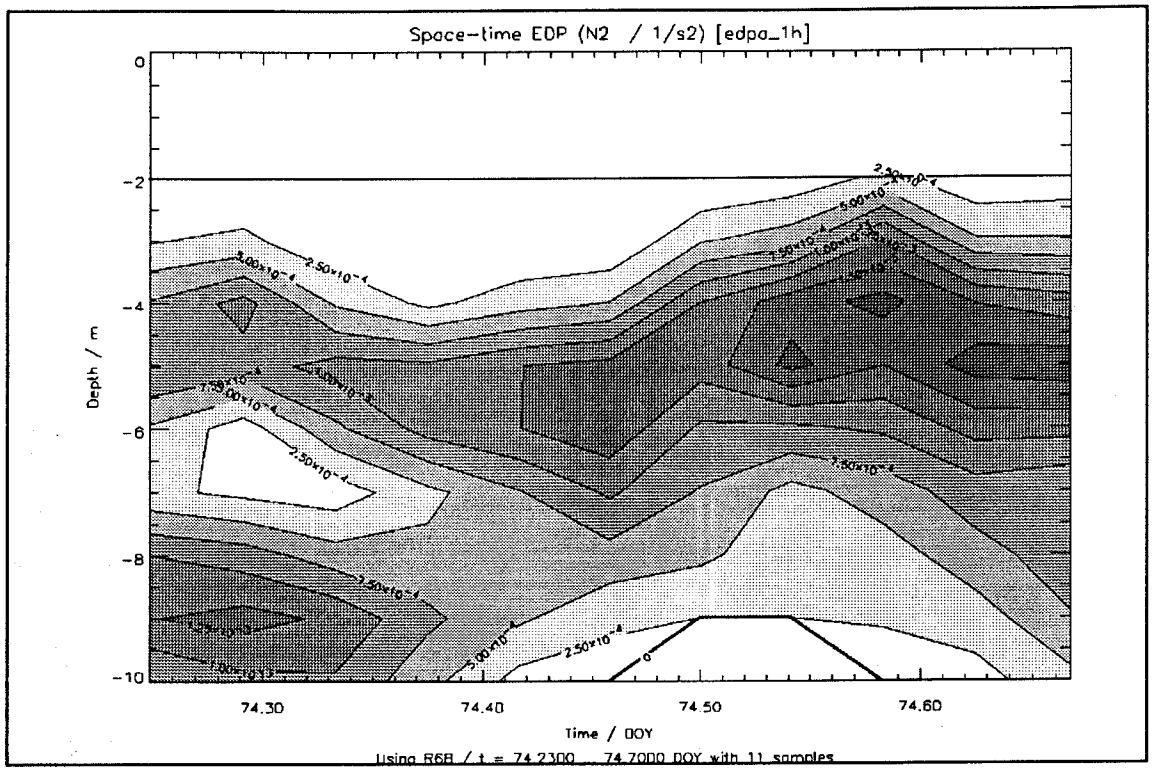

Fig. 2 As Fig.1 but for the squared Brunt-Väisälä frequency (N^2) with the contour spacing of 2.5 10^{-4} $1/s^2$.
(The overall stratification is relatively weak at the beginning but increases in time; a certain maximum (~ 1.5 10^{-3} $1/s^2$) develops between 4m and 6 m; the white zone near the top results from very small gradients while that located between 9m and 10m is based on reduced data.)

For instance, a well-pronounced peak value (K_ρ = 11.5 10^{-3} m^2/s) can be detected in the upper layer ($z_{1\text{-}2}$) at t = 74.29 DOY in Fig. 3. That event should be clearly attributed to the minimum in the stratification, Fig.2.

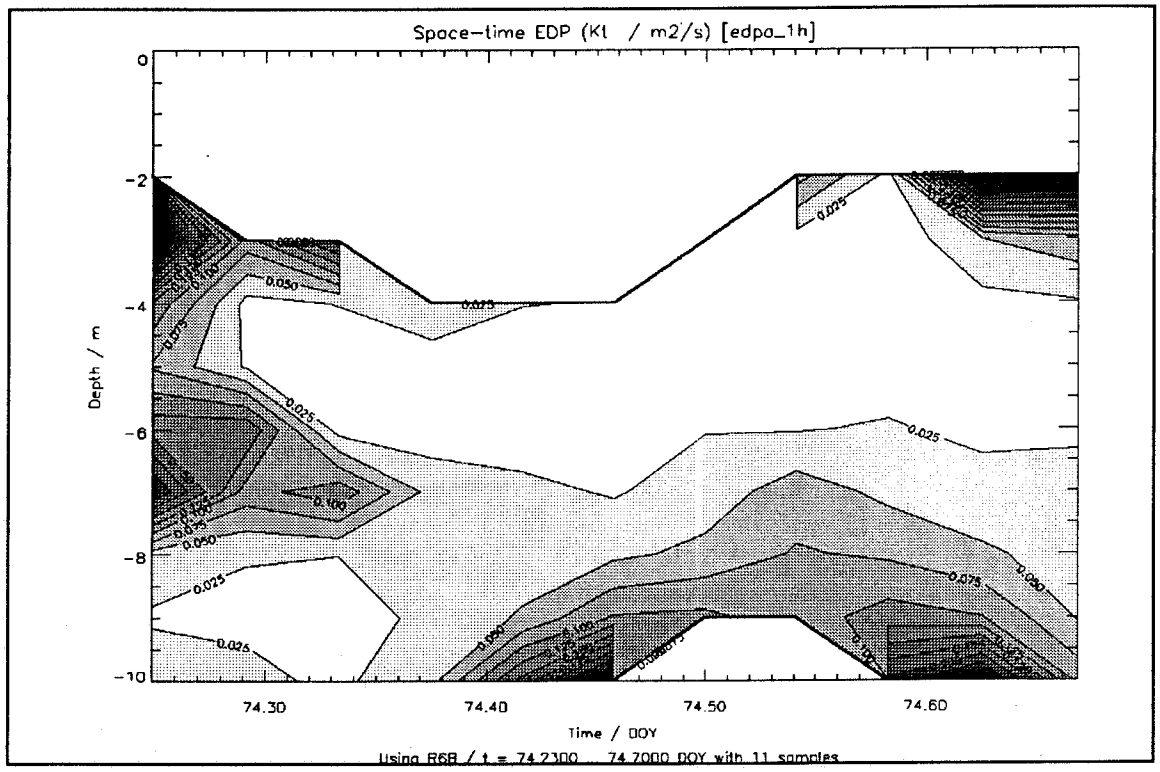

Fig. 3 As previous plots but for the exchange coefficient (K_ρ) with a line spacing of 0.025 m^2/s.
(Quite high values ($K_\rho > 0.1$ m^2/s) are estimated at the beginning and temporally occur in different layers located above 4m and below 6 m depth; the white region at the top corresponds to extremely low density gradients.)

A second peak value of about two hours duration can be found in the lower layer ($z_{2\text{-}3}$) for t ~ 74.54 DOY. The stratification was low again during that time. Variations in the vertical current shear visually follow that signal but seemingly with a little delay of about one hour. For example, the shear minimum, which is observed in layer ($z_{1\text{-}2}$) at t = 74.50 DOY, finds its response in changed exchange conditions at t = 74.54 DOY.

10-hourly averages

The corresponding coefficient of turbulent transports is given in Table 3. The location of the layer with maximal fluxes generally coincides with the level of minimal stratification.

Fluctuations of hourly means

Values of a similar regression than in Table 4, but for hourly and vertically averaged values, are compiled in Table 5 according to

$$<K_\rho>_{13} = \int dz/z_{13}\, K_{\rho z}. \qquad (22)$$

Regression coeff. ρ/ depth layer	$<K_\rho>_{13} \sim <\varepsilon>_{13}$	$<K_\rho>_{13} \sim (\partial u/\partial z)_{13}$	$<K_\rho>_{13} \sim 1/N^2_{13}$	$<K_\rho>_{13} \sim 1/Ri_{13}$
$z_{1\text{-}3}$	$+0.50 \pm 0.27$	$+0.41 \pm 0.29$	-0.29 ± 0.30	$+0.36 \pm 0.29$

Tab. 5 As Table 4 but for coefficients resulting from hourly means (80 % significance range)

It seems to be the dependence $<K_\rho>_{13}$ ($<\varepsilon>_{13}$, $1/N^2_{13}$) is mainly based on methodic uncertainties. Nevertheless, we state from Table 5 that the relative contribution of $<\varepsilon>_{13}$ is about two times larger than that of $(1/N^2_{13})$.

Bulk exchange coefficient

It was mentioned above that meter-estimates of the exchange coefficient lead to relatively noisy results. Here we attempt to calculate this quantity at a coarser scale from less noisy bulk estimates. Hence, we used for the bulk exchange coefficient

$$K_{\rho 13} = \gamma\, <\varepsilon>_{13}/N^2_{13}\ ;\ \gamma = 0.2 \qquad (23)$$

10-hourly averages

With respect to corresponding mean values we refer to Table 3. The difference between both meter and bulk estimates reveals the order of about two. That means, there are energy-rich fluctuations of the high frequency scale in both dissipation and stratification, which are not able to influence the averaged values substancially.

Fluctuations of hourly means

Corresponding regression coeficcients are tabulated in Table 6.

Regression coeff. ρ/ depth layer	$K_{\rho 13} \sim \langle \varepsilon \rangle_{13}$	$K_{\rho 13} \sim (\partial u/\partial z)_{13}$	$K_{\rho 13} \sim 1/N^2_{13}$	$K_{\rho 13} \sim 1/Ri_{13}$
$z_{1\text{-}3}$	+0.77 ± 0.20	+0.27 ± 0.30	-0.28 ± 0.30	0.68 ± 0.23

Fig. 6 As previous Tables but using hourly means for bulk estimates (80 % significance range)

For bulk estimates, the flux coefficients are mainly determined by $\langle \varepsilon \rangle_{13}$ and $(1/Ri_1)$ on the related temporal scale. For example, the correlation between (K_ρ) and (1/Ri) is significant at the 98 % level explaining a local variability of about 46 %.

Conclusions

It seems to be possible to use simultaneous measurements of dissipation rate, vertical current shear, and stratification to describe turbulent fluxes locally. For 10 hourly averages, the stratification was guiding the dissipation rate and associated fluxes whereas shorter fluctuations occurring at the hourly scale could be probably attributed to the current shear. From our data, we found a linear correlation between bulk exchange coefficient $(K_\rho)_{13}$ and the reciprocal gradient Richardson number $(1/Ri)_{13}$ explaining 46 % of the variance. Estimates of the exchange coefficient based on the meter-hour scale scatter remarkably more; only 13 % of $(K_\rho)_{13}$ could be explained by $(Ri)_{13}$. Sources of scattering are probably produced by dissipation as well as by density fluctuations. Beside these natural effects there exists a serious difficulty to determine correctly the needed gradients of both density and current on this scale.

Our dissipation measurements were done in near coastal zones. Within the whole water column investigated, the dynamical regime was mainly controlled by the vertical current shear. This circumstance was well expressed through very small values of the gradient Richardson flux number. Furthermore, the locally advected background field of stratification influenced the fluxes essentially. Vertical gradients both in the current and in the density field are quite large in coastal regions of the Baltic Sea. This is based on

the wind-induced mixing starting at the sea surface and the strong stratification due to advection processes of riverine input of fresh water and the spreading of salty water from Baltic basins. Hence, the Baltic seems to be a good candidate for the test of different flux parameterizations under extreme conditions. Measurements of dissipation, current and density profiles, which should be combined with direct measurements of vertical fluxes of density $<w'\rho'>$ at fixed depths, should be jointly performed with standard meteorological measurements including solar insulation and thermal radiation.

Finally, we may conclude that, with enough data in time, there is a good possibility to estimate turbulent quantities in a proper way. However, to attribute short-time and long-time effects more distinct to the turbulence / transport variability and to obtain more accurate numeric relations, it is necessary to extend the length of time series on several days. The sampling rate of 15 minutes was appropriate. Further improvement in the parameterization would be obtained by the usage of moored Acoustic Doppler Current Profiler (ADCP) for a better resolved current / shear profile. Another permanent challenge is the determination of the micro-structure in the density field.

Acknowledgement

We would like to thank Eberhard Hagen for encouraging continuous support.

References

GREGG, M. C., 1987: Diapycnal mixing: A review. J. Geophys. Res. **92**, C5, 5249 - 5286.

KRAUS, E. B., 1972: Atmosphere-Ocean Interaction. (Clarendon, Oxford).

LANDOLT and BOERNSTEIN, 1989: Numerical Data and Functional Relationships in Science and Technology. New Series V. Volume 3: Oceanography. Subvolume b (Springer; Berlin).

MONIN, A. S., OZMIDOV, R. V., 1982: Turbulence in the Ocean. (Reidel, Dordrecht).

OSBORN, T. R., 1980: Estimates of the local rate of vertical diffusion from dissipation measurements. J. Phys. Oceanogr. **10**, 83 - 89.

PETERS, H., GREGG, M. C., TOOLE, J. M., 1988: On the parameterization of equatorial turbulence. J. Geophys. Res. **93**, C2, 1199 - 1218;

Surface Energy Fluxes and Mixed Layer Depth

- A Spring / Autumn Case Study -

Christoph Zülicke
Institute for Baltic Sea Research, Warnemünde, Germany

Olaf Hennig
Department of Physics, University of Rostock, Germany

Introduction

Exchange processes between air and sea are essential parameters, which influence both atmospheric and oceanic dynamics. Coupled circulation models need their parameterization for a proper description of associated fluxes on different spatial and temporal scales. Unfortunately, many numerical approaches use coarse-grained grids, which can not resolve sufficiently the involved spatial/ temporal scale of contributing processes. To measure associated fluxes, field campaigns were carried out sporadically by research vessels, ships of opportunity, moored and drifting buoys, air crafts, and satellites in different regions during different environmental conditions. Therefore, only sparse data sets, which are based of joint meteorological and hydrographical measurements, are available in international data banks. The available data only cover a certain space-time window and can not be used generally for a correct formulation of such interaction processes. In shallow water areas of semi-enclosed basins, like that of the Baltic Sea, we have a similar situation due to the limited space-time window of joint measuring campaigns. Here, a wind-driven hydrographic regime mainly determines all circulation dynamics and associated fluxes on different spatial and temporal scales.

We attempt to discuss the temporal variability of important flux parameters by means of usual bulk estimates. However, the main aspect lies in different averaging procedures reflecting different temporal scales. We used hourly averages of standard meteorological parameters (wind velocity, wind direction, air pressure, dry and wet air temperature, short/ long wave radiation) as well as vertical profiles of standard hydrographic parameters (pressure, temperature, salinity), which were recorded on board of R/V "A.v.Humboldt" in the Arkona/ Bornholm Basin during March, but in the Bornhom/

eastern Gotland Basin during September, 1994. The compiled data set allows the rough estimation of the energy balance within the near-surface layer. Consequently, we also represent estimates of the thickness of the wind-mixed layer, which is a basic parameter not only for applications in analytical and numerical circulation modelling but also in the marine biology (primary production).

Methods

The material fluxes of density, momentum and heat were estimated with aerodynamic bulk formulae according to Landolt and Boernstein (1989), p. 332, and Price et al. (1978). Our calculations are based on hourly averaged quantities collecting most of the turbulent energy. Such means are representative if they are calculated from samplings with a frequency of at least 1000 times per hour, Foken (1990). For this study, the sampling rate was 50 times per minute, i.e. we got 3000 samples a hour. According to Foken (1990), we accepted the linear wind-dependence of the bulk coefficients. The flux of the latent heat (L_0) is related to the evaporation and can be approximated by

$$L_0 = L\, \rho_a\, C_{Ea}\, u_{a10}\, (q_{a0} - q_{a10}) \,.$$

Here, L is the latent heat of evaporation. The atmospheric parameters (cf. the Appendix for numerical values) are the air density (ρ_a), the atmospheric bulk coefficient for evaporation (C_{Ea}), wind velocity (u_{a10}) observed at 10-meter above the sea surface, and the specific humidity (q) at the sea surface (q_{a0}) and at the 10 meter level (q_{a10}). The analogous approximation for the sensible heat flux is given by

$$H_0 = c_{pa}\, \rho_a\, C_{Ha}\, u_{a10}\, (\, T_0 - T_{a10} - \gamma_{a10}\,)$$

and includes the values of atmospheric heat capacity (c_{pa}), the bulk coefficient for sensible heat (C_{Ha}), and temperature measurements at the sea surface (T_0) and at the 10 meter horizon (T_{a10}). The coefficient (γ_{a10}) reflects the adiabatic lapse correction according to the temperature decrease with decreasing pressure. Finally, the surface shear stress was estimated by the semi-empirical formulae

$$\tau_0 = \rho\, u_{*0}^2 = \rho_a\, C_{Da}\, u_{a10}^2 \,. \qquad \text{(directed downward)}$$

Here, $u_{*0}^2 = (\tau_0 / \rho)$ is the squared friction velocity. The basic parameter is, however, the bulk coefficient for momentum, the so-called drag coefficient (C_{Da}).

To estimate the short-wave flux of (solar) radiation (R_{SW}), we assumed a constant albedo (A) and directly measured the related downwelling component (R_{SW-}) by means of a pyranometer. Concerning more sophisticated ansatzes, we like to refer to Payne (1972). We adopted the balance

$$R_{SW0} = (1 - A)\, R_{SW-} . \qquad \text{(positive downward)}$$

The resulting bulk heat flux depends from the solar absorbtion length of several 10 m depth.

The long-wave (thermal) radiation (R_{LW0}) was derived from the following balance

$$R_{LW0} = \epsilon\, \sigma\, T_0^4 + (1 - \epsilon)\,(R_{tot-} - R_{SW-}) .$$

The first term on the right hand side is the radiation emitted by the sea surface with its thermal emissivity (ϵ) and the Stefan- Boltzmann constant (σ). The second term reflects the thermal backward radiation (downwelling) from the atmosphere. Its contribution was determined as the difference between the total downwelling radiation (R_{tot-}), which was measured by the pyrradiometer, and the short-wave downwelling radiation (R_{SW-}).

With respect to the exchange of heat we summarize:

$$J_0 = L_0 + H_0 + R_{LW0} \qquad \text{(positive upward)}$$

All terms of (J_0) must be balanced in the upper layer of several 10 μm thickness. Its positive sign, however, counts losses for the sea surface (cooling) and vice versa.

Data base

The data were acquired by two cruises of the R/V "Alexander von Humboldt" during running GOBEX activities in the Arkona, Bornholm, and eastern Gotland Basin in March and September, 1994. Our measurements were carried out in the framework of the sub-project "Baltic Radiation Budget (BARB)", which was jointly organized by the Institute for Baltic Sea Research Warnemünde (IOW) and the Institute for Remote Sensing Applications (IRSA) of the European Research Centre in Ispra, Italy, to provide new calibration procedures for remotely sensed data in the Baltic Sea. The used acronyms are tabulated in Table 1 together with time tables and target areas. Obtained data cover

standard meteorological parameters in combination with measurements of solar and thermal radiation.

Acronym	GX040301.AVH	GX940913.AVH
Time	01.03.94-10.03.94	013.09.94-29.09.94
Target region	Arkona Basin, Bornholm Basin	Bornholm Basin, Gotland Basin

Table 1: Data acronyms, time table, and target areas of the GOBEX sub-project BARB

Surface energy fluxes

Time series

The inspection of available time series indicates that the shear stress irregularly fluctuates on different temporal scales. Records of the March cruise are plotted in Fig. 1a and clearly reveal short-term variations (hourly scale), which are superimposed on more low frequency fluctuations (daily scale). During March, a relative silent phase is followed by a more active one. The September records are drawn in Fig. 2a. Peak values occur every 3-5 days. Such quasi-period corresponds to that of the synoptic weather cycle in the Baltic Sea. Visually, we may conclude that the amplitudes of contributing short term variations are relatively independent from the seasonal cycle while those of longer periods change significantly the amplitude between early spring (March) and late summer/ early autumn (September). Related peak values increased by a factor of about two from March (~ 0.4 N/m^2) to those in September (~ 0.7 N/m^2).
The corresponding response of the surface heat flux is shown in Fig.1b and Fig. 2b. Here, relatively small fluctuations determine the resulting curves. A strict downward trend occurs in March and the values change their sign at the mid of the observational

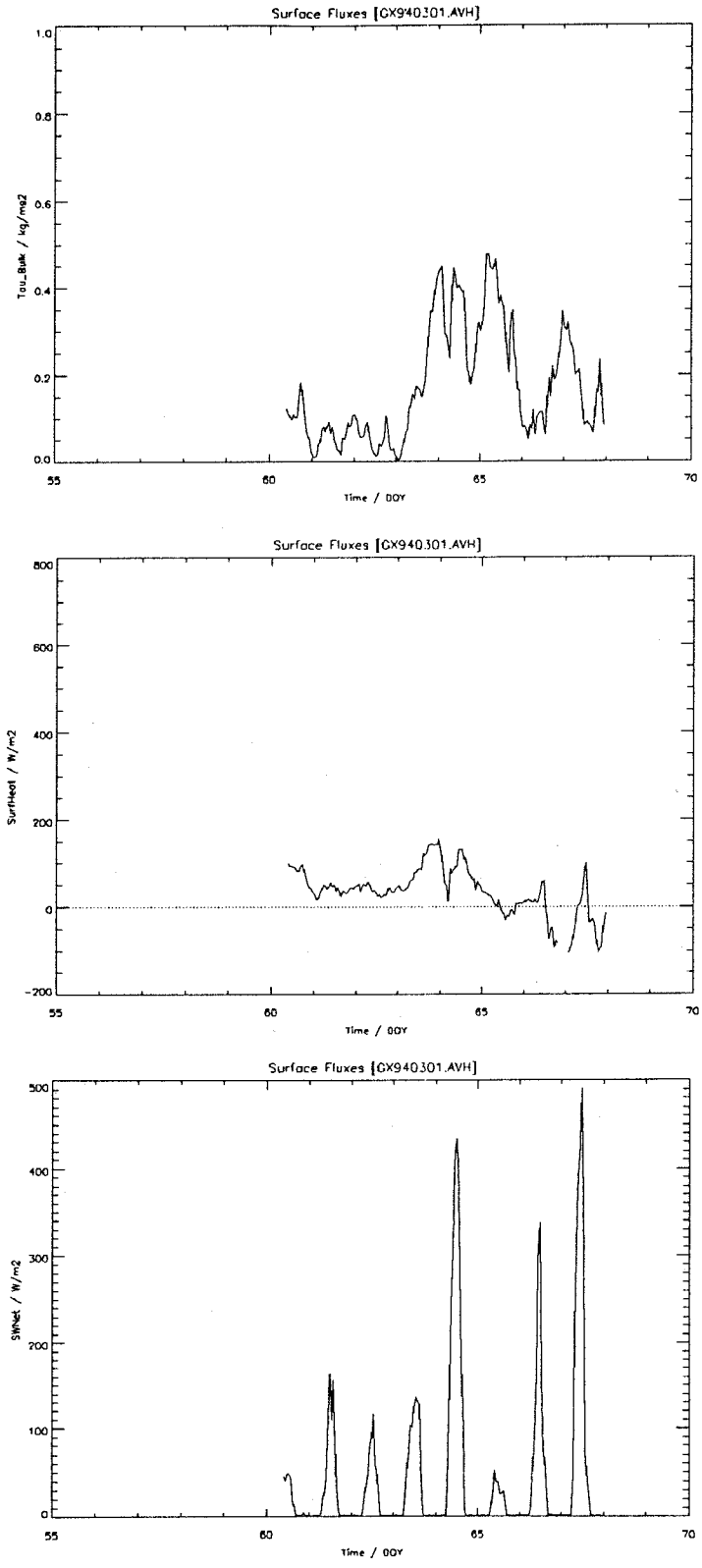

Fig.1 (a,b,c) Time series of surface heat fluxes for GX 0301.AVH (Hourly averages of shear stress (kg/ m s^2; upper panel], surface heat [middle panel] and solar radiation flux (W/ m^2; lower panel])

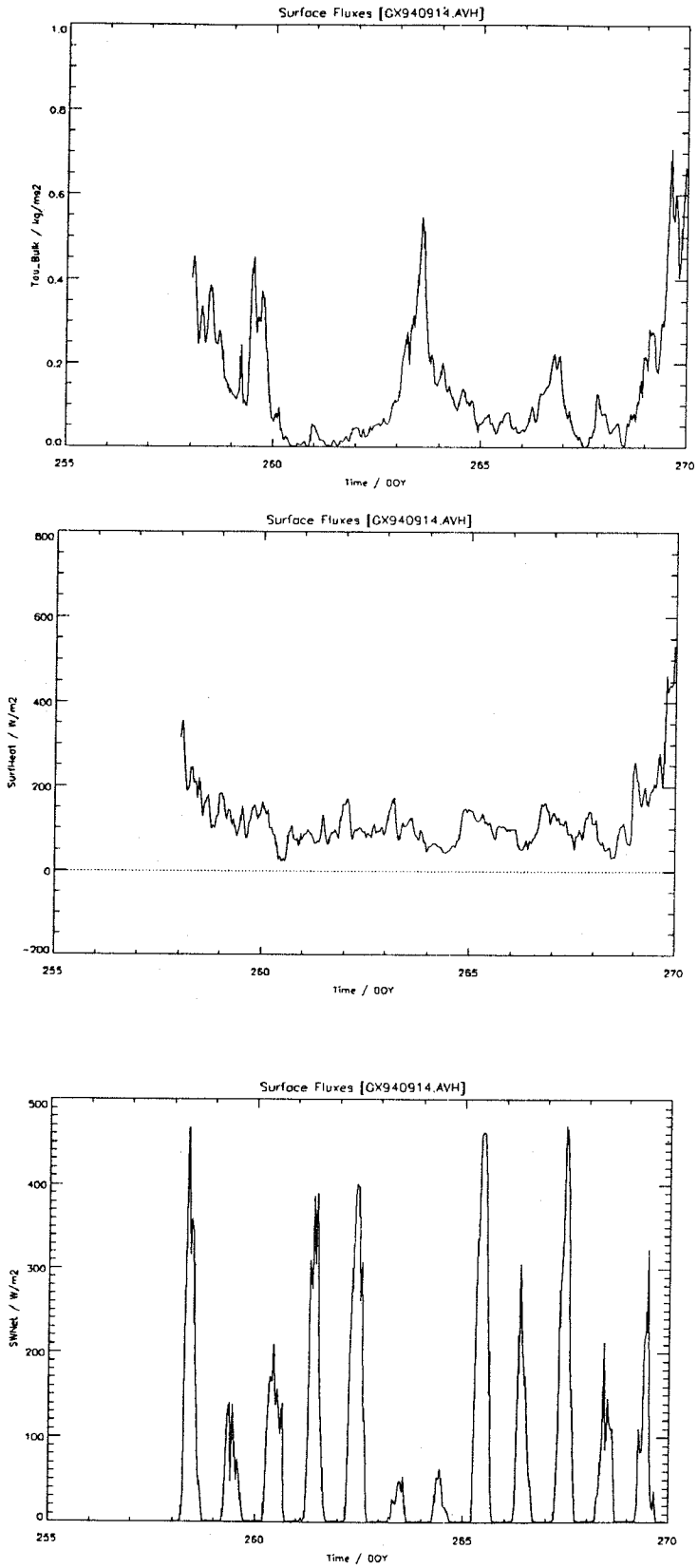

Fig.2 (a,b,c): As in Fig.1 but for GX940913.AVH

period. This fact indicates the turning from a negative heat balance during the first stage to a positive one during the last stage. There is some observational evidence that the trend is basically caused by increasing heating processes and associated changes are related to a (seasonally forced) warming of air masses within the atmospheric boundary layer. There is no similar signal recorded in September. Only positive values are plotted revealing larger amounts of cooling (up to a factor of about 2-3). The total curve suggests a very low frequency sine-like signal with peak values at the beginning and ending stage. This curve also suggests more intense fluctuations in the temporal range of several hours, which are characterized by fluctuating wind velocities. Consequently, periods with strong winds force a negative heat balance and support robust cooling in the order of 100 W/ m^2.

The astronomic watch is ticking through the diurnal cycle, Fig. 1c and Fig. 2c. Depending on the cloudiness, the solar radiation reaches peak values of about 500 W/ m^2. More in detail, it seems to be that the first observational stage in March is characterized by low insulation (Fig.1c), moderate heat loss (Fig.1b), and weak wind stress (Fig.1a). Nearly inverse conditions are recorded during the second stage. The synoptic weather cycle dominates in September. Strong winds and reduced solar insulation produce cooling. A drastic example is given by an extreme peak value observed at the last day of measurements (Fig.2). For daily periods, we state a positive correlation between wind speed and insulation during March (early spring) but a negative correlation in September (late summer/ early autumn).

Variability

In the following we compare flux quantities based on different averages for both cruises covering 9 days in March but 12 days in September. We want to quantify substantial changes of fluxes, which result from different average procedures. Here, we have to take into account the corresponding variance, too. All averages are constructed of different sub-samples smoothing out different temporal scales:

- hourly means (micro- scale / turbulence)
- 6-hourly means (meso- scale/ short term variations),
- daily means (diurnal cycle),
- 5-daily means (synoptic weather cycle).

All available data are considered for each averaging interval. Resulting shear stress

values are tabulated in Table 2a..

Shear Stress τ / kg/ms^2 based on	GX940301.AVH		GX940913.AVH	
1-h-means	0.174 ± 0.131	183	0.141 ± 0.142	288
6-h-means	0.170 ± 0.125	31	0.138 ± 0.135	48
1-d-means	0.158 ± 0.107	8	0.132 ± 0.118	12
5-d-means	0.129 ± 0.026	3	0.116 ± 0.050	3

Tab. 2.a: Shear stress values (kg/ m s^2=N/ m^2) given by (mean values +/- standard deviation) and the number of sub-samples)

Comparing hourly and five daily means, we state a systematic underestimation (about 20%). Consequently, the principal usage of hourly means is recommended. Otherwise the contributions of energy-rich fluctuations will be smoothed out and errors are produced systematically.

The consequences are not as clear for the surface heat flux. For changes in the latent heat flux, the corrections are given in terms of the cross- covariances between fluctuations in the wind-stress and humidity. Table 2b suggests that resulting means do not differ significantly. Comparing again hourly and five-daily means the corrections would be 5 W/ m^2 in March but -2 W/ m^2 in September.

Surface heat flux J_0 / W/m^2 based on	GX940301.AVH		GX940913.AVH	
1-h-means	30.9 ± 59.2	181	120.2 ± 71.8	285
6-h-means	32.6 ± 56.4	31	119.8 ± 68.2	48
1-d-means	34.3 ± 53.2	9	123.1 ± 25.4	12
5-d-means	35.3 ± 51.9	3	118.2 ± 25.4	3

Tab. 2.b: As Table 2a but for the surface heat flux

Both values are fairly below the methodic accuracy. Nearly constant variances indicate a homogeneous energy distribution over all averaging intervals in March. Different conditions result from the September campaign. Here, variances permanently decrease with increasing averaging interval. That suggests a higher energy accumulation in the high frequency range.
Similar tendencies are obtained in corresponding variances, which result from estimates of the solar radiation flux. Their interpretation must be attributed to the diurnal cycle. Independent from different averaging intervals, the means are roughly constant while related variances decrease with increasing averaging interval, Tab. 2c.

Solar radiation flux J_{sw0} / W/m^2 based on	GX940301.AVH		GX940913.AVH	
1-h-means	50.2 ± 97.7	182	71.1 ± 116.9	287
6-h-means	49.8 ± 78.1	31	72.0 ± 105.0	48
1-d-means	48.9 ± 24.9	9	65.1 ± 32.2	12
5-d-means	46.1 ± 29.3	3	67.2 ± 17.6	3

Tab. 2.c: As previous Tables but for the solar radiation flux

Mixed layer energy balance

In general, we are interested in the seasonal cycle of mixed-layer properties. Our data provide, at least, two characteristic values for spring (March) and autumn (September). Therefore, we estimated the depth of the wind-mixed layer by means of surface energy fluxes mentioned above.

We start our study with a simple model, which is described by Kraus and Turner (1967) and by Niiler and Kraus (1977). The Surface Mixed Layer (SML) is completely homogenized by the action of the turbulent kinetic energy. For simplification, we proceed with a resting SML of thickness (h) under stationary conditions. Hence, the stationary turbulent kinetic energy equation for this case reads

$$0 = m_1 u_{*0}^3 + h/2\, B_0 + (h/2 - 1/\gamma)\, R_0 - \epsilon_1 h \,.$$

It allows the estimation of (h). Here, (m_1) is an empirical constant to be determined. The

surface buoyancy flux is formulated by

$$B_0 = g \left(\alpha/c_p\rho \, J_0 - \beta \, S_0 \, (E_0 - P_0) \right) .$$

The extinction coefficient for solar radiation is given by (γ), the normalized solar radiation flux at the sea surface by

$$R_0 = g \, \alpha/c_p\rho \, R_{sw0} ,$$

and the mean dissipation rate by (ϵ_1). We get finally

$$h = [\, m_1 \, u_{*0}^3 - R_0 / \gamma \,] / [\, \epsilon_1 - B_0/2 - R_0/2 \,] .$$

This depth is directly proportional to the shear production by wind and gravity waves released. Its reduction is caused by the stabilizing effect of stratification due to solar heating. If the dissipation becomes dominant, (h) decreases. Both terms (B_0) and (R_0) are responsible for increasing (h) due to destabilization effects near the sea surface.

Following Niiler and Kraus (1977) we leave $m_1 = 1.0$ and the extinction depth scale ($1/\gamma$) = 10 m. The dissipation rate is fixed to a certain check value ($\epsilon_1 = 10^{-5}$ W/ kg). Neglecting the salt effect on buoyancy, we tabulated our check values of both cruises in Table 3.

Parameter/ Cruise	GX940301.AVH	GX940914.AVH
Shear-production ($m_1 u_{*0}^3$ / m^3/s^3)	$2.197 \pm 2.535 \, 10^{-6}$	$1.728 \pm 2.592 \, 10^{-6}$
Surface buoyancy flux (B_0 / m^2/s^3)	$28.2 \pm 42.3 \, 10^{-9}$	$85.9 \pm 51.3 \, 10^{-9}$
Solar radiation flux (R_0 / m^2/s^3)	$35.8 \pm 69.9 \, 10^{-9}$	$51.2 \pm 83.4 \, 10^{-9}$
Dissipation rate (ϵ_1 / W/kg)	$1.0 \, 10^{-5}$	$1.0 \, 10^{-5}$
Mixed layer depth (h / m)	18.4	12.2

Tab. 3: Characteristic surface energy budget and mixed layer depth for the March (second column) and September cruise (third column); cf. related constants in the Appendix.

During March, the shear-production ($m_1 u_{*0}^3$) and the associated mixed layer depth (h)

indicate larger values than those observed in September. Opposite conditions are estimated for the surface buoyancy flux (B_0) and the solar radiation flux (R_0) reflecting more intense heat losses and solar insulation. We got a positive heat balance in March ($R_0 > B_0$) but a negative one in September ($R_0 < B_0$). However, for both cases listed in Table 3, the most important contributions result from terms of the shear stress and dissipation. Therefore we can simply use the following approximation

$$h = m_1 u_{*0}^3 / \epsilon_1 .$$

Discussion

We measured surface energy fluxes during spring and autumn at two cruises in the Baltic Proper. During spring environmental conditions, the wind was fresh and the solar insulation was relatively large. In autumn, however, strong cooling occurred under moderate winds.

Different averaging procedures elucidated that flux quantities need properly sampled hourly means of standard meteorological parameters including radiation. To achieve this goal, continuous records with a sampling frequency of about one Hertz are needed. Hourly mean values should be available at least four times a day. To study the impact of different averaging lengths on flux estimates, the statistical properties of the meteorologic parameters must be studied carefully to obtain the wanted correction for the bulk formulae under discussion.

Estimates of the depth of the wind-mixed layer showed the dominating influence of wind-generated vertical current shear and dissipation during spring and autumn. These findings could be strictly modified for summer periods by the solar insulation but for winter periods by increased cooling at the sea surface. Our investigations of the Surface Mixed Layer only used meteorological standard observations. For the next future, however, joint hydrographic in-situ measurements are needed together with records of dissipation rates and current measurements from moored current meters/ ADCP's. This comprises more sophisticated estimates of spatial/ temporal turbulence- scales under different environmental conditions. According to Stevenson (1979), carefully determined dissipation rates are needed to check the entrainment, which couples the near-surface dynamics with those in superficial layers.

Acknowledgement

Funding of one of the authors (CZ) was provided by the *Kultusministerium des Landes Mecklenburg-Vorpommern*, grant no. 0710, M604, 68101-05, and the EU programme *Human Capital and Mobility*, contract no. ERBCHRXCT930312. This paper benefited from helpful comments of Eberhard Hagen.

References

FOKEN, TH., 1990: Turbulent energy exchange between atmosphere and surface. Berichte des Deutschen Wetterdienstes **180**, Dt. Wetterdienst, Offenbach/Main, pp. 287, (in German).

KRAUS, E. B. AND J. S. TURNER, 1967: An one-dimensional model of the seasonal thermocline. II: The general theory and its consequences. Tellus, **19**: 98-106.

LANDOLT AND BOERNSTEIN, 1989: Numerical data and functional relationships in science and technology, New Series V/3b, Springer, Berlin.

NIILER P. P. AND E. B. KRAUS, 1977: One-dimensional models of the upper ocean. In: Modelling and Prediction of the Upper Layers of the Ocean,Editor: E.B.Kraus, Proc. NATO Advanced Study Inst., Pergamon, Oxford, pp. 143-172.

PAYNE R. E., 1972: Albedo of the sea surface. J. Atm. Sci., **29**: 959-970.

PRICE J. F., CH.N. K. MOERS, J. C. VAN LEER, 1978: Observation and simulation of storm-induced mixed- layer deepening. J. Phys. Oceanogr., **8**: 582-599.

STEVENSON, J. W., 1979: On the effect of dissipation on seasonal thermocline models. J. Phys. Oceanogr., **9**: 57-64.

Appendix: Material constants

$\rho_a = 1.203$ kg/m^3	air density
L = 2.5 10^6 J/kgK	latent heat of evaporation
$c_{pa} = 1000$ J/kgK	(isobaric) heat capacity of air
$\gamma_{a10} = 0.1$ K	atm. adiabatic lapse rate for 10 m height
g = 9.81 m/s^2	gravitational acceleration
$\alpha = 3.0\ 10^{-4}$ 1/K	(isobaric) thermal expansion coefficient
$\rho = 1025$ kg/m^3	water density
$c_p = 2000$ J/kgK	(isobaric) heat capacity of water
	atm. bulk coefficients

$C_{Ea} = C_{Ha} = 10^{-3}$	: $u_{a10} < 7.0$ m/s
$C_{Ea} = C_{Ha} = 10^{-3}\ (\ 1.0 + 0.054\ (u_{a10} - 7.0\ )\ )$	: $7.0 < u_{a10} < 20.0$ m/s
$C_{Da} = 10^{-3}\ 1.2$	: $u_{a10} < 7.0$ m/s
$C_{Da} = 10^{-3}\ (\ 1.2 + 0.065\ (u_{a10} - 7.0\ )\ )$	: $7.0 < u_{a10} < 20.0$ m/s

---

A = 0.06	Albedo of sea water (for diffuse solar irradiation)
$\epsilon = 0.98$	Emissivity of sea water (in the thermal range)
$\sigma = 5.67\ 10^{-8}$ W/m^{2}K^4	Stefan-Boltzmann constant
$\gamma = 0.1$ 1/m	Solar extinction coefficient

The Carbon Budget in Gotland Sea Surface Waters: October to February

B. Schneider, H. Thomas, A. Stamer
Institute for Baltic Sea Research, Warnemünde, Germany

Summary

The carbon budget of the Gotland Sea surface waters was investigated by measurements of total carbonate (Ct), particulate organic carbon (POC) and the surface CO_2 partial pressure (pCO_2) during two cruises in October 1995 and February 1996. The surface Ct pool increased by 0.66 mol/m² during the time span between the cruises. This could partly be explained by CO_2 uptake from the atmosphere (0.18 mol/m²) and input by diapycnal mixing (0.06 mol/m²). The remaining Ct excess and the almost negligible loss by advection (0.02 mol/m²) must be balanced by decomposition of POC (0.44 mol/m²). Since the total decrease of POC between October and February was 0.61 mol/m², the difference of 0.17 mol/m² is attributed to sedimentation.

Introduction

The marine carbon cycle has gained increasing attention during the last decade, because it is closely linked to the atmospheric CO_2 budget and thus to the fate of anthropogenic CO_2 emissions. In addition to this aspect, which is of minor importance for the Baltic Sea, the carbon cycle plays a central role for the cycles of many seawater constituents such as nutrient elements, trace metals and organic contaminants.

In a first step, our investigations on the carbon cycle in the Baltic Sea are confined to surface waters in the eastern Gotland Sea. The approach is based on measurements of total carbonate (Ct), particulate organic carbon (POC), dissolved organic carbon (DOC) and the surface CO_2 partial pressure (pCO_2). The data are used to calculate seasonal changes of the pools of Ct, POC and DOC, and to explain these changes by internal transformations and external fluxes. Unfortunately, data for DOC are not yet available. Nevertheless, an attempt is made to construct a scheme for the carbon budget for the time span between two cruises in October and February.

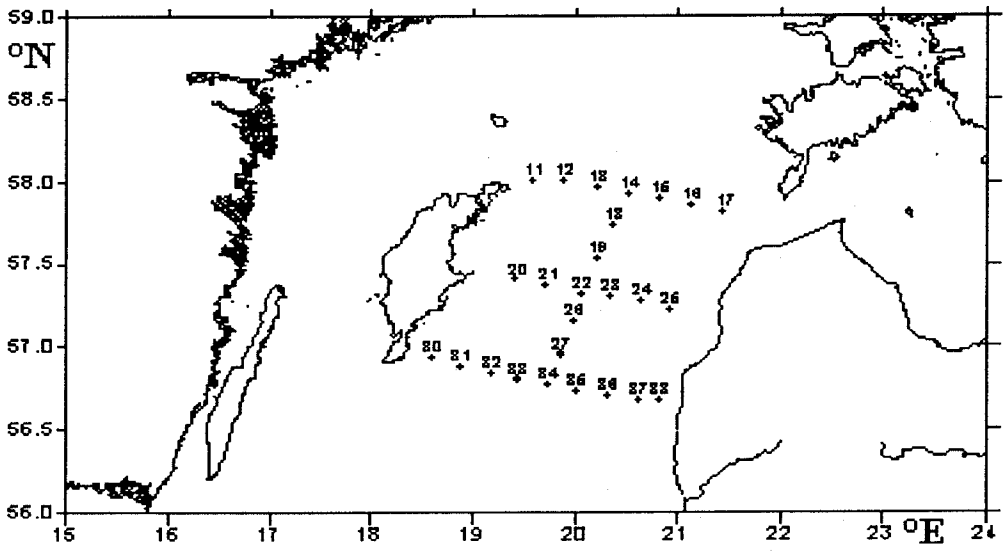

Fig. 1: Station map for the Gotland Sea surface box.

Methods

A box is defined, which ranges from the sea surface to the halocline and is horizontally bordered by the northern and southern connecting lines between Gotland and the Latvian coast (Fig.1). The vertical profiles of Ct and POC were determined at 26 stations during two cruises with "A.v.Humboldt" in October 1995 and February 1996. The vertical sampling resolution was adjusted to the stratification pattern of the water column. Surface pCO_2 was continuously measured in the box area.

Samples were analyzed for Ct by the coulometric SOMMA system according to Johnson et al. (1993). For the determination of POC, suspended particulate matter was collected on glass fiber filters, combusted in an oxygen flow and the carbon content measured as CO_2 by infra-red spectrometry. The estimated accuracy of the Ct and POC measurements was (+/- 2) μmol/kg.

The pCO_2 was determined with an accuracy of (+/- 2) μatm by continuous equilibration of surface water with a closed loop of air and integrated infra-red CO_2 detection, cf Schneider et al. (1992) and Körtzinger et al. (1996). CTD profiles were recorded at each sampling station.

Results and Discussion

The carbon pools

The pools of Ct and POC in the Gotland Sea surface box are calculated for each sampling period on the basis of the corresponding vertical profiles. The concentrations of Ct and POC are integrated over depth between the sea surface and the halocline. Values between the sampling depths are obtained by linear interpolation. Averaging the integral Ct and POC values over all stations yields the pools of Ct and POC in terms of mol/m^2.

Total carbonate

Typical vertical Ct distributions for October and February are shown in Fig.2. The situation in October is characterized by a flat (20 m) thermic surface layer which preserves the Ct depletion caused by biomass production. Below this layer, Ct is increasing because decomposition of organic matter prevails over production. In February convective mixing leads to a homogenous distribution of Ct between the surface and the halocline. Concentrations closed to the surface are by approximately 60 μmol/kg higher than in October. But the increase can only partly be explained by mixing, since the integral Ct in February exceed the corresponding values in October by up to 3 mol/m^2.

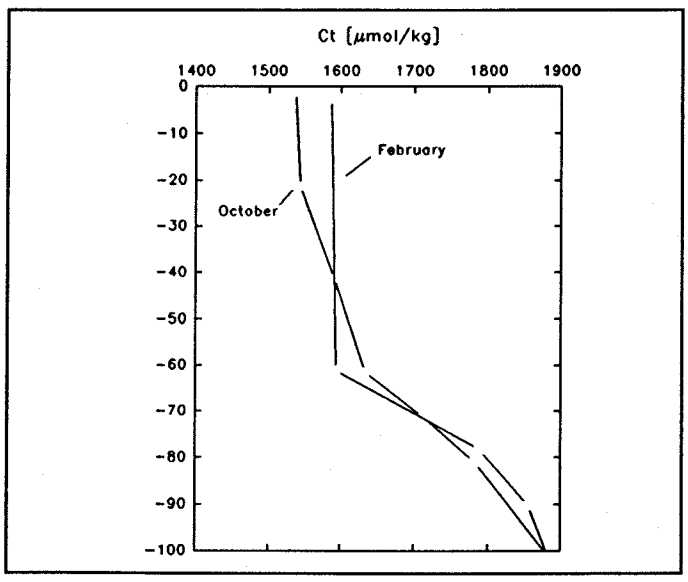

Fig. 2: Vertical profiles (depth/m) for total carbonate in October and February.

Only at three stations a minor Ct deficiency was observed. The mean difference between the integral Ct in February and October amounts to 0.66 mol/m² and represents the increase of the Ct pool. This value corresponds to a mean increase of Ct in the surface box of 10 μmol/kg which is well beyond the accuracy of our measurements.

Particulate organic carbon

An example for the vertical profiles of POC is given in Fig.3. High concentrations of about 25 μmol/kg in the thermic surface layer during October can be attributed to continual biological production. The standard deviation of the mean value is only (+/- 4) μmol/kg and indicates a low spatial variability. Below the thermocline, POC concentrations are decreasing rapidly to values of about 5 μmol/kg. This concentration level is also observed in February, but throughout the water column between the surface and the halocline. Hence, the POC pool is decreasing and the difference between the mean integral POC in October and in February yields a deficiency of 0.61 mol/m².

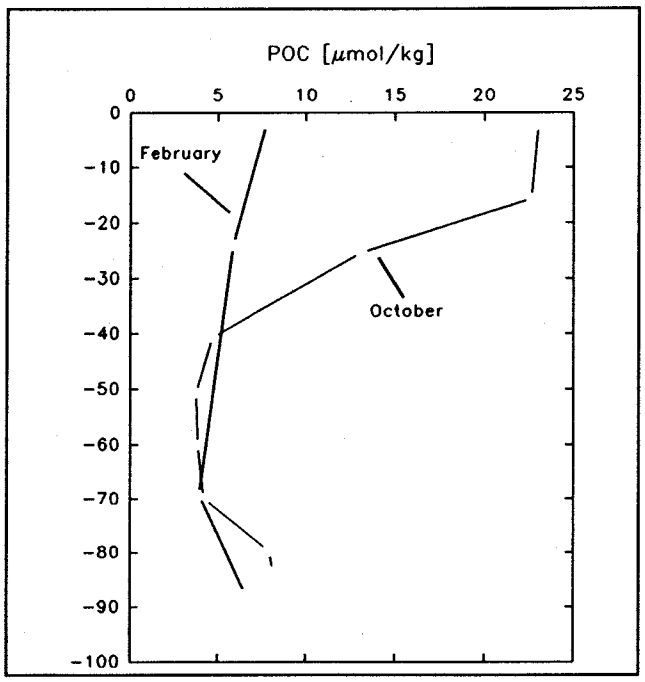

Fig. 3: Vertical profiles (depth/m) for particulate organic carbon in October and February.

The carbon fluxes

The carbon fluxes across the vertical and horizontal interfaces are calculated in order to establish the carbon budget for the Gotland Sea surface box. On the basis of our measurements, an estimate is given for the CO_2 exchange with the atmosphere, for the Ct flux by diapycnal mixing at the halocline and for the advective Ct transport across the northern and southern margins of the box.

CO2 exchange with the atmosphere

The exchange of CO_2 with the atmosphere is driven by the CO_2 partial pressure difference between surface water (sw) and the atmosphere (atm):

$$\Delta pCO_2 = pCO_2(sw) - pCO_2(atm).$$

The $pCO_2(sw)$ at the surface of the Gotland Sea box as well as the mean $pCO_2(atm)$ are plotted against latitude in Fig.4. An extreme variability is observed for $pCO_2(sw)$ during both seasons. This is the consequence of variations in temperature, salinity, total carbonate and alkalinity in the box area and demonstrates the outstanding sensitivity of the $pCO_2(sw)$ with regard to changing physical and chemical conditions. The $pCO_2(sw)$ in October is below the $pCO_2(atm)$ and indicates a CO_2 flux from the atmosphere into the surface water. In February the $pCO_2(sw)$ exceeds the atmospheric value and leads to the release of CO_2 from the sea surface.

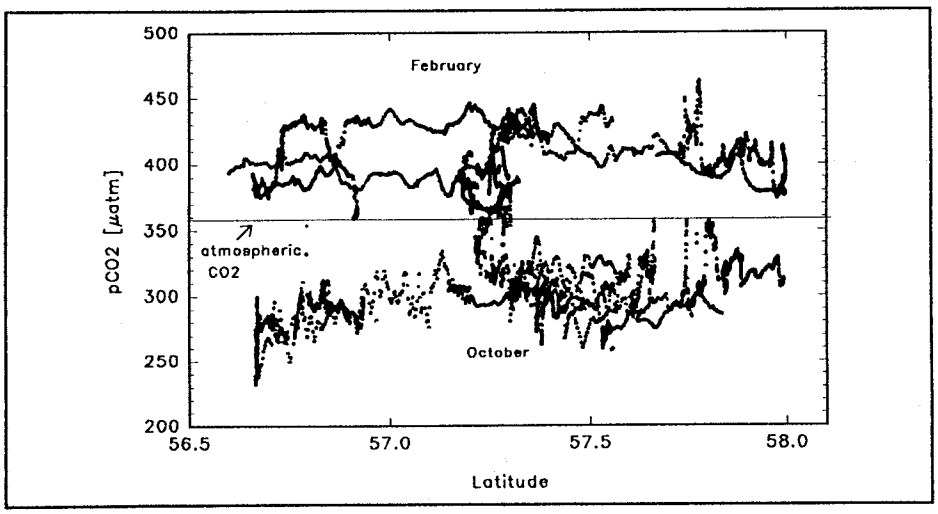

Fig. 4: CO2 partial pressure in surface waters of the Gotland Sea during October and February.

To account for the spatial variability of $pCO_2(sw)$, the surface of the box is covered by a grid with a resolution of 0.2°(latitude) X 0.4°(longitude). Assuming a linear increase of $pCO_2(sw)$ between October and February, mean ΔpCO_2 are calculated for each grid element. Approximately 75 % of the grid values were negative and imply a net flux of CO_2 from the atmosphere into the sea surface. Positive ΔpCO_2 and thus a CO_2 flux into the atmosphere were found for the northeastern region of the box which is influenced by the Gulf of Riga.

To estimate the CO_2 fluxes according to

$$F(atm) = k_{ex} * \Delta pCO_2, \qquad (1)$$

the exchange coefficient k_{ex} is calculated for a mean wind speed of 10 m/s on the basis of two alternative parameterization schemes. The approach by Liss and Merlivat (1986) yields a mean CO_2 uptake for the entire box area of 0.12 mol/m², whereas by calculations according to Peng and Takahashi (in Tans et al., 1990) a value of 0.24 mol/m² is obtained. This discrepancy shows that the uncertainties in quantification of the CO_2 air/sea exchange are still high. Since it cannot be decided, which of the two approaches is the more realistic one, the results are averaged and a value of 0.18 mol/m² is used for the budget calculations.

Total carbonate exchange across the halocline

Diapycnal mixing in connection with strong Ct gradients across the halocline (Fig.2), which is approximately identical with the pycnocline, generates a Ct flux from the deep water into the surface box:

$$F(diap.) = D * \Delta Ct/\Delta z \qquad (2)$$

The diffusion coefficient D is determined by the density gradient at the main pycnocline using the relationship suggested by Broecker and Peng (1982). The mean density gradient of $7.8*10^{-7}$ g/cm^{-4} calculated from the CTD profiles, yields a diffusion coefficient of $5*10^{-3}$ cm²/s. The corresponding mean Ct gradient is approximately 130 μmol/kg over a depth interval of 10 m and equivalent to 1.3 mol/cm^4. By multiplication with D, a flux of 0.06 mol/m² is obtained for the period October to February.

Advective Ct flux

Since no horizontal gradients were observed for POC, only advective Ct fluxes are considered. Assuming a net volume flow (v) through the box from the north to the south and taking into account the Ct difference between the northern and southern margin of the box, the advective Ct flux is given by:

$$F(Ct) = (v/A) * (Ct[north] - Ct[south]) \quad (3)$$

The area of the box (A) is introduced in order obtain flux units. In analogy to (3), the advective salt flux can be expressed and combination with (3) gives:

$$F(Ct) = F(S) * (Ct[north] - Ct[south]) / (S[north] - S[south]) \quad (4)$$

If we assume a steady state for the salinity in the surface box, the salt flux by advection must be equal to flux by diapycnal mixing and can be calculated according to (2) ($4.8 * 10^{-9}$ g/cm² sec). Since also the mean Ct and S differences between the northern and southern box margins are available by the measurements (11 μmol/kg and 0.23 ‰, respectively), equation (4) can be used to estimate the net advective Ct flux. For the period between October and February a net outflow of 0.02 mol/m² is obtained. This estimate is a first order approximation and contains considerable uncertainties. However, these can be tolerated, because the contribution of the advection term to the carbon budget seems to be of minor importance.

The carbon budget

Based on the temporal changes of the carbon pools and the flux estimates, a carbon budget for the time span between October and February is outlined for the Gotland Sea surface box (Fig.5). With regard to the Ct pool, an increase of 0.66 mol/m² results from the measurements. The atmospheric input (0.18 mol/m²) and the diapycnal mixing (0.06 mol/m²) account for about one third of this excess. Taking into account the removal of Ct by advection (0.02 mol/m²), a Ct source of 0.44 mol/m² must exist. Due to missing data for DOC, we attribute this remaining increase to the decomposition of POC. Since the total decrease of the POC pool is 0.61 mol/m², the difference of 0.17 mol/m² is explained by sedimentation.

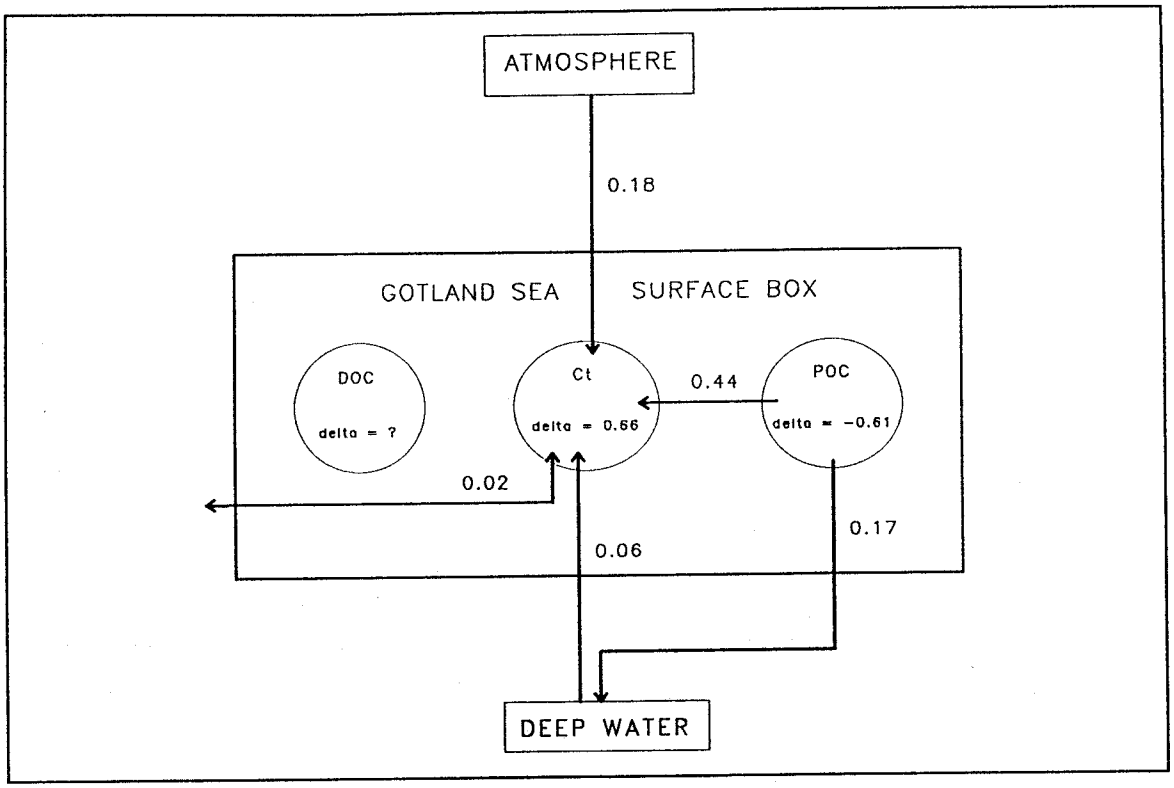

Fig. 5: The carbon budget for the Gotland Sea surface box.

Conclusions

A first step towards the comprehensive description of the Baltic Sea carbon cycle was made by our investigations in a well defined surface box in the eastern Gotland Sea. Due to a dense station network and high quality analytical data, a scheme for the carbon budget from October to February could be constructed, which will serve as the basis for future investigations. It is planned to resolve the complete seasonal carbon cycle and to include DOC into the budget calculations. Finally, we intend to deploy sediment traps to determine the POC export independently and to examine the internal consistency of the carbon budget.

References

BROECKER W.S., T.H. PENG, 1982: Tracers in the Sea. Lamont Geological Observatory, Columbia University, Palisades, Eldigio Press, New York.

JOHNSON K.M., K.D. WILLS, D.B. BUTLER, W.K. JOHNSON, C.S. WONG, 1993: Coulometric total carbon dioxide analysis for marine studies: maximizing the performance of an automated gas extraction system and coulometric detector. Mar.Chem., **44**, 167-187.

KÖRTZINGER A., H. THOMAS, B. SCHNEIDER, N. GRONAU, L. MINTROP, J.C. DUINKER, 1996: At-sea intercalibration of two newly designed underway pCO_2 systems: encouraging results. Mar.Chem., **52**, 133-145.

LISS P.S., L. MERLIVAT, 1986: Air-sea gas exchange rates. Introduction and synthesis. In: The Role of Air-Sea Exchange in Geochemical Cycling. Editor: P. Buat-Menard, NATO ASI Series, C185, Reidel, 113-127.

SCHNEIDER B., K. Kremling, J.C. DUINKER, 1992: CO_2 partial pressure in Northeast Atlantic and adjacent shelf waters: Processes and seasonal variability. J. Mar. Syst., **3**, 453-463.

Optically Active Components and Their Relationship With Meso-Scale Features in Baltic Coastal Zone

M.D. Dowell, Department of Oceanography, University of Southhampton, UK

Introduction

The Baltic Sea represents one of the major European semi-enclosed seas. Changing conditions in the policies of the bordering eastern European countries have catalyzed a sudden increase in collaborative research initiatives in the region. Additionally increased sampling possibilities due to the rapid technological advancement on research vessels as well as in laboratories, increased computer power, and a new generation of satellites have made, interdisciplinary oceanographic surveys more attainable, cf. DICKEY (1991).

Recently there has been much interest in the interaction of processes involving physical forcing and biological response in the marine environment, NIHOUL (1986). LEGENDRE and DEMERS (1984) termed this situation "Dynamic Biological Oceanography". Areas of enhanced primary production, coinciding with specific physical conditions defined as ergoclines by LEGENDRE et al. (1986), have been described regionally and seasonally in the literature. The highest values of chlorophyll concentration and primary production in the Baltic region are, reported as being in the highly dynamic coastal zones, LASSIG et al.(1978). Processes in these areas play a substantial role in the whole of the seas ecology, SEMOVSKI (1995). Consequently, the hydrographic regime of the Baltic Sea with low salinity and highly eutrophicated coastal zones influences the net productivity of the entire Baltic Sea on the decadal time-scale, NEHRING (1990). Therefore considering the recent tendency in the temporal development of the Baltic ecosystem, the examination of exchange processes between coastal zones and deep basins is obviously very important.

This was a principal topic of investigation of the international Gotland Basin Experiment (GOBEX), which was carried out during 1994/ 1995. No permanent currents exist in the Baltic such as the Norwegian Coastal Current in the North Sea. Here, wind-driven motions are forced by alternating wind conditions on the synoptic time-scale of several days. Due to the relatively small size of the Arkona Basin, Bornholm Basin, and Gotland Basin with a horizontal scale of several 100 km and the averaged depth of some 100 m,

the dominating motion dynamics are of the meso-scale. Their spatial patterns are determined by the baroclinic radius of deformation, which regionally and seasonally varies between 2 km and 7 km, FENNEL et al. (1991). Well known hydrodynamic features, such as coastal zones fronts with embedded eddy-like features and filaments, are associated with upwelling/ downwelling processes in the region. This results in a modification of the regional Sea Surface Temperature (SST) as well as the distribution of Optically Active Components (OAC) represented by suspended particulate and dissolved organic matter. The former is often but not always directly related to corresponding structures in the surface chlorophyll distribution. Both SST and the relative distributions of the different OACs can be observed through satellite techniques with a greater synopticity than that attainable by standard in-situ measurements from research vessels and/or ships of opportunity. Using multispectral ocean colour and infrared imagery the pigment concentration and the SST can be easily monitored above relative large regions. The ocean colour sensors provide quantitative information on the different bio-optical parameters through specific algorithms SIEGEL et al.(1994), BARALE (1994)., however the local meteorological conditions must also be accounted for by specific atmospheric algorithms, KONDRATYEV et al. (1992).

Thus, to adequately make a synergetic interpretation of remotely sensed data and hydrographic measurements regionally adjusted calibration procedures are required. Although the cloud cover in the region is relatively high during a typical seasonal cycle, it has been recognised for over two decades that the use of remotely sensed data offers a powerful tool for snapshot studies, HORSTMANN and HARDTKE (1980). Qualitative series of detailed images elucidate the complex nature of the highly dynamic coastal processes. Furthermore, changes in associated patterns show positive relationships with simulations of current fields by means of numerical models, SEMOVSKI et. al. (1995). Such comparisons yield some hints for prevailing dynamics, especially when hydrographic observations are available for the same time.

Furthermore quantitative results from maps of individual optically active components, such as CDOM, when correlated with significant geophysical parameters such as Dissolved Organic Carbon (DOC) could also prove to be important inputs for analyses of flux budgets. Chromophoric parts of dissolved organic matter interact with sunlight absorbing quanta in the same range of the phytoplankton, thus subtracting to the water body radiant energy for marine photosynthesis, KALLE (1938). In the Baltic CDOM can be responsible for up to 70% of total absorption in the blue. Measurements of both CDOM and DOC provide the input data for models simulating the local primary

productivity, BACASTOW and MEIER-REIMER (1991). In this investigation, we are also interested in the detailed optical properties of these substances in an attempt to differentiate between their terrestrial (riverine run-off) and autochotonous origin.

Several cruises were carried out. The main objective of the field campaign was the development of methodologies for the interpretation of satellite ocean colour data with specific reference to the forthcoming and recently launched sensors MOS, OCTS and SeaWiFS. Resulting data will be used in monitoring and modelling of the bio-optical state and an estimation of the local primary productivity. The experimental part of the activities was to collect data for

- the concentration of Optically Active Components like chlorophyll pigments, suspended particulate matter, and CDOM, as well as for
- the vertical and spectral distribution of the irradiance.

The following section describes the field campaigns and methods used. In the later section characteristic examples of meso-scale features are discussed, which have been initially identified by of the Coastal Zone Colour Scanner (CZCS) historical data. In conclusion a summary of our measurements in context of existing literature is given and a proposal for a specific bio-optical investigation in the Baltic region is suggested.

Data Base and Methods Used

The Institute of Oceanology of the Polish Academy of Science in Sopot/ Poland (IO-PAS) and the Space Applications Institute (IRSA) of the Joint Research Centre of the EU in Ispra/ Italy carried out a series of four oceanographic cruises onboard R/ V "Oceania" during 1993-1994, OOMS (1996). The first being a pilot cruise in September, 1993. Three campaigns followed in April, August, and September 1994. The area investigated was the Polish coastal zone, plus several open Baltic Sea stations as mapped in Fig.1. In order to detect the largest gradients in the measured parameters, all station locations were operatively determined. Therefore, the irregularly distributed station positions also reflect changes in the actual weather conditions.

Repeated measurements were carried out along a transect running from the Vistula mouth, which flows into the Gulf of Gdansk, and then on into the direction of open waters. Coastal normal sections were sporadically performed starting at the threshold of some small rivers, especially during the 1994-campaigns. Meteorological standard parameters were recorded continuously at the 10m-level above the sea surface. These observations included visibility, coded in accordance with the 'International

Meteorological Codes' of the World Meteorological Organization (WMO), as well as cloud cover, wind direction and velocity, dry-wet air temperature, and air pressure.

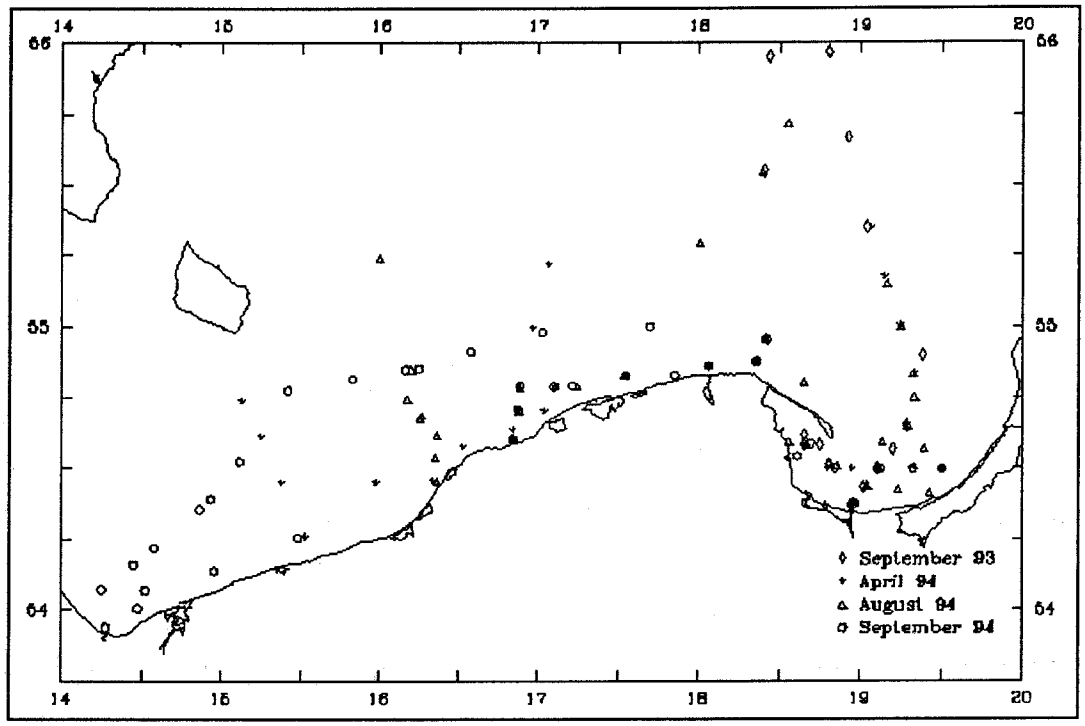

Fig.1 Image showing the region of interest in the Southern Baltic Proper and the station positions for the field campaigns, carried out in 1993 and 1994 by SAI JRC and IOPAS Sopot

Continuous measurements of incident solar radiation at the sea surface were taken daily by pyranometers. Their glass domes (295-2800 nm transmission range) were mounted on a Cardan suspension at an elevated position on the stern. The irradiance was recorded by means of a Kipp and Zonen CM-5 pyranometer during September, 1993, and April, 1994, cruises while an Eppley precision pyranometer PSP was also available in August and September, 1994. Both instruments were factory calibrated. Their signals were finally integrated over 30 seconds.

Within the water column, conductivity (C), temperature (T) and pressure/depth (D) were measured at each hydrographic station using a CTD-system, either that of Guildline 87104 or Sea-Bird SBE. The data validation was provided by the IO-PAS for 1m standard layers after each cruise.

Vertical profiles of downwelling irradiation, obtained from MER 2040, were used as source data for the calculation of the reflectance at certain wavelengths, which correspond to those of MOS, OCTS and SeaWiFS sensors channels. We observed the upwelling radiance in the nadir direction just under the sea surface and the associated downwelling irradiance impinging on the surface was obtained from measurements when the instrument was just above the water. As it is not possible to place the instrument at the theoretically needed "zero depth", its value was estimated as follows: for each wavelength the diffuse attenuation coefficient for the upwelling radiance was computed by linear regression between logarithm of the upwelling radiance and depth. Within the near surface layer, between 0.5m and 4 m depth, the slope of that regression was nearly constant. The searched "zero-value" was then simply extrapolated. Furthermore, the attenuation coefficient of a light beam at the wavelength of 655 nm was measured using a transmisometer built in IO-PAS. Its light path length was 1m within the water column. That probe combined the transmisometer with sensors for temperature and a standard chlorophyll fluorometer. Finally, all profiled data were also integrated over 1m intervals.

All measurements of Suspended Particulate Matter (SPM) were carried out on preweighed filters, which were prepared before each campaign after having been carefully washed with distilled water and left in the oven at 60°C or 24 hours. The volumes filtered were typically between 1000 and 2000 ml. Thereafter the filters were stored in a freezer at -20°C On return to the laboratory the samples were once again heated in the oven at 60°C for 24 hours, left for four hours at room temperature and then reweighed to obtain the dry temperature weight.

The chlorophyll-a concentration measurements were carried according to the method described by STRICKLAND and PARSONS (1972). The absorption spectra were taken for the wavelength range (350-750) nm with the spectrometer SPECORD M40. Related measurements, such as that of phaeophytine "a" concentration, were not performed. Furthermore, absorption measurements by phytoplankton pigments were performed using an alternative approach to the conventional method of particles retained on glass fibre filter. This method is described more in detail by TASSAN and FERRARI (1995). Their method consists in a combination of light transmission and light reflection measurements using a Perkin-Elmer Lambda 19 dual beam spectrometer, equipped with a 60mm integrating sphere, so as to remove the spurious contribution to the measured absorption by the sample backscattering. The phytoplankton absorption was obtained by bleaching the sample with NaClO solution inducing a depigmentation of organic particles involved. The absorption spectra of particles retained on a filter are converted in an equivalent

particles-suspension absorption, using an empirical expression.

Samples for pigment analysis by the High Pressure Liquid Chromatography (HPLC) were filtered onto GF/F filters under gentle vacuum. The dried filters were then wrapped in aluminium foil, labelled and quick frozen, then stored in liquid nitrogen. Thereafter the filters were placed in 15 ml test-tubes with 6 ml of 100% acetone. These samples were disrupted with a Teflon tipped tissue grinder and allowed to extract for 24hrs in the freezer. Afterwards, enough water was added to the extracts to obtain a final concentration of 90% acetone. Then the tubes were centrifuged to settle the cell and filter debris. Twenty- five microliters of the clear supernatant were injected in a Hewlett-Packard 1050 series HPLC apparatus. A Spherisorb ODS 2 column (5 mm, 250x4 mm) was used to separate the pigments using the solvent scheme. The diluted pigments were detected with a spectrophotometer (1050 series) set at 440 nm and a fluorometer (1046A; ex:440 nm; em:664 nm). The pigments were identified based on their relative retention times and absorption spectra. Fluorometer data were also used for the identification of the chloropigments. The pigments were quantified according to their peak values.

A further data set was calculated for the description of the geochemical composition of particulate matter and its variations, both geographically and seasonally. The Millepore 0.22 nm filters resulting from CDOM (yellow substance) filtrations were preserved in petridishes and frozen at -20°C. The analysis itself was carried out using a Siemens SRS 300 sequential X-ray spectrometer.

Much attention was placed, during these field experiments, on the analysis and characterisation of CDOM. This is primarily due the fact that in this region the absorption of these substances contribute so much to the total optical properties of the water column (as it does also in other coastal regions). The filtration for the analysis was made through 0.2 micron Millipore filters. The filtrate was then stored in amber bottles, an inhibitor of anaerobic growth was added (sodium azide Na2N3). Measurements of spectral absorbance were made with the Perkin Elmer Lambda19 dual beam spectrophotometer with fused quartz cuvettes of 0.04 or 0.10 m and Milli-Q water as a blank. All of the subsequent analysis was carried out within 10 days of the end of field measurements. To test the portability of the samples, some fluorescence spectra were made again on return to the laboratory. In all cases, the change in the fluorescence spectra, and therefore in the absorption, was negligible and smaller than 2%. The absorbance (A) was converted by means of the path-length (L) of the cell (in metres) in absorption coefficient using the relationship 2.3*(A/L).

Fluorescence were made so as to permit a more detailed analysis of the CDOM and to attempt to differentiate between different sources. The analyses were made with a Perkin Elmer LS50B fluorometer with a 0.01m cuvette, quinine sulphate was used as a standard. The instruments were used in the range (300 -750) nm with a spectral resolution of 1 nm.

Three fluorescence techniques were used to analyze CDOM:

- Emission spectra: These spectra are obtained by exciting at 355 nm wavelength (the value as those for laser fluorescence from airborne sensors, VODACEK et al.(1995)) and measuring the emission in between the range (375-650) nm. At this excitation the peak of the Raman is at 408 nm and this can be used as well as the quinine sulphate to standardise the CDOM fluorescence, FERRARI and TASSAN (1991).
- Synchronous spectra: These spectra basically consist of a diagonal cut across the emission excitation matrix. Excitation is performed at a certain wavelength and the emission is then measured at a wavelength which is at a fixed interval of 25 nm. The excitation is then moved on and the measurement is made at a 1 nm increments. Such spectra have not been used as much as emission spectra in CDOM experiments but they contain more diverse qualitative information than the above, FERRARI and MINGAZZINI (1995).
- Emission excitation matrices: The matrix itself consists of a series of 20 or 30 spectra each with the same emission range and each with a sequential increase in its excitation, i.e. emission range (375- 650) nm and excitation from 260 nm to 450 nm in increments of 10 nm. This approach is definitely the most innovative, GREEN and BLOUGH (1994).

However, questions remain as to whether the additional information provided, compared to the synchronous spectra, really justifies the difficulty both in the processing and following interpretation of these spectra.

The regional relationship between CDOM and DOC was also considered as it could prove invaluable for the input into Carbon Cycle models and principally models of New Production, BACASTOW and MAIER-REIMER (1991), using remotely sensed data (through a CDOM algorithm). Such measurements were made for the last three cruises. Seawater samples collected with a 10l-Nansen bottle were stored in a 15l preconditioned PVC-container in order to reduce contamination. The filtration was performed under gentle depression on a precombusted GFF filter rinsed with filtered seawater to eliminate the main fraction of particulate matter. In each filtration, the initial aliquots ($\sim$200 ml)

were discarded to prevent any possible source of contamination by the filters. The final filtrate was transferred to a 250 ml glass ambered bottle preinserted with the same filtered seawater. After the addition of sodium azide the sample was stored at 4°C. The DOC analyses were performed at the SAI for the High Temperature Carbon Oxidation (HTCO) method, cf. SUGIMURA and SUZUKI (1988). A Carlo Erba-Fisons TMC 480 analyzer was used which involves a high temperature oxidation reactor thermoregulated at 1020°C. The resulting methane was measured with a Flame Ionisation Detector (FID) whose signal is fed to a potentiometric chart recorder and it is directly proportional to the amount of organic carbon present in the original sample. Corresponding measurements were performed by means of the LTO (Low Temperature Oxidation) method at the University of Venice/ Italy. We used a Technicon Instrument Rotterdam Autoanalyzer II able to detect the DOC concentration in the range between 8-830 microMC. This method also requires an accurate removal of inorganic carbon by acidification and is described more in detail by MENZEL and VACCARO (1964).

Meso-scale Features in CZCS- Images

According to KAHRU et al. (1986), meso-scale patterns occur not only along open Baltic frontal zones but also in areas of coastal upwelling/downwelling. "Level 3"-images of the Coastal Zone Colour Scanner (CZCS) were available from the southern Baltic Sea region for 1979-1986. The relative number of images per month, which roughly cover the seasonal cycle, are shown in Fig. 2.

The largest number of scenes (35-40) in May and August when suitable conditions exist for remotely sensed detection due to the annual minimum in the cloud coverage. Relative minima are present for the early summer season and during spring, and autumn. No valid data were available for the winter season (November-February). All images were processed at SAI using an algorithm for the retrieval of chlorophyll-like pigments according to that defined by GORDON and MOREL (1983). However, previous investigations by SIEGEL et al. (1995) have shown that the application of this algorithm is certainly not very accurate for our area of investigation. Here, a set of local algorithms are required, because terrestrial anthropogenic and local atmospheric inputs provide a large source of optically active material not specifically accounted for by these more general models. Depending on the regional precipitation season, river discharges contribute strong freshwater inputs during March and April. Associated problems of the water budget for the whole Baltic area are still under investigation by the international,

interdisciplinary BALTEX-programme, RASCHKE (1992).

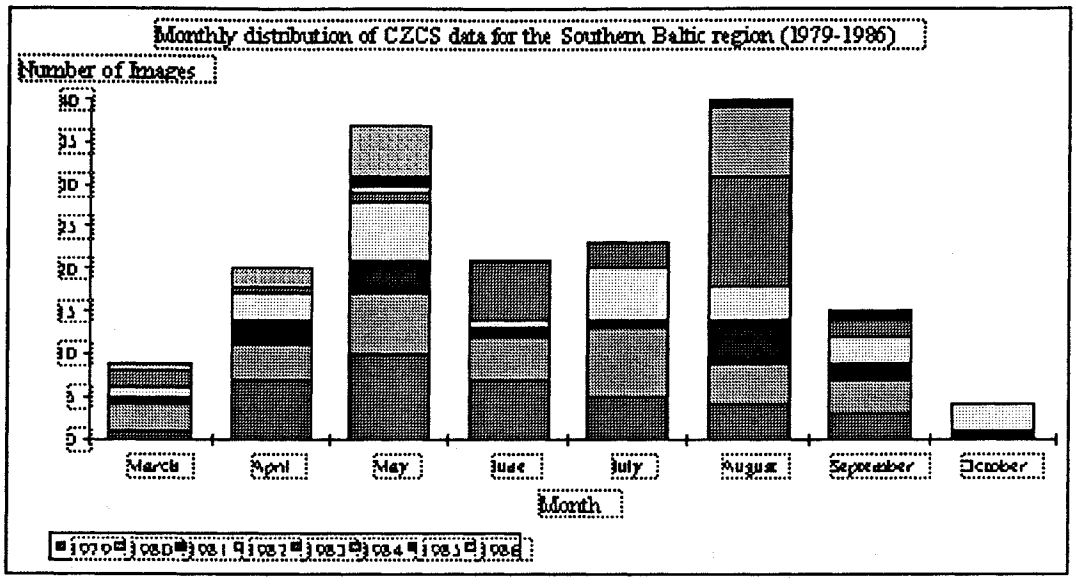

Fig.2 Stacked histogram showing the availability of CZCS data (1979-1986) in the Baltic Proper.

With respect to the rivers influence on structures observed of the optically active materials, it may be hard to differentiate in many circumstances between the contribution by fluvial inputs and the contribution due to spring blooms. In an attempt to clarify this point, the influence of two very different rivers was investigated; the Vistula River in the Gulf of Gdansk and the Oder River in the Pomeranian Bay.

The first of these transports an extremely high nutrient concentration into the southeastern part of the Gulf of Gdansk and causes high plume-like concentrations in the phytoplankton distribution roughly corresponding to the known dispersion of the river. An example representing this plume is shown in Fig.3. Such patterns and the related dispersions produce different distributions in the chlorophyll field as seen from CZCS-data. Many of the investigated images for the region display an isolated feature with extremely high pigment concentration in the centre of the Gulf of Gdansk. This feature is most probably controlled by topographically trapped eddy-like motions.

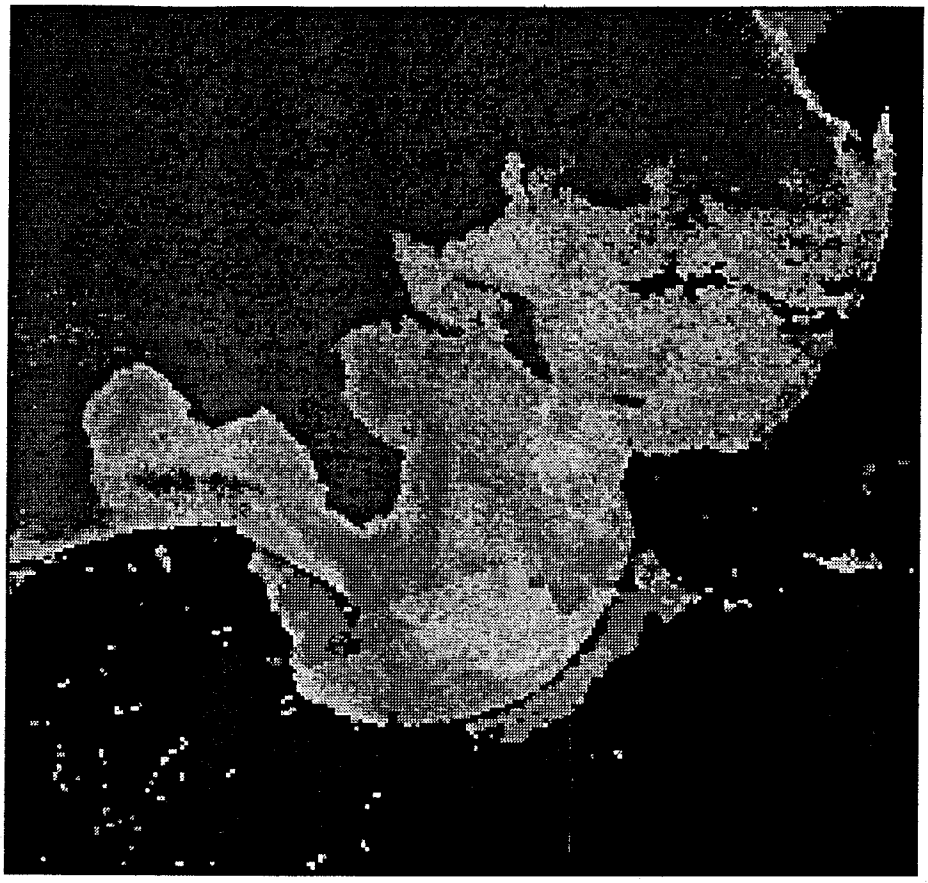

Fig.3 CZCS scene (11/04/1979) showing the Vistula river plume in the Gulf of Gdansk

These, result in simple anticyclonic circulation, and produce convergences in the motion field with centred downwelling processes, thus accumulating passive tracers as shown by the bright grey pattern in Fig.3. Such eddy-circulation usually depends on the prevailing wind direction and the path of the continuation of the Vistula river within the gulf. The gulf-size controls its diameter. The presented example suggests that the continuation of the Vistula river crosses the gulf from southeast to northwest. Furthermore, it seems that the continuation of the river discharge forms break-off filaments as it disperses in the northwest part of the gulf. These features suggest that locally generated wind-driven currents, which usually follow the shelf slope off the gulf, were only weak during this situation. And also that the easterly winds, along the slope turned the filament direction into more westward directions outside the gulf, in the region North of the Hell peninsula. The above mentioned peninsula is a narrow sand spit which borders the Gulf of Gdansk along its northwest coast. The bathymetric structure in the region is extremely diverse as a result of post-glacial regression. Local winds with an alongshore component sporadically induce upwelling features along the spit. Eastern or southeastern winds result

in Ekman-offshore transport of warmer coastal water. The generated divergence zone is associated with upwelling of cold deeper water along the coastal slope as shown by low values of the SST illustrated in Fig.4a

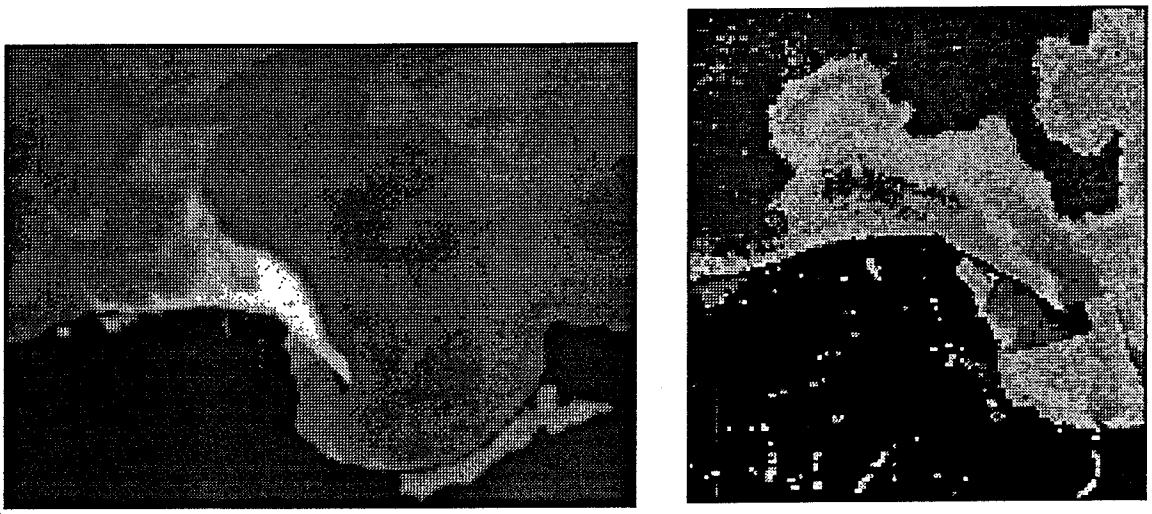

Fig.4 (a,b) AVHRR image (26/09/1982) showing the thermal structure in the Hel peninsula region (left panel); CZCS image (12/04/1979) mapping the distribution of OACs (right panel)

The events themselves show varying spatial and temporal scales, from very localized events to occasions during which the feature covers the whole of the spit. Commonly, upwelled water inputs nutrients into the euphotic layer and induces a significant increase in the production of phyto- and zooplankton. However, if the upwelled water are anoxic or at least depleted in nutrients with respect to the surrounding surface waters there will not be the biological response described. In the case at hand if we compare the relatively low nutrient concentration upwelled water with the much higher concentrations of the river discharge, we may expect a poor chlorophyll concentration for upwelling events off the Hell peninsula, this is in fact extremely well represented depicted in Fig.4b. This is a marked difference with well-known oceanic upwelling, which tend to be associated with high chlorophyll concentration, GABRIC et al.(1993).

On a number of similar satellite images for the Gulf of Gdansk area, a jet-like structure is observed with a high pigment content or biologically produced suspended matter. This jet occurs at the entrance to a narrow strait, this strait occurs adjacent to the highly eutrophicated, low saline Vistula Bay. Generally, wind-driven motions control the volume-mass transport through the strait into the gulf, SEMOVSKI et al. (1995). In some instances, observation has given evidence that the magnitude of this input can be greater than that from the Vistula river. Completely different conditions occur in the Pomeranian

Bay. Here, wind-driven motions rapidly disperse the discharge from the Oder river along adjacent coasts. Westerly winds force a eastward flowing coastal plume and associated spreading of riverine water while easterly winds support its west-northwestward displacement. This bay is much larger in its spatial scale than the gulf of Gdansk and consists of a complex bottom topography with a shallow water region placed in front of the river plume limits (i.e. Oder Bank). Dynamically, this shallow water region aides in the generation and maintenance of eddy-like features, which locally influence stratification and associated transport conditions. A plume of high pigment concentration occasionally takes place in the centre of the Pomeranian Bay as shown in Fig.5. This plume suggests anticyclonic motions, however the effect of the Oder Bank is obvious as the shape of the plume clearly follows the shape of the banks topography and this feature may even possibly result from bottom reflectance.

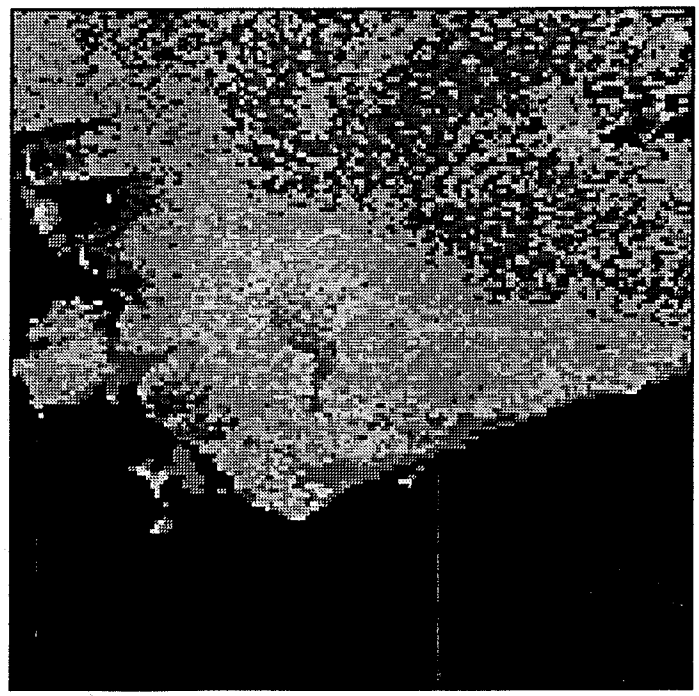

Fig.5: CZCS scene for the Pomeranian Bay (06/05/1980) showing the Oder river 'plumes' along the eastern shore and the high eddy-like concentration above the Oder Bank

Inspecting all available CZCS-images of the Pomeranian Bay, the large river inflow appears to be quite constant throughout the year in terms of input of optically active material, this consistent nature can be attributed to the role of the eutrophicated Szczecin lagoon which provides a constant input of OACs.

Frequently, no clear frontal system can be detected in the sea surface layer, separating both the large mouth of the Pomeranian Bay and the Gulf of Gdansk waters from the open Baltic Proper. Conversely, a hydrographic frontal zone is found quasi-permanently across the much smaller mouth of the Gulf of Finland, HEINANEN et al. (1995). This feature was frequently detected in the CZCS imagery.

High concentrations dominate in April imagery during spring blooms and the enhanced fluvial input but also in July/ August when the cyanobacteria blooms occur. These anomalous blooms can be usually observed in the open Baltic Sea during the summer season (July/ August) during SST of $>16^{\circ}C$ and low to moderate wind velocities, KAHRU and RUD (1995). In other words, these blooms occur during fairly stagnant conditions of wind-driven mixing processes.

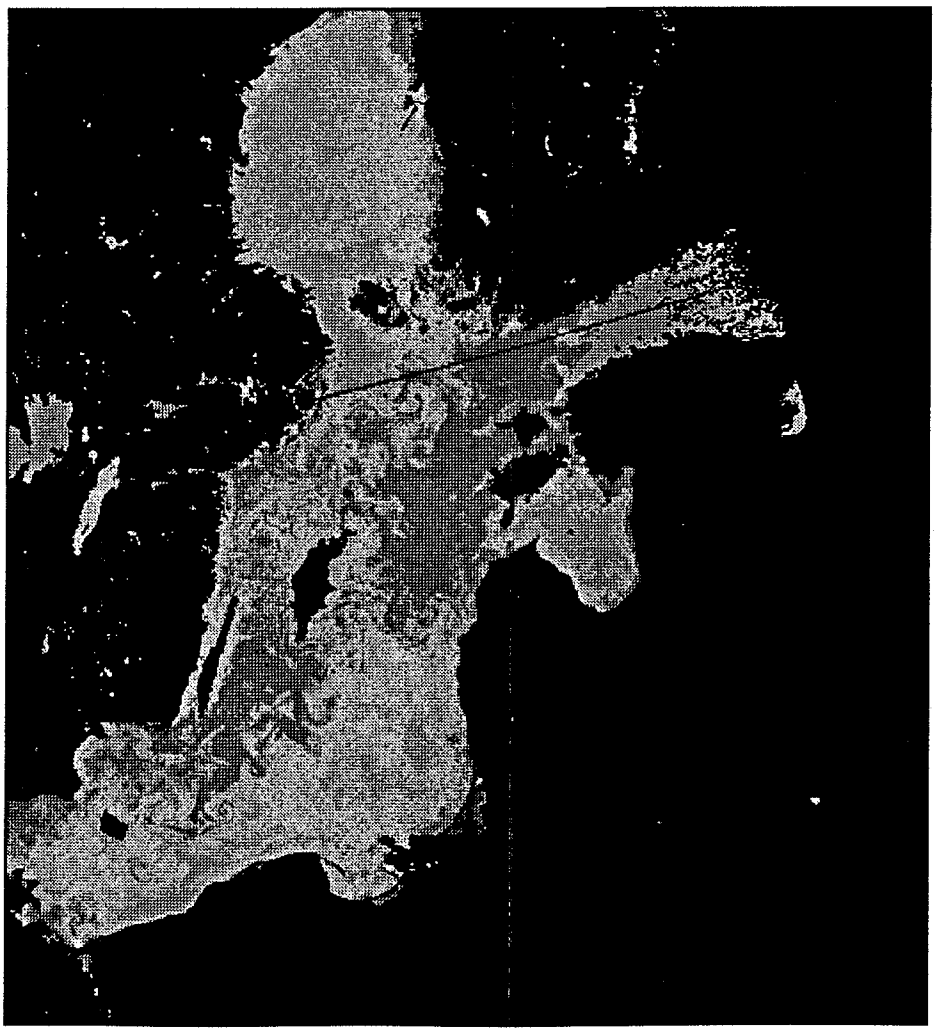

Fig.6: CZCS image showing an example of a cyanobacteria bloom (dark grey) with significant filament structures in the Baltic Proper (09/08/1983)

At a certain point of their life-cycle, the blooms undergo inverse sedimentation and form massive mats at the sea surface. At this point they become subject to external forcing allowing them to trace hydrographic patterns associated by frontal systems and filaments mapped in Fig.6.

Wind induced dynamics are also responsible for the Hiiumaa upwelling in the Northeast of the Baltic Proper in the region the Gulf of Riga, NOMMANN et al.(1991). Resulting patterns of cold water locally coincide with nutrient concentrations and an accumulation of chlorophyll. There is also some observational evidence that such features are more intense and productive during the summer season due to favourable winds.

According to LASS and SCHMIDT (1994), such a feature is represented by a clear signal in the SST imagery off the Darss Sill. They concluded that its occurrence was relatively independent of the local Ekman offshore transport but more related to abnormal situations in coastal normal pressure gradients, which are associated with geostrophic alongshore currents. Frequently, pairs of cyclonic and anticyclonic eddies form dipole-like motion patterns, as it is described, for instance, more in detail by FEDOROV and GINSBURG (1989). An example is shown in Fig.7.

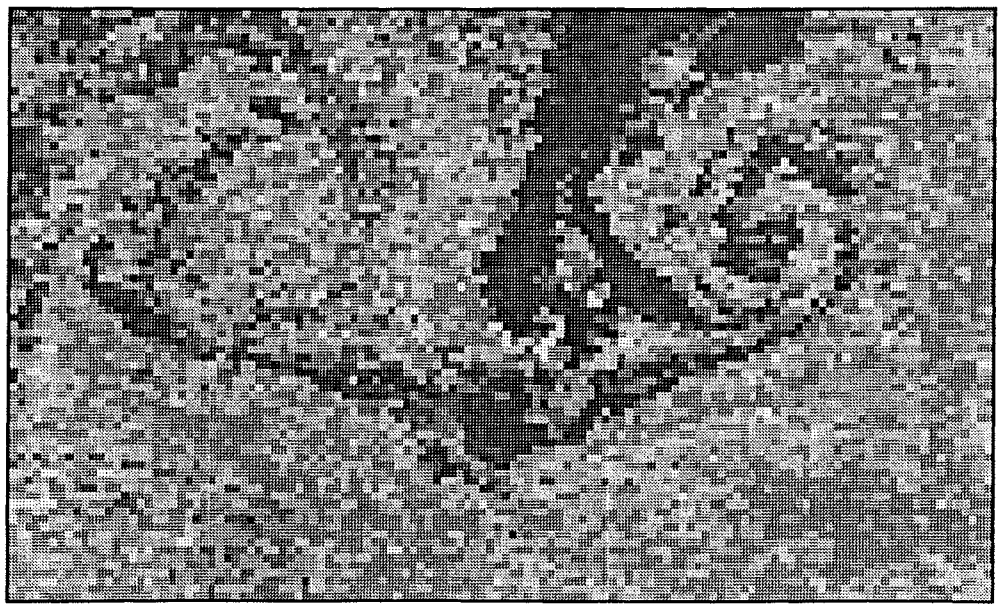

Fig.7: Vortex Dipole shown in a CZCS image (09/08/1983) northeast of Bornholm Island

Due to the conservation of potential vorticity in nearly barotropic motions of shallow water regions, anticyclonic motions dominate above topographic 'bumps' while cyclonic cells of rotation lie more frequently above deeper waters. We have therefore used this notion to interpret the quasi-permanent structures mapped in our figures, here illustrated by the image shown in Fig.6 and Fig.7. Island and coastal wakes also play an important role in the generation of eddy-like circulation patterns via 'Karman's Vortex Street'. Their dynamics are, for instance, discussed by PATTIARATCHI et al.(1986) and DENNISS et al.(1995). No data is available at present demonstrating such phenomena clearly. However, some images suggest the existence of these phenomena in the vicinity of both Bornholm and Gotland Island.

Finally, the features identified are often associated with frontal zones separating coastal upwelling regimes from the Baltic Proper. Upwellings sporadically occur and affect the biological productivity on different spatial and temporal scales, cf. NOMMANN et al. (1991) and SIEGEL et. al.(1994). This response clearly suggests supplementary external forcing which cannot always be explained exclusively by the bottom topography but which in many cases are also influenced by the coastal configuration and geometry.

The use of first generation ocean colour sensors (CZCS) for the quantitative interpretation of pigment concentrations has in the past shown its limitations. The shortcomings of these original sensors require the development of more accurate bio-optical algorithms for the next generation of ocean colour sensors. On the other hand, it is still important to recognise the importance of existing historical data sets of the CZCS and its potential in qualitative studies, as it was proposed by STURM et al.(1992). In this study, such data has been used to identify and characterize both spatially and temporally specific meso-scale features occurring in the Baltic Sea region.

In order to improve the interpretation of meso-scale dynamics by means of remotely sensed images, new techniques are needed. Time series resulting from sequential images illustrate the evolving dynamics of the individual features much more realistically than simple snapshot images. Well known statistical procedures can be used such as Empirical Orthogonal Functions (EOF) these techniques are useful both in comparing individual scenes of different parameters (SST and Chlorophyll like pigment for example) as well as in making time series analysis of sequential imagery. In the latter the EOF's decompose the given variance pattern from each pixel point into a set of orthogonal eigenfunctions, which are spatially fixed. Their temporal changes are described by

corresponding development coefficients. Usually the first few empirical mode numbers sufficiently reflect the total variance. Therefore, the contribution of higher mode numbers can be rejected. This way, we obtain a statistical separation between real signals and the noise level superimposed. Following, the eigenfunctions and corresponding coefficients of significant mode numbers can be composed to construct resulting patterns for a dynamical interpretation. For further details on this technique refer to LAGERLOEF and BERNSTEIN (1988). An alternative statistical technique to be investigated is that of the 'maximum cross correlation'. Its basic idea is the identification of the maximum cross correlation in a lagged matrix between two subareas of a pair of sequential scenes. This method was first used for mapping SST images (AVHRR) by EMERY et al.(1986), and later for CZCS data by GARCIA and ROBINSON (1989).Considering the whole pattern, the resulting vectors indicate direction and velocity of associated shifting and deformation. An example is shown in Fig.8.

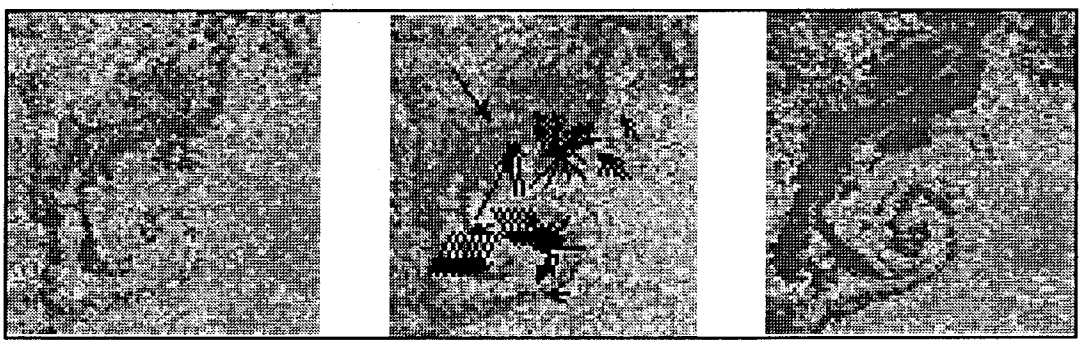

Fig.8: Two sequential images showing a cyclonic feature in the Baltic Sea (left and right panel) and the results on a MCC computation for August 1983 (08 & 09/08/1983, middle panel).
(The arrow show the vectors resulting from the best correlated lagged matrix and therefore represent the motion of the features observed.)

Neural networks, however, also represent a powerful tool. Comparing them to the last two techniques, COTE and TATNALL (1995) concluded that such networks adequately resolve local variations not only in their characteristic distribution but also in their intensity. All of such statistical approaches suppose the availability of proper working calibration algorithms, which transform the pixel information into values of the chlorophyll like pigment.

Preliminary Results

The hydrography of the coastal area under consideration is characterized by a high degree of variability in space and time. A homogeneous top layer, which is well stirred by wind-induced mixing processes, covers depths between 5m and 25 m.. Temperatures range from 3.0°C to 3.5°C in April and 14°C to 18°C in August while salinities range from 7 to 11 PSU in April to 6.2 to 7.0 PSU in August. Due to increased salinity in near bottom layers, a strong pycnocline separates the upper from the deeper layers. Its thickness considerably fluctuates locally and temporally in response to the wind forcing. This pycnocline controls all vertical exchange processes and, in this way, also the local concentration of the Coloured Dissolved Organic Matter (CDOM) with its main origin in the euphotic zone.

In the Baltic Sea, the stratification mainly depends from the vertical distribution of the salinity. The influence of the temperature structure on that of the density profile is of secondary importance. Therefore, a positive regression between the salinity distribution and the CDOM absorption could be accepted. The measurements made for CDOM absorption, indicate in fact small values in deep layers with relative high salinities but large amounts in near surface layers. Furthermore if we consider only the surface values, the scatterplot shown in Fig.9, we observe an extremely 'good' correlation between salinity and CDOM absorption.

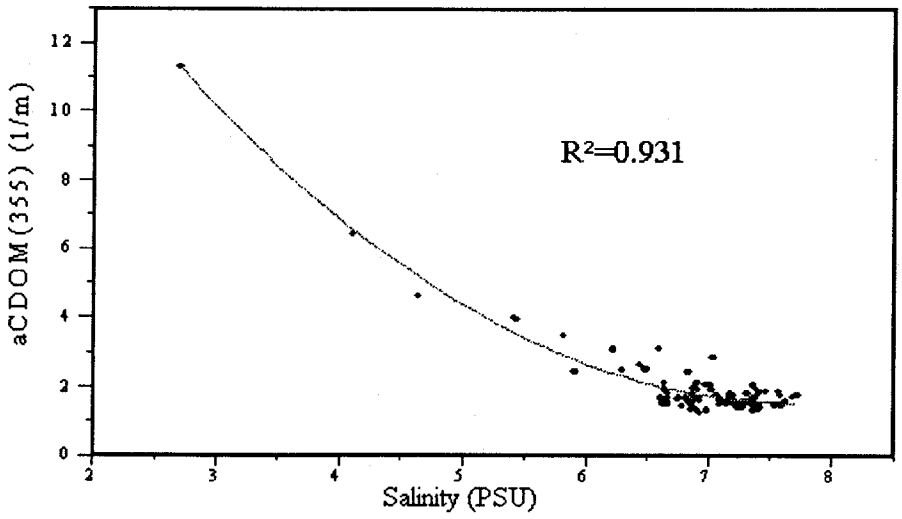

Fig.9: Regression between Salinity and absorption of CDOM at 355nm for all of the cruises surface measurement only.

This relationship is extremely significant as it verifies the potential use of CDOM absorption (a parameter which can be detected remotely) as passive tracer at least in the nearshore area. Furthermore we can therefore also assume that processes, which are related to the local production of turbulence, should affect the Dissolved Organic Carbon (DOC) distribution in the same manner than that of CDOM. The linear relationship between DOC and CDOM is shown in Fig.10. The large CDOM absorption coefficient at 355 nm in this region is clearly correlated to the DOC concentration. This relationship is undoubtedly invaluable as DOC is a important input to models for the determination of new production (BACASTOW and MAIER-REIMER, 1991) and a method for determining this parameter remotely would therefore represent a notable accomplishment.

The discrimination between different OACs, which may not be correlated amongst themselves or are subject to local specific correlations described by TASSAN (1994), could not be achieved with the historical data presented here above. This factor greatly influenced the choice of the channels for the new sensors by the introduction of a channel at 412 nm (408nm for the MOS sensor), SATHYENDRANATH et al.(1989).

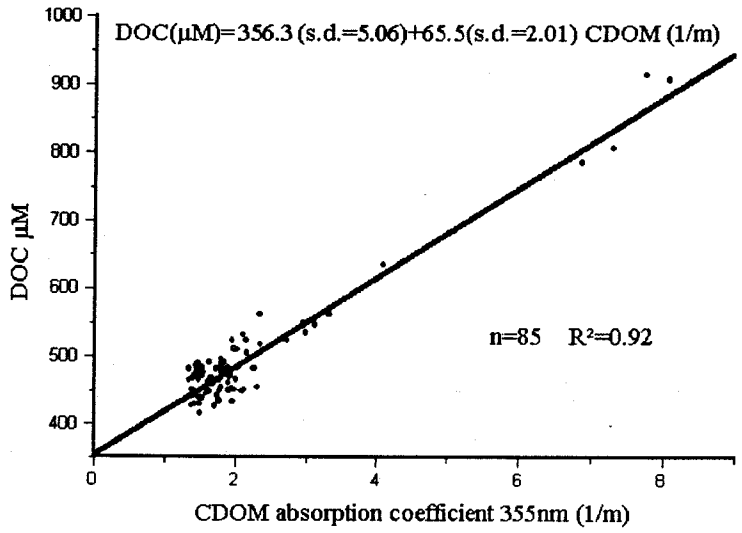

Fig.10: Plot showing the relationship between a-CDOM and DOC concentration.

This channel allows to differentiate between the absorption due to CDOM and the absorption due to chlorophyll like pigments.

One important aspect in the analyses of the optical budget is that 'optical closure'. This

simple concept involves the consideration that at the end of all investigations all of their compartments must add up. There are always several problems in achieving complete closure mainly because not all of the contributing fractions to both absorption and scattering are accounted for adequately. For example, the auxiliary pigments included in the pigment spectra and their effect on the total absorption of a spectral deconvolution is discussed by HOEPFFNER and SATHYENDRANATH (1991).
The peaks of certain phycoerytherin pigments, which are associated with blue-green algae, can be seen at the wavelength of 495 nm and 545 nm. Furthermore, we may speculate that additional absorption can come from a fraction not measured by standard methods, i.e. the fraction of absorbing substance in the size range between GFF(median 0.8 microns) and Millepore (0.2 microns), and the possibility of ultrafine particles (diameter < 0.22 fm), which pass through Millepore-filters. Such particles could be composed of small bacteria, virus or small colloids and could contribute both to the absorbing and the scattering parts of the energy conservation equation, MOBLEY (1994). These are all important considerations which need to be considered when developing reflectance models in Case II models required to adequately distinguish the distinct Optically Active Components, and consists of a principal objective of the author's investigation into the region at present.

Discussion

The history on the development of bio-optical models for the interpretation of satellite imagery in the visible range has been a subject of investigation for over 15 years. Early studies allowed the determination of chlorophyll like pigment in oceanic (Case I) waters with an error margin of about 40%, GORDON et al. (1983). For these regions, they used ratios between the blue and green channels, GORDON and MOREL (1983). However the capabilities of the use of CZCS imagery for investigations in the coastal (Case II) waters was greatly limited by the number of spectral bands available. Some historical and future ocean colour sensors and their wavelengths with spectral bands are tabulated with respect to their application in Table 1.

The closure concept mentioned above requires a simple conservation of energy and, thus, the attention c(l)= absorption a(l) + scattering b(l) [here, (l) is the wavelength]. For its verification, it is necessary to quantify all subsets of individual components, and therefore a(l) is subdivided into the absorption of:

- aph(l) chlorophyll like pigments,
- ancp(l) non-chlorophyllous particles,

- ay(l) CDOM,
- aw(l) sea water.

The scattering coefficient b(l) is also subdivided into contributions from:

- bp(l) chlorophyll like pigments,
- bncp(l) non-chlorophyllous particles,
- bw(l) water molecules.

CZCS	SeaWiFS	POLDER	OCTS	MERIS	Specific uses, defined for MERIS channels.
	412(20)		412 (20)	410 (10)	CDOM (Gelbstoff)
443 (20)	443 (20)	443 (20)	443 (20)	445 (10)	Chlorophyll
	500 (20)	490 (20)	490 (20)	490 (10)	High concentration Chlorophyll
520 (20)			520 (20)	520 (10)	Turbidity
550 (20)	565 (20)	565 (20)	565 (20)	565 (10)	Chlorophyll
				620 (20)	Sediments
670 (20)	665 (20)	670 (20)	665 (20)	665 (10)	Chlorophyll
				682.5 (5)	Fluorescence
				710 (10)	
750 (100)				755 (10)	Atmospheric correction
	765 (40)	765 (40)	765 (40)	765 (25)	Oxygen (top of cloud height)
	865 (44)	865 (40)	865 (40)	880 (10)	Aerosols, land vegetation
		910 (20)		900 (10)	Clouds
				960 (10)	Vegetation
10200			3715	1022.5	Aerosols

Table 1: Historic, current, and future ocean colour sensor their spectral channels (nm) and the potential usefulness of each channel; translated and modified from ANTOINE (1995).

The measurement of some of the listed features is feasible whereas that of others is extremely difficult. Nevertheless, the enhanced spectral resolution of satellites like MERIS permits the development of new empirical and/or semi-analytical approaches, which describe the bio-optical properties of coastal water much better than in the past.

Moreover, SATHYENDRANATH et al.(1989) and TASSAN (1994) expect that the available bands if the SeaWiFS and OCTS sensors could be sufficient to adequately interpolate the full spectra. In this investigation the interest is in the development of a three component approach for chlorophyll-like pigments, SPM, and CDOM. Matrices are being compiled for each of the cruise containing information about concentration and absorption values together with reflectance values at SeaWiFS and OCTS wavelengths. Possible complications with our Baltic Sea data are already becoming apparent and include extremely low values of the reflectance.

Nevertheless, the comparison of individual ocean colour scenes of newly derived distinct parameters (Chlorophyll like pigment, Non Chlorophyllous Particles and Coloured Dissolved Organic Matter) with AVHRR SST imagery will facilitate the interpretation and analysis of meso-scale patterns and their dynamics in the Baltic Sea, as well as provide additional information on their effect and role in the dynamics of the local ecosystem of the Baltic region.

References

ANTOINE D., 1995: Utilisation des mesures spatiales de la "couleur de l'océan" pour l'estimation dela production primaire et la modelisation du cycle du carbone dans l'océan. Thesis, Doctorat, Université P. & M. Curie (Paris VI), Paris, France. p. 206.

BACASTOW R., E. MAIER-REIMER, 1991: Dissolved Organic Carbon in modelling oceanic new production. Global Biogeochemical Cycles, **5**, 71- 85.

BARALE V., P.M. SCHLITTENHARDT, 1994: Monitoring the marginal seas of Europe with optical observations. In: Remote Sensing- from Research to Operational Applications in the new Europe., Proceedings of the 13th EARSeL Symposium, Dundee U.K., R. Vaughen Ed., Springer-Verlag, Budapest, 293-298.

COTÉ S., A.R.L.TATNALL, 1995: Estimation of ocean surface currents from satellite imagery using a Hopfield Neural Network. Proceedings of the Third Thematic Conference on Remote Sensing for Marine and Coastal Environments, Seattle, Washington, 538- 549 .

DENNISS T., J.H. MIDDLETON, R. MANASSEH, 1995: Recirculation in the lee of complicated headlands: a case study of Bass Point. J. Geophys. Res., **100**, 16087- 16101.

DICKEY T.D., 1991: The emergence of concurrent high-resolution physical and bio-optical measurements in the upper ocean and their application. Reviews of Geophysics, **29**, 383- 413.

EMERY W.J., A.C. THOMAS., M.J. COLLINS, W.R. CRAWFORD, D.L. MACKAS, 1986: An objective method for computing advective surface velocities from sequential infrared satellite images., J. Geophys. Res., **91**, 12865- 12878.

FEDOROV K.N., A.I. GINSBURG, 1989: Mushroom-like currents (vortex dipoles): one of the most widespread forms of non-stationary coherent motion in the ocean. In: J.C.J.Nihoul (Editor), Mesoscale/ synoptic coherent structures in geophysical turbulence. Elsevier, Amsterdam, 1- 14.

FENNEL W., T. SEIFERT, B. KAYSER, 1991: Rossby radii and phase speeds in the Baltic Sea. Continental Shelf Research, **11**, 23- 36.

FERRARI G.M., S. Tassan, 1991: On the accuracy of determining light absorption by "yellow substance" through measurements of induced fluorescence. Limnol. Oceanogr., **36**, 777- 786.

FERRARI G.M., M. MINGAZZINI, 1995: Synchronous fluorescence spectra of dissolved organic matter (DOM) of algal origin in marine coastal waters. Mar. Ecol. Progr. Ser., **125**, 305- 315.

FERRARI G.M., M.D. DOWELL, S. GROSSI, C. TARGA, 1996: CDOM absorption, fluorescence and DOC relationships in the southern Baltic Sea (Baltic Proper). Evaluation of seasonal aspects. Marine Chemistry, in press.

GABRIC, A.J., L. GARCIA, L. van CAMP, L. NYKJAER, W. EIFLER, W. SCHRIMPF, (1993): Offshore export of shelf production in the Cape Blanc (Mauritania) giant filament as derived from coastal zone colour scanner imagery. J. Geophys. Res., **98**, 4697- 4712.

GARCIA C.A.E., I.S. ROBINSON, 1989: Sea surface velocities in shallow seas extracted from sequential Coastal Zone Colour Scanner satellite data. J. Geophys. Res., **94**, 12681- 12691.

GORDON H.R., A.Y. MOREL, 1983: Remote assess of ocean colour for interpretation of satellite visible imagery: A review. Lecture Notes on Coastal and Estuarine Studies, 4, Springer- Verlag, pp. 114.

GORDON H.R., D.K. CLARK, J.W. BROWN, R.H. EVANS, W. W., BROENKOW, 1983: Phytoplankton pigment concentrations in the middle Atlantic bight: Comparison of ship determinations and CZCS estimations, Appl. Opt., **22**, 20–36.

GREEN, S.H., N.Y. BLOUGH, 1994: Optical absorption and fluorescence properties of chromophoric dissolved organic matter in natural waters. Limnol. Oceanogr., **39**, 1903- 1916.

HEINANEN A., K. KONENEN, H. KUOSA, J. KUPARINEN, K. MAKELA, 1995: Bacterioplankton growth associated with physical fronts during a cyanobacterial bloom. Mar. Ecol. Prog. Ser., **116,** 233- 244.

HOEPFFNER N., S. SATHYENDRANATH, 1991: Effect of pigment composition on absorption properties of phytoplankton. Mar. Ecol. Prog. Ser., **73,** 11- 23.

HORSTMANN U., P. G. HARDTKE, 1980: Transport processes of suspended matter, including phytoplankton, studied from LANDSAT images of the southwestern Baltic Sea. In: J.F.R. Gower (Editor), Oceanography from Space, Plenum Press, New York, 429- 438.

KAHRU M., S. NOMMANN, M. SIMM, K. VILBASTE, 1986: Plankton distributions and processes in the Baltic Boundary Zones. In: J. C. J. Nihoul (Editor), Marine Interfaces Ecohydrodynamics. Elsevier Amsterdam, 273-294.

KAHRU M., O. RUD, 1995: Monitoring the decadal- scale variability of cyanobacteria blooms in the Baltic Sea by Satellites. Proceedings of the Third Thematic Conference on Remote Sensing for Marine and Coastal Environments, Seattle, Washington, 76-83.

KALLE K.,1938: Zum Problem der Meereswasserfarbe. Berlin, Ann. Hydrography, **66**, 1- 13.

KONDRATYEV K.Y., V.V. KOZODEROV, O.I. SMOKTY, 1992: Remote sensing of the Earth from space. Springer Verlag, pp. 478.

LAGERLOEF G.S.E., R.L. BERNSTEIN, 1988: Empirical orthogonal function analysis of Advanced Very High Resolution Radiometer surface temperature patterns in Santa Barbara Channel. J. Geophys. Res., **93**, 6863- 6873.

LASS H.U., T. SCHMIDT, 1994: On the dynamics of upwelling observed at the Darss Sill, 19th Conference of Baltic Oceanographers, Sopot, Poland, pp. 65.

LASSING J.J., M. LEPPANEN, A. NIEMI, G. TAMELANDER, 1978: Phytoplankton primary production in the Gulf of Bothnia 1972 - 1975 as compared with other parts of the Baltic Sea. Finn. Mar. Res., **244**, 101-115.

LEGENDRE L., S. DEMERS, 1984: Towards dynamic biological oceanography and limnology, Can. J. Fish. aquat. Sci., **41**, 2- 19.

LEGENDRE L., S. DEMERS, D. LEFAIVRE, 1986: Biological production at marine ergoclines, In: J.C.J. Nihoul (Editor), Marine Interfaces Eohydrodynamics. Elsevier, Amsterdam, 1 - 29.

MENZEL D.W., R.F. VACCARO, 1964: The measurement of dissolved organic carbon and particulate carbon in seawater. Limnol. Oceanogr., **9**, 138-142.

MOBLEY C.D., 1994: Light and water: Radiative transfer in natural waters. Academic Press, San Diego, pp. 592.

NEHRING D.,1990: Eutrophication in the Baltic Sea., In: R.A. Vollenweider (Editor), Marine Coastal Eutrophication. Elsevier, Amsterdam, 673- 682.

NIHOUL J.C.J. (Editor), 1986: Marine Interfaces Ecohydrodyanmics, Elsevier, Amsterdam, p. 670.

NOMMANN S., J. SILDAM, T. NOGES, M. KAHRU, 1991: Plankton distribution during a coastal upwelling event off Hiiumaa, Baltic Sea; impact of short-term flow field variability, Continental Shelf Research, **11**, 95- 108.

OOMS M., 1996: ULISSE Baltic '93/ 94' Data Catalogue, SAI JRC Special Publication I. 96. 29.

PATTIARATCHI C., A. JAMES, M. COLLINS, 1986: Island wakes and headland eddies: A comparison between remotely sensed data and laboratory experiments., J. Geophys. Res., **92**, 783- 794.

RASCHKE E. (Editor), 1992: Scientific plan for the Baltic Sea Experiment (BALTEX). BALTEX Conference, 30 November to 1 December, 1992, at the GKSS Research Centre in Geesthacht, Germany, pp. 49.

SATHYENDRANATH S., L. PRIEUR. A. MOREL, 1989: A three-component model of ocean colour and its application to the remote sensing of phytoplankton pigment in coastal waters. Int. J. Remote Sensing, **10**, 1373- 1394.

SEMOVSKI S.V., R. HAPTER, A. BESZCZYNSKA- MÖLLER, W. WALCZOWSKI, M. DARECKI, J. SZCZUCKA, M.D. DOWELL, A. STACEKIEWICZ, 1995: Remote sensing of mesoscale features in the Baltic coastal phytoplankton field: Contact observations and models incorporating. In: Proceedings of the Third Thematic Conference on Remote Sensing for Marine and Coastal Environments, Seattle, Washington, 18-20 September 1995, 210- 221.

SIEGEL H., M. GERTH, A. HOELL, T. SCHMIDT, 1994: Typical chlorophyll distribution patterns in the Pomeranian Bight derived from satellite data. In: 19th Conference of the Baltic Oceanographers Proceedings, Gdansk, Poland, August 29–September 1, 1994, Vol.1, 268– 277.

SIEGEL H., M. GERTH, M. BECKERT, 1995: The variation of optical properties in the Baltic Sea and algorithms for the application of remote sensing data.In: Ocean Optics XII, Bergen, Norway, Proceedings, 894- 905.

STRICKLAND L.D.H., T.R. PARSONS, 1972: A practical handbook of sea water analysis. Bulletin 167, Fishering Research Board, Canada, pp. 311.

STURM B., M. KUZMIC, M. ORLIC, 1992: An evaluation and interpretation of CZCS-derived patterns on the Adriatic shelf, Oceanologia Acta, **15**, 13- 24.

SUGIMURA Y., Y. SUZUKI, 1988: A high-temperature catalytic oxidation method for the determination of non-volatile dissolved organic carbon in seawater by direct injection of a liquid sample. Mar. Chem., 105- 131.

TASSAN S., 1994: Local algorithms using SeaWiFS data for the retrieval of phytoplankton, pigments, suspended sediment, and yellow substance in coastal waters. Applied Optics, **33**, 2369- 2378.

TASSAN S., G.M. FERRARI, 1995: An alternative approach to absorption measurements of aquatic particles retained on filters. Limnol. Oceanogr., **40**, 1358- 1368.

VODACEK A., F.E. HOGE, R.U. SWIFT, J.K. YUNGEL, E.T. PELTRER, N.V. BLOUGH, 1995: The use of in situ airborne fluorescence measurements to determine UV absorption coefficient and DOC concentration in surface waters. Limnol. Oceanogr., **40**, 411- 415.

An Adjusted Picture of the Upper Layer in Kattegat

Bjarke Rasmussen

Institute of Hydrodynamics and Hydraulic Engineering, Technical University of Denmark, Building 115, DK-2800 Lyngby, Denmark.

Present Address: Department of Marine Ecology and Microbiology, National Environmental Research Institute, P. O. Box 358, DK-4000 Roskilde, Denmark.

Abstract

The valuable description of stratification in Kattegat developed in the beginning of this century has been used with much success by many authors. Here, two main layers are considered, often including different water masses in the lower layer. The upper layer has primarily been described as a single layer without horizontal and vertical discontinuities. It is suggested to extend the description to include stratification of the upper layer. This upper layer stratification is created by the horizontal spreading of large pulses of Baltic Proper water having recently entered Kattegat. After horizontal spreading, the plume water covers the saltier layer of former Kattegat surface water. This stratification lasts for days. The water column becomes homogeneous to depths of (10 - 15) m only under events of strong wind mixing. The pycnocline, which separates both layers, is then strengthened. The seasonal cycle of stratification develops due to the annual cycle in wind mixing and volume flow through the Belt and the Sound. Spring and summer stratification are found to be similar.

Introduction

Kattegat, the Great Belt and the Sound resemble a transition area between the less salty Baltic Proper and the North Sea. The morphology is mapped in Fig. 1. It is customary to describe the stratification of Kattegat as having two main layers separated by a pycnocline, cf. KNUDSEN (1899, 1900), BO PEDERSEN and MØLLER (1981), STIGEBRANDT (1983), and HANSEN et al. (1995). For the bottom layer a sublayering is often considered, JENSEN (1937). Here, near-bottom Atlantic water and intermediate water from Skagerrak at depths of 40 - 50 m have been identified by KNUDSEN (1905), as well as intrusions of water from the so-called Jutland Coastal Current by JAKOBSEN et al. (1994).

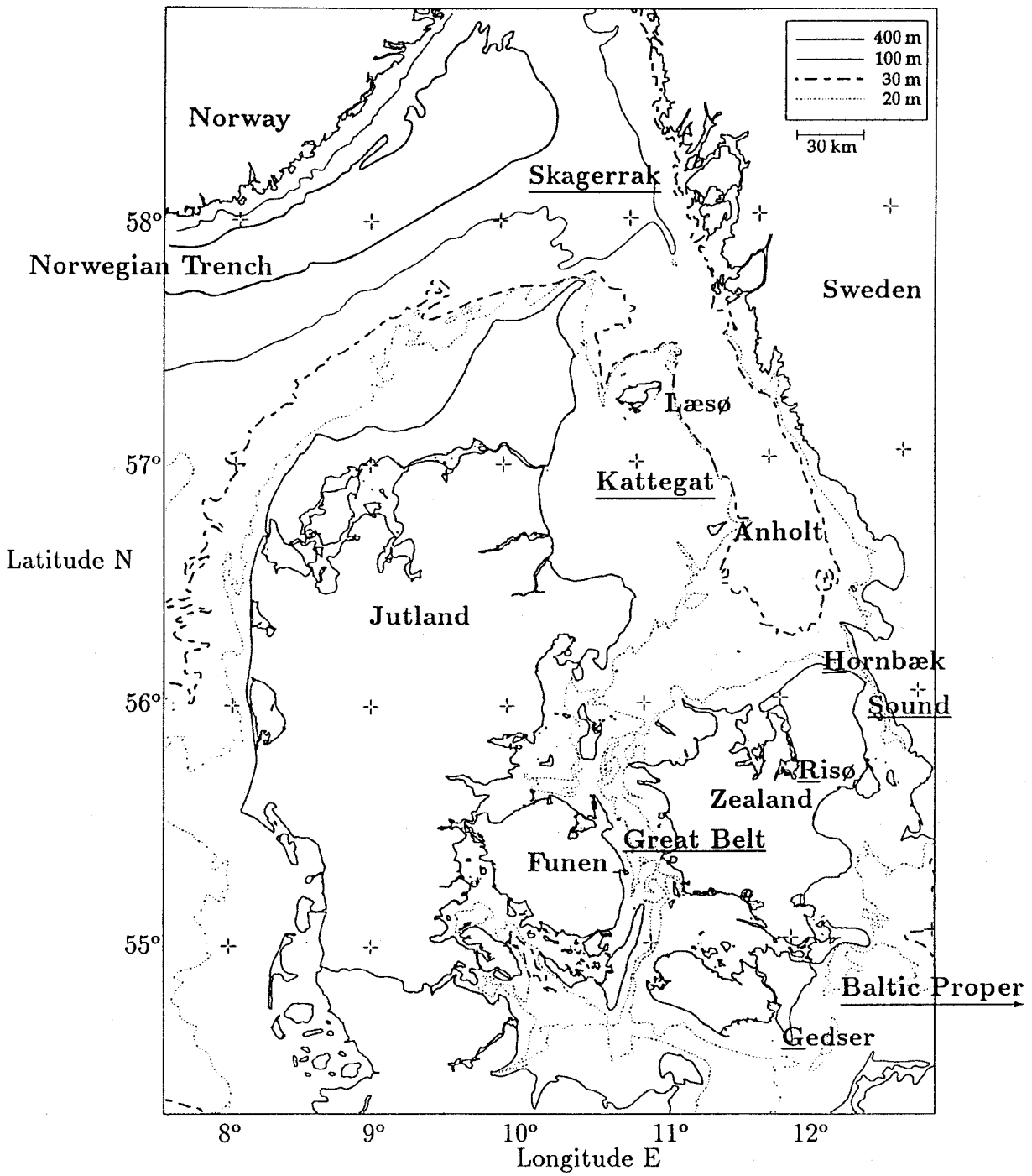

Fig. 1 Locations and morphology; wind data were collected at Risø; the tidal gauge data from Gedser and Hornbæk were used by Jacobsen (1980, 1994) to calculate the volume flux through the Great Belt.

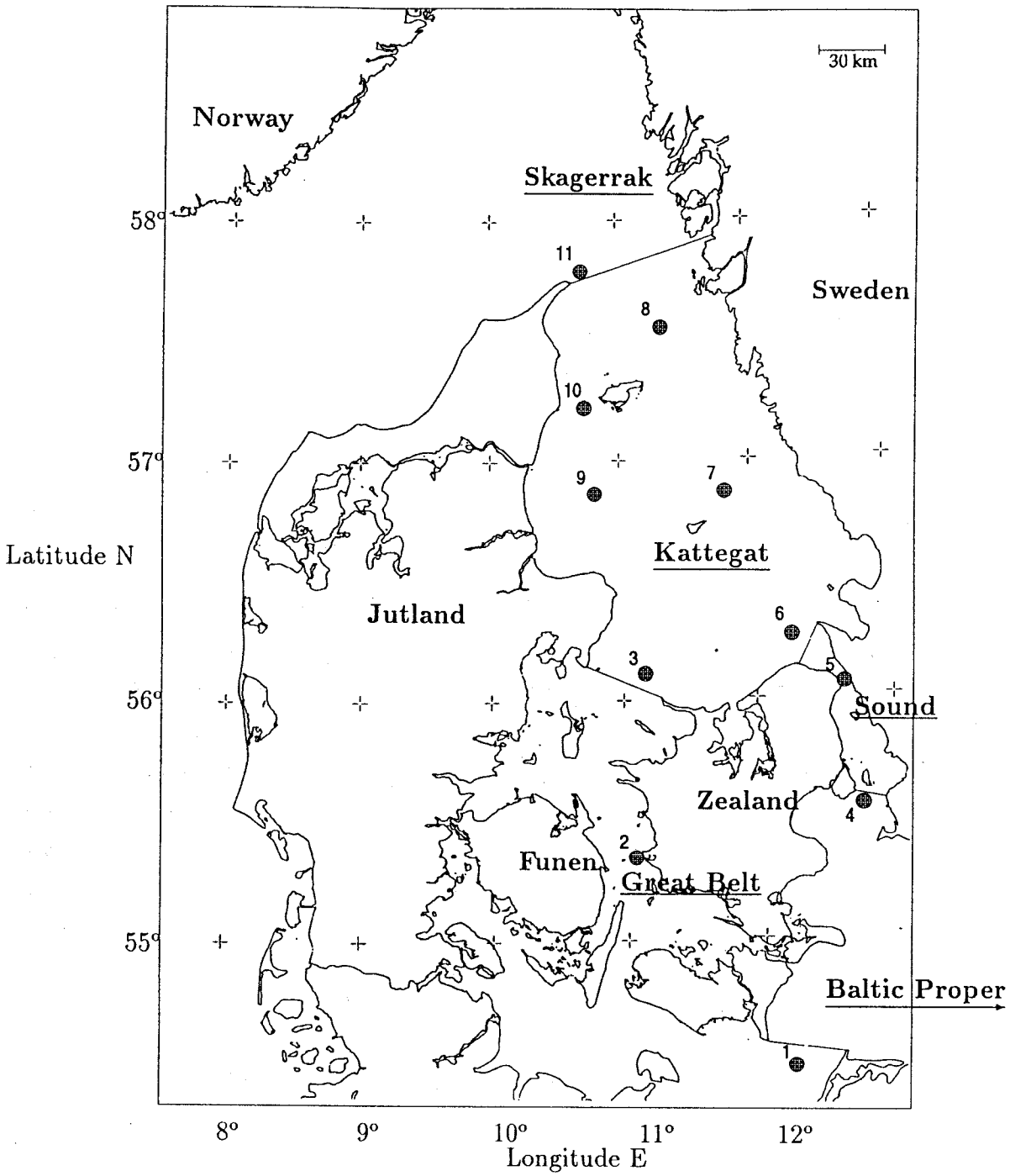

Fig. 2 Positions of light vessels (L/V) in the Great Belt, the Sound and Kattegat:

1) Gedser, 2) Halsskov Rev, 3) Kattegat Sydvest,
4) Drogden, 5) Lappegrunden, 6) Kattegat Syd,
7) Anholt Nord, 8) Læsø Nord, 9) Ålborg Bugt,
10) Læsø-Rende 11) Skagens Rev

(Straight lines indicate the borders of the different regions.)

Often the pycnocline is present at a depth of 10 - 15 m in Kattegat. This has been used to identify the depth of the well-mixed, turbulent upper layer (JENSEN, 1937). Vertical density differences in the upper layer are rarely considered (JACOBSEN and HANSEN, 1985), and marine monitoring programs of Scandinavian countries focus their effort towards a two-layered description of the hydrography in the Kattegat (Anonymous, 1993). The presence of different water masses in the upper layer of Kattegat has been investigated during the last years by BO PEDERSEN (1993) and RASMUSSEN (1995 b). This paper aims to provide a qualitative insight into the formation of stratification above the pycnocline in the Kattegat.

Methods

The hydrodynamics leading to the formation of density difference above the pycnocline are illustrated by light vessel (L/V) data from 1966. The light vessels were located at different positions in the Danish Straits as shown in Fig. 2.The year 1966 was chosen to be representative for a year without extreme events such as major inflows to the Baltic Proper, cf. MATTHÄUS and FRANK (1992). Furthermore, the data coverage is sufficient for 1966. In particular statistics of salinity and vertical density difference from L/V Anholt Nord are discussed. Observations from this light vessel are consistent with observations from other light vessels in Kattegat, RASMUSSEN (1995b). The light vessel observations cover the years 1930 - 76 (1948 - 76). The methods of measuring density and temperature are described in Sparre (1984). Wind velocity data are from Risø. The wind velocity was obtained from measurements taken during the first 10 minutes of each hour from 1958 to 1994 at a height of 76 m. Using a log-profile with a roughness height of 1 mm, the wind velocity was recalculated to the height 10 m above the sea according to Petersen et al. (1981). The wind velocity is given by it's cubed value, as this can be taken to be proportional to the theoretical wind mixing. The volume transport through the Great Belt was estimated by Jacobsen (1994) using the water level difference between tidal gauges at Gedser and Hornbæk covering the years 1893 - 1980. Seasonal cycles have been calculated for salinity, wind velocity and volume flow by calculating a daily mean value, and excluding events with a time scale less than 3 months, Rasmussen (1995b).

Results

Strong winds were observed during most of March as depicted by cubed wind velocities (W^3)in the upper panel of Fig. 3. Outside of this period, only shorter periods of strong winds occurred, which lasted for a few days as also given by peak values in September/

December. Such events were followed by longer periods (weeks) with lighter winds. The transport (Q) through the Belt is correlated to the wind velocity and direction. Inflow ($Q < 0$) of Kattegat Water to the Baltic Sea tends to occur under strong westerly winds, while outflow ($Q > 0$) occurs during calm periods or under easterly winds. Periods of outflow from the Baltic Sea can last for half a month. One larger outflow event was in 1966 observed from end of March to mid May, middle panel of Fig. 3. During such periods the volume transported through the Great Belt is (100 - 200) km^3. Such values are equal to (50 - 100) % of the volume in the upper 10 m-layer of the Kattegat. Periods of large inflow also occur, as for example at end of August. Periods of minor volume transport may last for one or two months.

The volume transport results in large salinity changes in the Danish Straits. The large outflow at end of March brought water from the Baltic Proper into the Kattegat. For instance, the surface salinity then decreased from 26 to 13 (PSU) at L/V Kattegat Sydvest as shown by the upper curve in the lower panel of Fig. 3. This effect decreases with the depth and is only slight visible at 40 m depth. During inflow periods, the salinity generally increases, as it was the case in March. However, not all salinity changes follow the alternating flow through the Great Belt and Sound. Only a small net-flow was present by the end of June, when the salinity increased to 17 ‰. This was older and saltier Kattegat Water that reached the entrance of the Great Belt after an outflow situation transporting Baltic Proper water with salinities of about 12 (PSU) within superficial layers. The flow events also change the near-bottom salinity. Large outflows force the halocline to move downwards in the Great Belt and can result in a northbound near-bottom flow through the Great Belt. This flow may reduce the near-bottom salinity at L/V Kattegat Sydvest in mid-January shown in Fig. 3 c. This Great Belt Water, enters the Kattegat with an intermediate density peak at the halocline depth. The amplitude of salinity variation in the bottom layer is small compared to variations in salinity observed at the sea surface. The salinity difference between bottom and surface observations is therefore largely determined by corresponding fluctuations in the surface waters. The magnitude of this salinity difference fluctuates in the range of (8 - 18) PSU, Fig. 3 c.
Time series of the surface salinity from L/V Gedser Rev to L/V Skagens Rev well reflect the response of the hydrographic regime on changes in the volume transport. Examples are plotted in Fig. 4. During outflow and periods of a small net-flow the salinity at L/V Gedser Rev was about 8 (PSU) over most of the summer period. At the northern boundary of the Kattegat the large volume flow from the Baltic Proper forces the frontal zone between the waters of the Skagerrak and the Kattegat to move northwards and Kattegat Water ($S < 30$) was observed at L/V Skagens Rev.

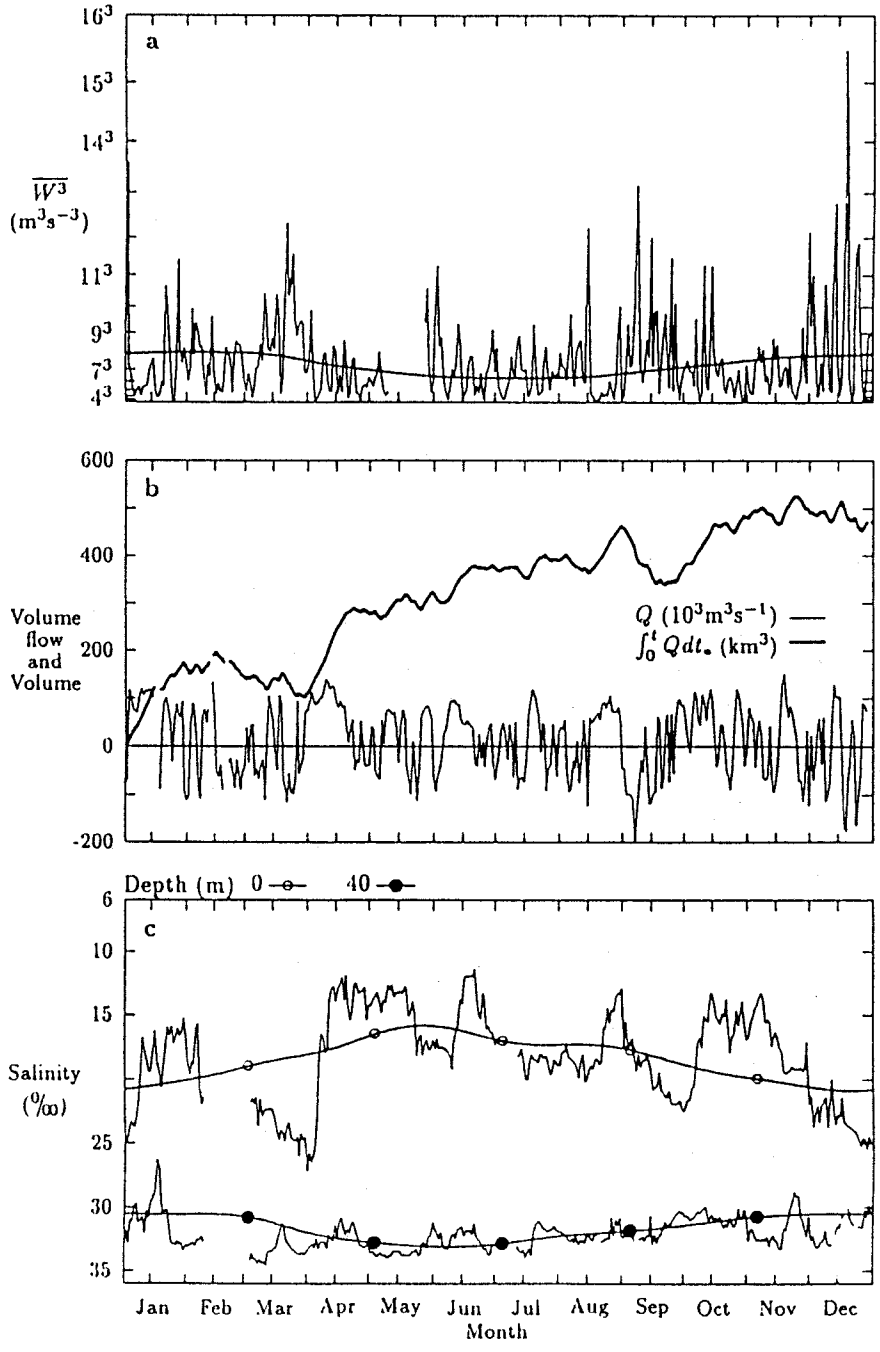

Fig. 3 Year 1966: a) Data of the wind velocity cubed (W^3) and its seasonal mean;
b) volume flow (Inflow: $Q < 0$; Outflow: $Q > 0$) and the associated volume (km^3) transported through the Great Belt;
c) the actual salinity (PSU) and the seasonal means at the surface and at the depth of 40 m observed at the L/V Kattegat Sydvest.

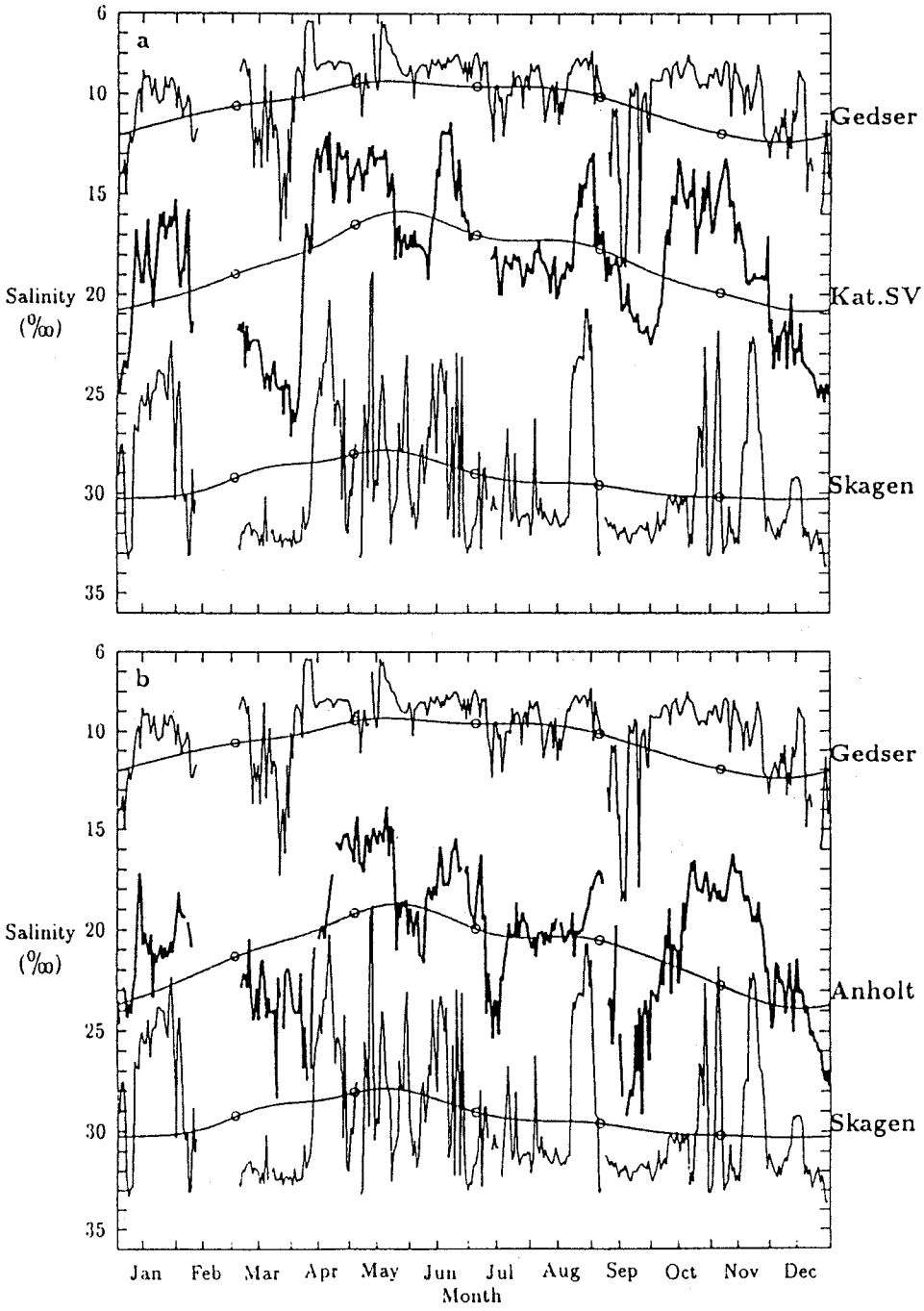

Fig. 4 Year 1966: The surface salinity (PSU) at
a) L/V Kattegat Sydvest (Kat.SV, bold line);
b) L/V Anholt Nord (bold line)
and at the boundaries L/V Gedser Rev and L/V Skagens Rev (thin lines); smoothed curves represent seasonal means.

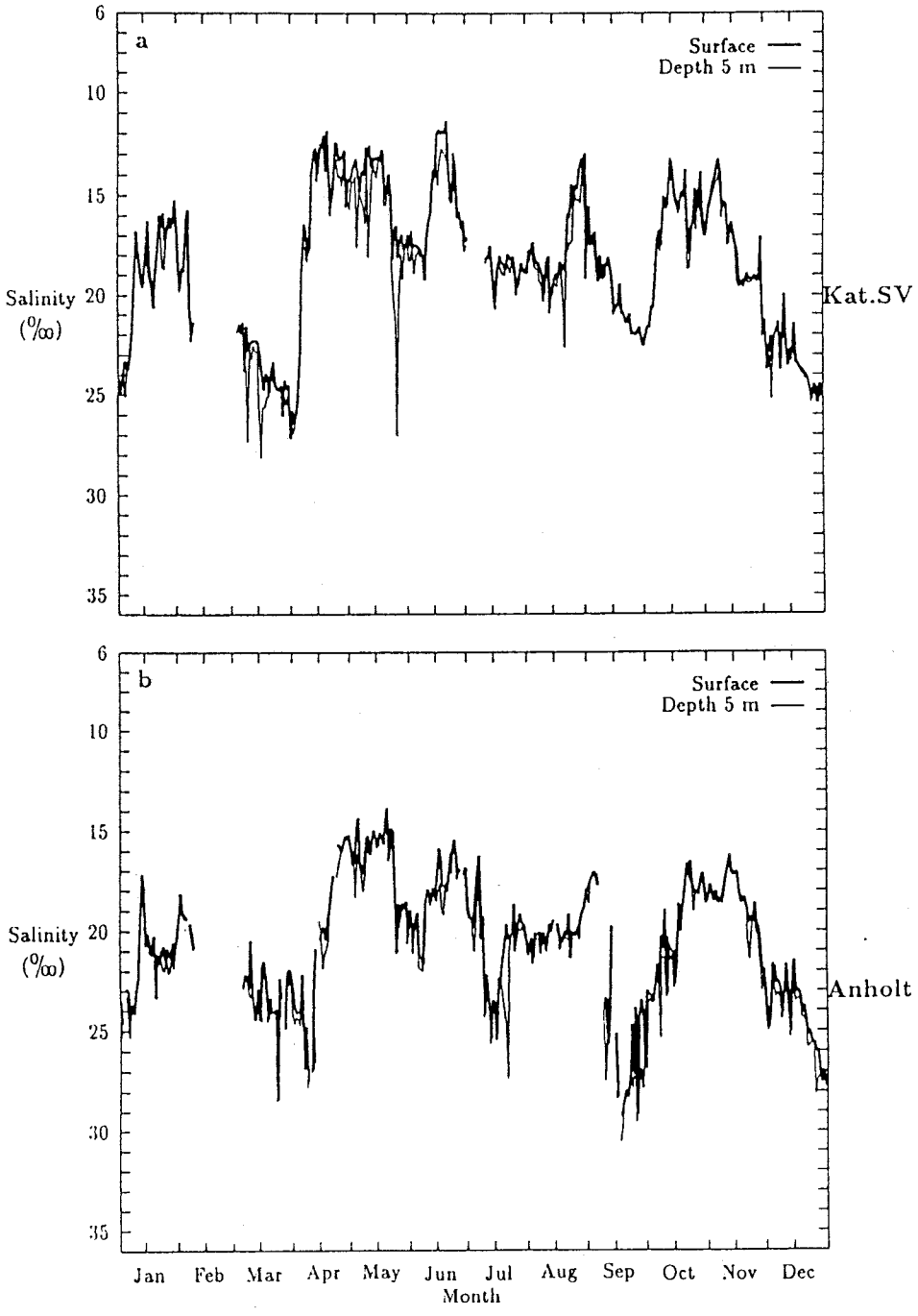

Fig. 5 Year 1966: The salinity at the surface (bold curve) and at 5 m depth for
a) L/V Kattegat Sydvest;
b) L/V Anholt Nord.

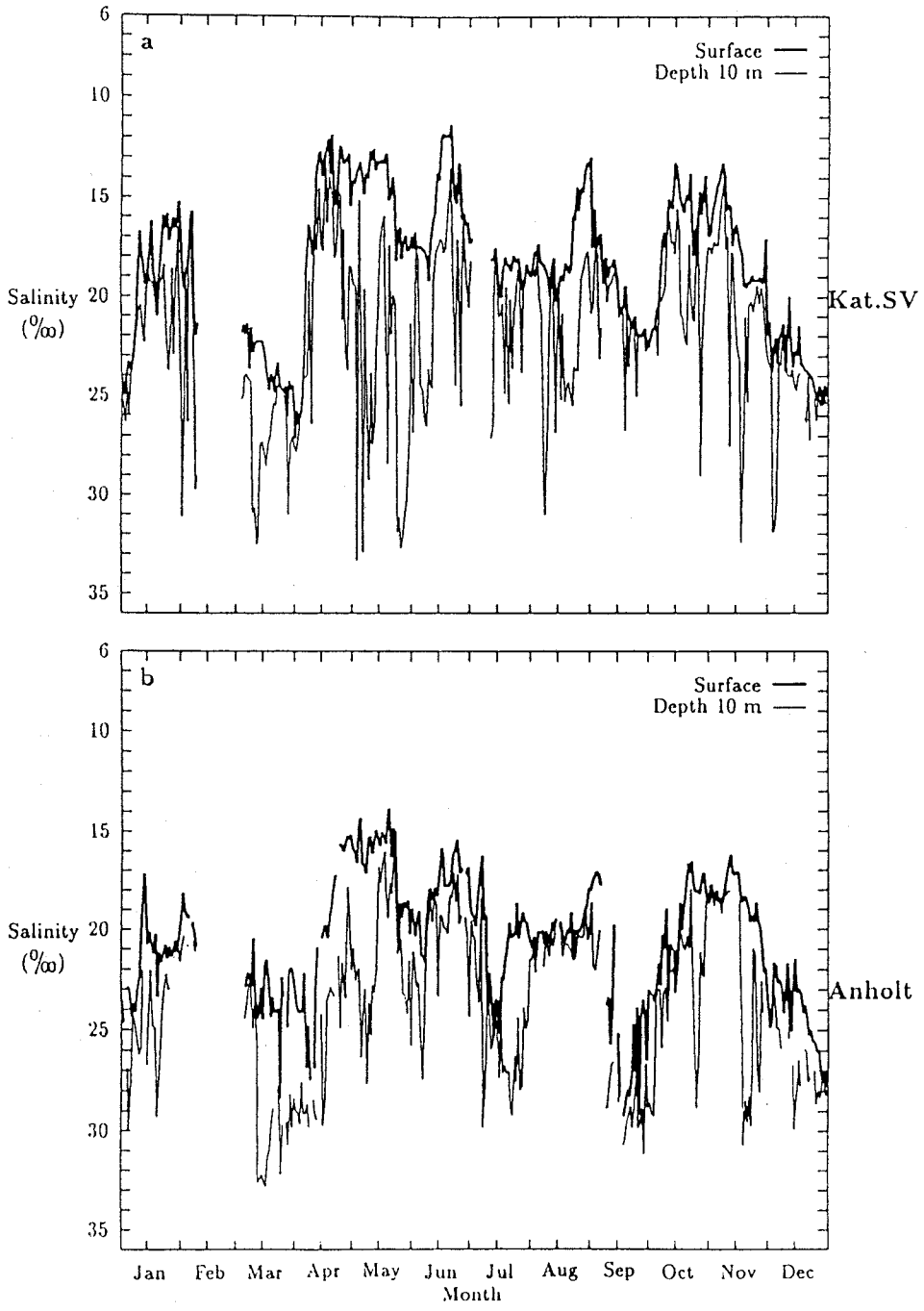

Fig.6 Year 1966: The salinity at the surface and at 10 m depth for
a) L/V Kattegat Sydvest;
b) L/V Anholt Nord.

During an inflow situation, the Skagerrak/Kattegat frontal zone moves southwards, and Skagerrak Water is found at L/V Skagens Rev throughout most of March. Salinity changes at either end of Kattegat (L/V Kattegat Sydvest and L/V Skagens Rev) occurred within (7 - 14) days over most of the Kattegat.

The salinity distributions at the surface and at 5 m depth are generally similar, but periodically the salinity at 5 m depth is larger than at the surface. Such series are plotted in Fig. 5. Resulting differences are seldom greater than 5 (PSU), and they are presumably caused by an upward movement of the halocline as observed at the end of May and in early July, Fig. 5 (a, b). In general, the salinity difference is less than 1 (PSU) and probably caused by a horizontal spreading of low-salinity water. The salinity difference in the upper 10 m is only occasionally less than 1 (PSU). Such value can be explained in terms of the flow direction; outflow increases the salinity difference but inflow causes its reduction. The short-term salinity variations are much larger at 10 m depth than those at 5 m depth or at the sea surface. Corresponding series are drawn in Fig. 6 (a, b). Therefore, the effect of up- and downward movements of the halocline cannot be neglected at 10 m depth.

Above, the changes in salinity and density difference have been described with respect to the horizontal advection and pycnocline movements. Within superficial layers, the vertical density differences are influenced by wind mixing. Related salinity differences in the upper 5 m visually have, however, no obvious linkage to the wind velocity cubed, compare Fig. 3a with Fig. 5 (a, b). In order to elucidate the role of wind mixing and advection on the formation/ maintenance of vertical density gradients in the upper layer, the seasonal cycles and probability functions are calculated for wind velocity cubed (W^3), volume flow (Q), salinity (DS) and density differences (Dr). The wind velocity cubed has a magnitude of (4^3 - 10^3) m^3s^{-3} for approximately 80 % of all observations (Fig. 7 a). The cubed wind velocity has a seasonal cycle (Fig. 7 b) with an annual mean of approximately 7.4^3 m^3s^{-3}. During winter (December - February) the largest values occur (8^3 m^3s^{-3}) and autumn values are slightly lower. In June and July the lowest mean values are found (6.7^3 m^3s^{-3}), which is a factor two lower than the winter values. The standard deviation of the wind velocity cubed has the same magnitude as the mean values and follows the same seasonal cycle (Fig.7 c).

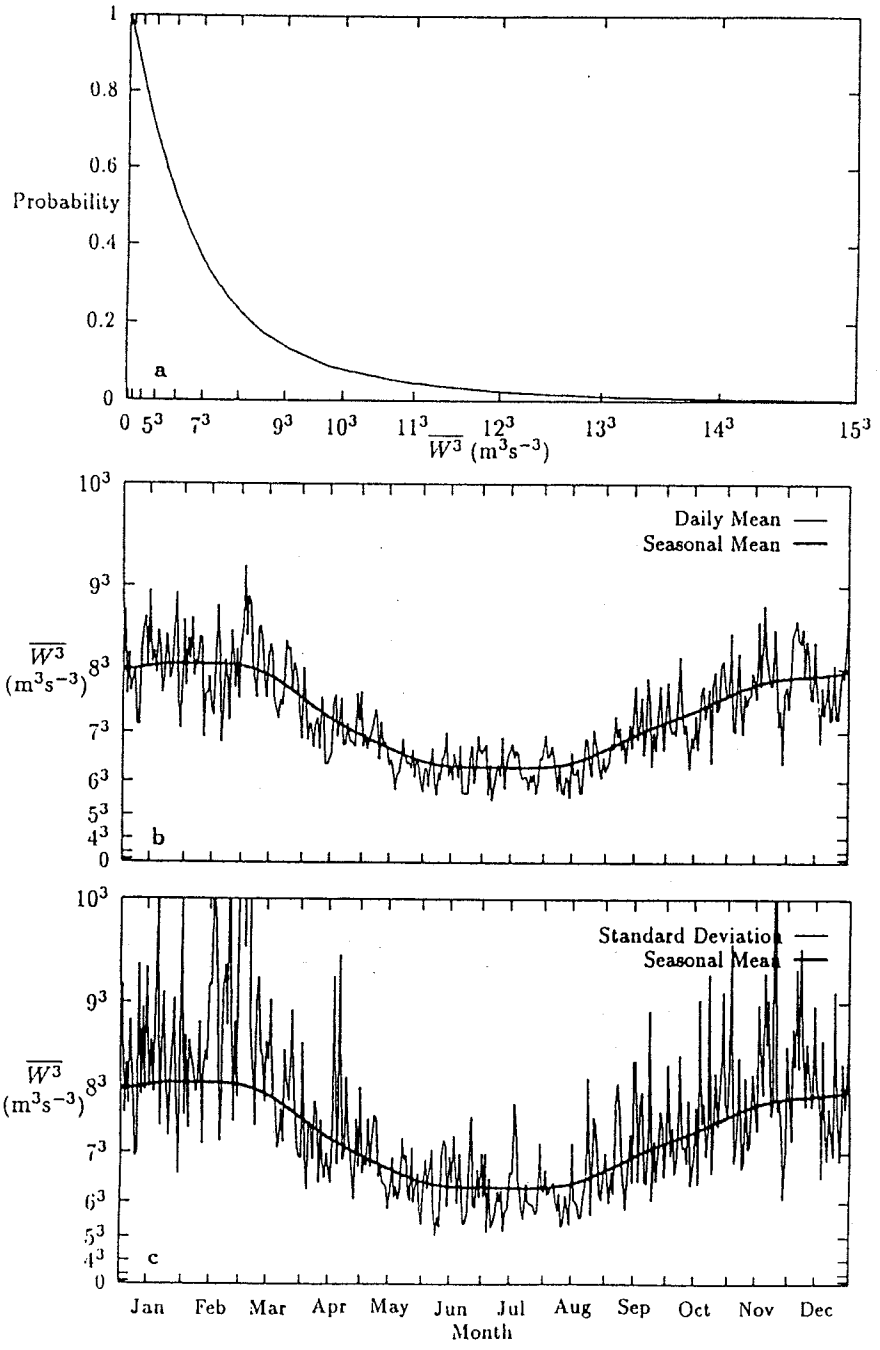

Fig. 7 Wind velocity cubed (W^3) at Risø, recalculated to the height of 10 m:
a) probability distribution;
b) the daily mean values and the smoothed seasonal cycle;
c) the standard deviation of (b) and its smoothed seasonal cycle.

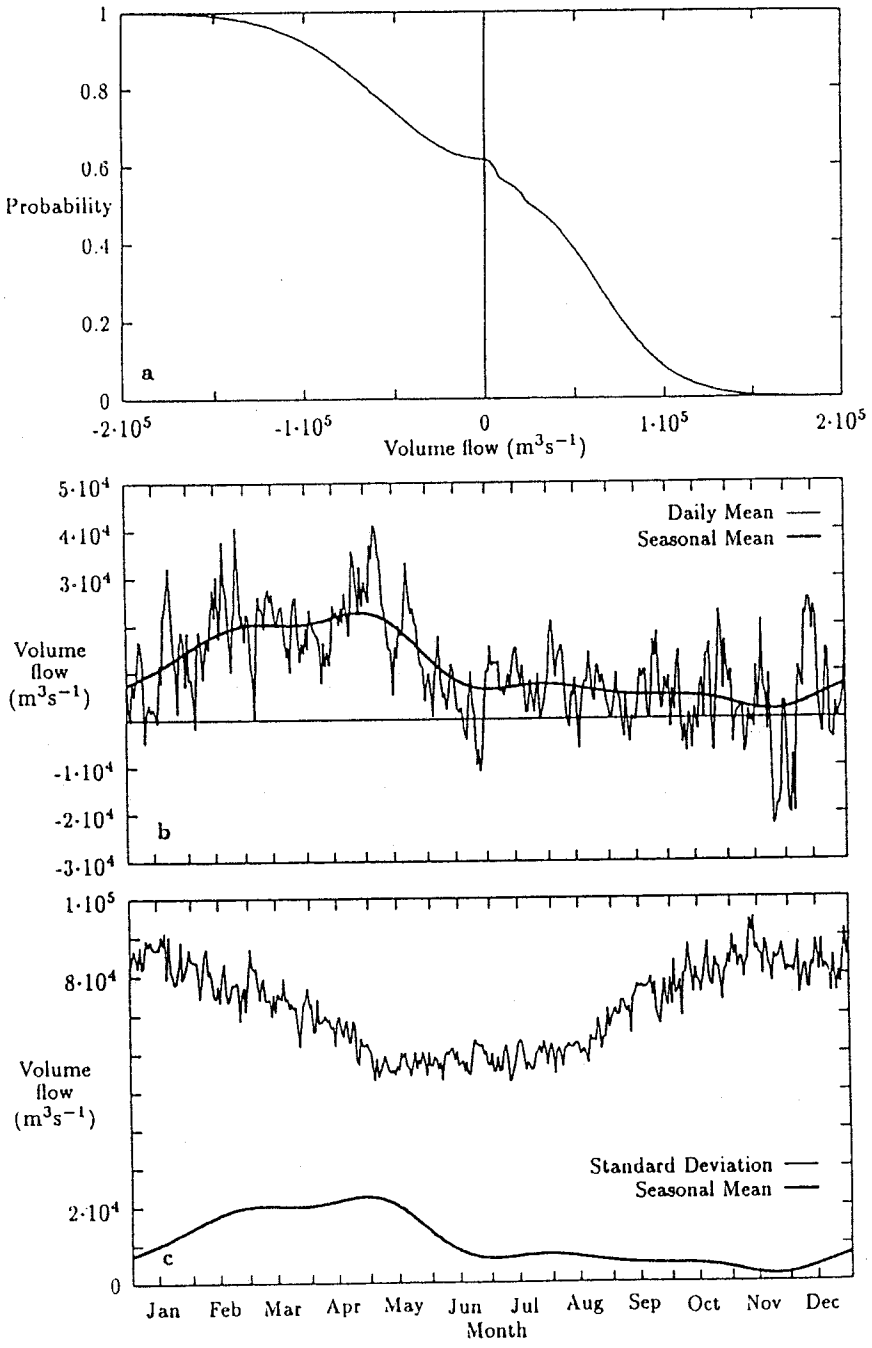

Fig.8 Volume flow through the Great Belt:

a) the probability distribution

b) daily mean values and the smoothed seasonal cycle (bold line);

c) the standard deviation of the daily mean values and its smoothed seasonal cycle.

Generally, it is expected that enhanced wind conditions will be followed by well-mixed conditions in the upper part of the water column, i. e. the well-mixed layer deepens. Due to the seasonal cycle in wind mixing, the upper 5 - 10 m layer of the Kattegat should generally be homogeneous in winter, while stratified in summer. However, as seen from the description of the hydrographical changes in 1966, the volume flow plays a dominant role in the salinity changes. According to Fig. 8 a, of the daily flow through the Great Belt approximately 38 % of the observations correspond to outflow situations larger than $5 \cdot 10^4$ m^3s^{-1}, while 25 % of the inflow events are only larger than $5 \cdot 10^4$ m^3s^{-1}. The mean flow through the Great Belt is enhanced from the end of winter until the beginning of summer as demonstrated in Fig. 8 b, while it is reduced in the remaining part of the year to $(2.1 - 0.8) \cdot 10^4$ m^3s^{-1}, for autumn and winter respectively. The standard deviation of the mean flow is a factor of (4 - 12) larger than its mean value, Fig. 8 c. The seasonal cycle of the mean flow and associated fluctuations are not similar. Large in- and outflow events occur during autumn and winter, while the summer period has minor volume flows. Generally, the largest outflow should correspond to the formation of density differences in the surface layer, as the outflow brings low-salinity water to the Kattegat. At the end of winter and in spring, the largest outflow from the Baltic Proper is found, and, it can be expected that stratification in the upper layer mainly should be observed during the late winter and in spring.

The surface layer depth and stratification is, for instance, evaluated from the statistics of salinity and vertical density differences at L/V Anholt Nord. The broad salinity range observed (10 - 15, PSU) at L/V Anholt Nord is mainly due to short-term changes as shown in Fig. 9a. The annual variation is only of (3 - 5) PSU, Fig. 9 b. The observations show a large difference in the salinity distribution in the layer between 5 m and 15 m depth. A similar distinction is found in the seasonal-mean values of salinity. Here observations at the surface and at 5 m depth have a similar seasonal cycle, while those at 10 m depth and deeper are different. Surface layer water is found above 10 m depth. In May the mean salinity reduces to its minimum in the upper 5 m, Fig. 9 b. The reduction of the surface salinity takes place from early spring, during the period of maximum mean outflow from the Baltic Proper. The surface salinity reduction coincides with an enhanced probability to observe vertical density difference in the upper (5 - 10) m layer at L/V Anholt Nord, Fig. 9 (c, d). The probability functions of the density differences for winter and autumn are similar. Furthermore, these functions are also similar for spring and summer environmental conditions. The probability of observing no-density differences in the upper 5 m layer with values $\Delta\rho < 0.1$ kg m^{-3} at Anholt Nord is only slightly enhanced during the winter months (0.25) compared to spring and

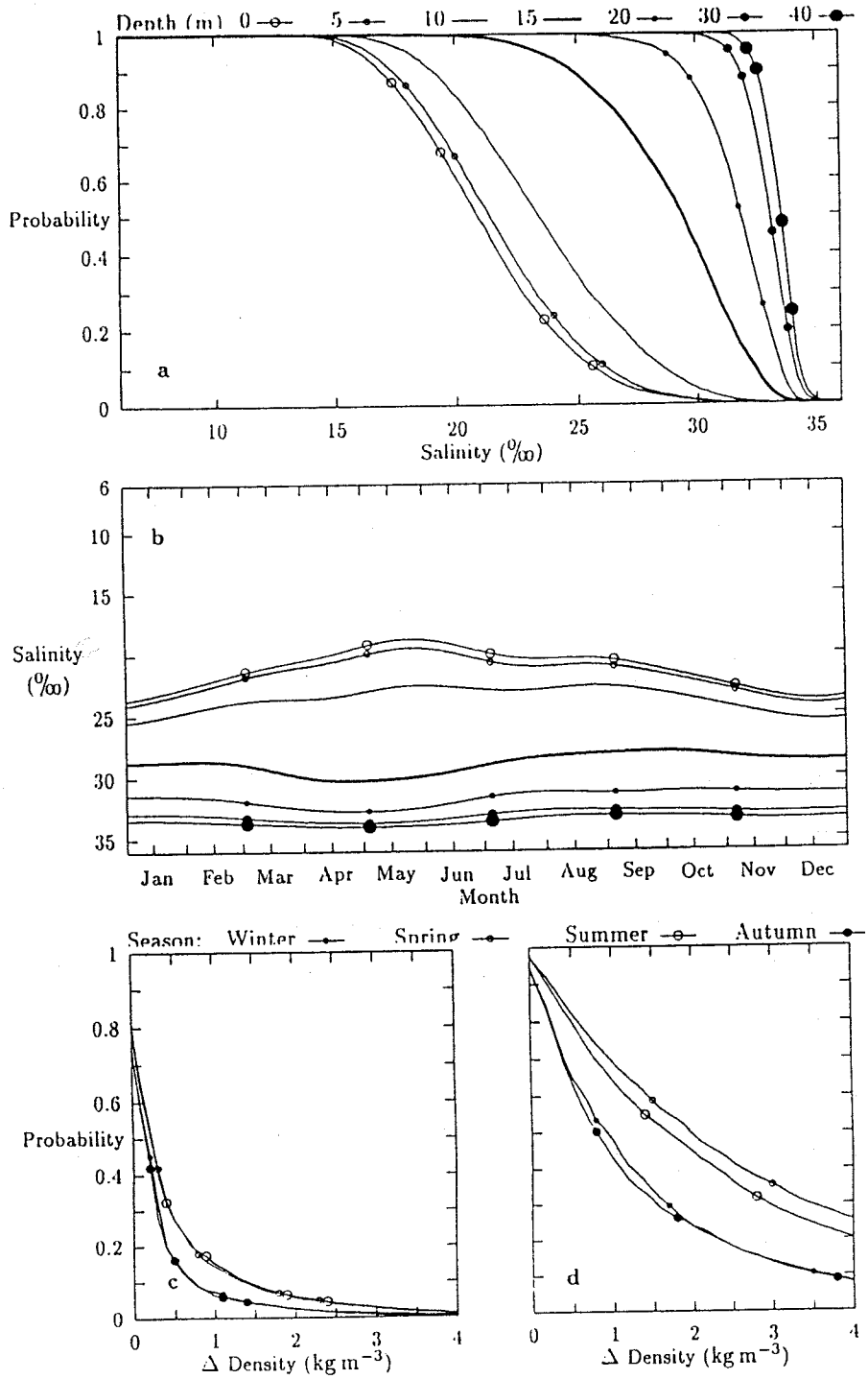

Fig. 9 L/V Anholt Nord (depth range between the surface and 40 m):

a) probability functions of salinity;

b) the seasonal cycle in salinity;

c) the seasonal variation of the vertical density difference in the upper 5 m layer

d) as c) but in the upper 10 m.

	Stratification:		Stratified		Homogeneous	
	Light Vessel	h (m)	$\overline{W^3}$ (m^3s^{-3})	Period (Days)	$\overline{W^3}$ (m^3s^{-3})	Period (Days)
1	Gedser Rev	5 10 15	398.9 398.9 404.6	2.4 7.0 19.0	444.5 512.0 631.8	2.7 1.7 1.4
2	Halsskov Rev	5 10 15	416.2 421.9 421.9	4.5 17.1 81.9	467.3 517.6 706.2	1.9 1.4 1.2
3	Kattegat Sydvest	5 10 15	346.2 381.4 410.3	3.5 10.7 64.4	528.5 653.3 679.8	2.4 1.5 1.3
5	Lappegrunden	5 10 15	387.3 421.9 427.5	7.3 49.8 184.5	637.2 946.7 946.7	1.4 1.2 1.2
6	Kattegat Syd	5 10 15	427.5 450.3 456.0	7.7 21.2 109.4	637.2 727.1 727.1	1.7 1.2 1.2
7	Anholt Nord	5 10 15	381.4 398.9 393.0	3.6 15.2 129.9	517.6 550.6 784.3	2.0 1.4 1.3
8	Læsø Nord	5 10 15	369.8 393.0 398.9	3.6 11.4 32.7	550.6 626.6 679.8	2.0 1.4 1.4
9	Ålborg Bugt	5 10	358.1 398.9	4.9 22.3	556.0 695.7	2.3 1.7
10	Læsø Rende	5 10 15	346.2 381.4 393.0	3.4 13.2 43.9	495.3 626.6 820.3	2.3 1.5 1.5
11	Skagens Rev	5 10 15	387.3 404.6 410.3	4.2 9.6 18.5	523.0 556.0 517.6	2.0 1.5 1.4

Table 1 Mean values of the wind velocity cubed and the duration for stratified [$\Delta\rho > 0.1$ kg m^{-3}] and homogeneous periods observed at different light vessel (L/V) from 1958 to the end of the light vessel period; positions are mapped in Fig.2.

summer (0.20). In the upper 10 m layer, the probability of observing no-vertical density difference is reduced to be 0.05 during winter/autumn but 0.03 during spring/summer. The water column is only homogeneous during events of strong wind mixing. This follows from Table 1. The wind velocity cubed is enhanced by a factor of 2 during such homogeneous periods (1 - 3 days), which are short compared to the duration of stratified periods (2 - 8 days).

Discussion

The salinity changes in the Danish Straits are mainly governed by the volume flow. The volume flow results in halocline and frontal movements, where outflow increases the halocline depth, while the Skagerrak/Kattegat surface frontal zone moves to the north, MØLLER (1980). To the south of the Kattegat, the plumes passing through the Great Belt and the Sound also result in frontal structures of superficial layers. The Great Belt plume flows into Kattegat and where it then turns slightly to the right due to the influence of the Coriolis force, while it gets horizontally dispersed, and wind mixing entrains denser water into the plume. During outflow, the Sound plume follows the Swedish coast. According to BO PEDERSEN (1993), this plume moves laterally due to flow reversal. In the Kattegat, the structure of surface salinity distributions is reduced during outflow but much more patterned during inflow events. Due to the horizontal inhomogeneities, which are introduced by the plumes of Baltic Proper Water, departures occur from this general picture. A regionally forced estuarine circulation causes older and saltier Kattegat Water to increase the surface salinity during or just after outflow events.

At all light vessels a broad salinity range is found, and plumes of recent Baltic Proper Water seem, therefore, to reach most of the Kattegat. This notion is supported by other studies analysing single events, cf. POULSEN (1991), and JAKOBSEN et al. (1994). An outflow from the Baltic Proper often lasts 4 - 6 days, JACOBSEN (1980), and allows approximately 40 km^3 of less salty water to enter the Kattegat. This volume represents 20 % of that in the upper 10 m layer of the Kattegat. Such value causes large horizontal density differences before the plumes become mixed and so loose their identity in terms of salinity. Therefore, the simple assumption that the whole near surface layer in the

Kattegat has a horizontally slightly increasing density can not be maintained, even though it has been implicit in some of the recent modelling efforts, cf. JENSEN (1937), PEDERSEN and MØLLER (1981), STIGEBRANDT (1983), JACOBSEN and HANSEN (1985), and HANSEN et al. (1995).

Due to the horizontal density gradients, intrusion is often identified as discussed in BO PEDERSEN (1993) and RASMUSSEN (1995a). Associated plumes involve vertical density differences larger than 0.1 kg m^{-3} to remain for 2 - 8 days within the upper 5 m layer. Since such vertical density differences are present in 75 % of all observations, the buoyancy input can compete with wind mixing at this shallow depth. Considering the two layer approach, only during events of strong wind mixing do these two layers become mixed to strengthen the pycnocline at a depth of 10 to 15 m. Hence, it is suggested that the two layer description of the Kattegat, which was originally given by KNUDSEN (1899, 1900), may be extended to include two layers above the pycnocline. Here, the saltier Kattegat Water generally lies below a surface layer formed by Baltic Proper Water. These two top-layers are found temporally between alternating events of intense wind mixing.

The main mixing agent in the Kattegat is the wind, which provides a supply of external energy. Considering the vertical displacement of the associated pycnocline, the tidal effect is only small in most Kattegat areas, according to SVANSSON (1975) approximately 0.1 m. If the wind mixing was dominating the seasonal cycle of stratification, a similarity between the wind velocity cubed and the stratification could be expected. Such a linear relationship is not present, as the distribution of vertical density differences are similar in winter and autumn as well as in spring/autumn. That is the stratification during the windy spring and the calm summer are similar. The seasonal cycle of stabilisation of the surface layer therefore needs to be considered. It is suggested that the stabilisation causing summer-like stratification during spring is a result of enhanced fresh-water flux, which carries large volumes of less salty water from the Baltic Proper to the Kattegat. Solar heating as estimated by HANSEN and JACOBSEN (1985) gives only a minor contribution to the stabilisation of the upper 5 - 10 m in the Kattegat, RASMUSSEN (1995b).

In the Kattegat, the presence of minor density differences above the pycnocline has been used by JENSEN (1937) as an argument for an ongoing vertical exchange between the two main layers. Increasing vertical density gradients can, however, be due to events of strong wind mixing, PHILLIPS (1969). The density gradient within near-surface layers temporally prevents wind-generated turbulence reaching depths deeper than (5 - 10) m. Temperature inhomogeneities can then persist for weeks, RASMUSSEN (1995a), and the formation of

oxygen minimum and maximum layers is possible according to JACOBSEN (1908), KRUSE and RASMUSSEN (1995), and RASMUSSEN (1995b). This suppression of turbulence by minor density differences is well documented by both laboratory experiments in TURNER (1986) and in the field by BRAINERD and GREGG (1993). Hence, the presence of vertical density gradients above the pycnocline must in general be considered as being an indication of reduced turbulence rather than an ongoing exchange between the two main layers.

Conclusion

It is suggested to modify the valuable understanding of the stratification of the Kattegat, which was originally given by KNUDSEN (1899, 1900), by extending the upper layer description to include a near-surface stratification. Large volumes of less salt, Baltic Proper Water periodically entering Kattegat cause the near-surface stratification to develop. Horizontal density gradients are then established by frontal zones to force intrusions, which involve vertical density gradients within the upper 5 to 10 m layer of the Kattegat. Such stratification within the top layer can be understood to be produced by a layer of older Kattegat Water below a less-salinity layer of Baltic Proper Water. During wind mixing events the water properties of both sublayers are well mixed and the main pycnocline may be strengthened at depths of (10 - 15) m. With respect to the stratification, the transition area of the Kattegat must be considered as filled up by an inhomogeneous water body with both vertical and horizontal gradients. Both wind mixing and volume flow of less dense water need to be included in the description of the resulting hydrography.

Acknowledgements

This paper describes some of the results in the authors Ph.D.-thesis written under supervision of Torkel Gissel Nielsen, Flemming Bo Pedersen and the late Torben Schelde Jacobsen. The paper has further benefited from the contributions of Daniel Conley, Anders Højgård Petersen, David Larkin and Adolf Stips. Wind velocity data from Risø have kindly been provided by the Research Centre Risø by Jørgen Brandt and Søren Larsen. The work has been financed partly by the National Environmental Research Institute and partly by the National Environmental Protection Agency under the research program HAV90 (project nr. 2.36).

References

ANONYMOUS, 1993: Inventering av hyrdrodynamiska modeller och valideringsda før Kattegat-Skagerrak. Nordiske Seminar - og Arbejdsrapporter, 56 pp.

BO PEDERSEN, F., 1993: Fronts in the Kattegat: The hydrodynamic regulating factor for biology. Estuaries, **16**: 104 - 112.

BO PEDERSEN, F. AND J. S. MØLLER, 1981: Diversion of the river Neva. Nordic Hydrology, **12**: 1 - 20.

BRAINERD, K. E., AND M. C. GREEG, 1993: Diurnal restratification and turbulence in the oceanic surface mixed layer. Journal of Geophysical Research, **98**: 22645 - 22664.

HANSEN, I. S., G. ÆRTEBJERG, AND K. RICHARDSON, 1995: A scenario analysis of effects of reduced nitrogen input on oxygen conditions in the Kattegat and Belt Sea. Ophelia, **42**: 75 - 94.

JACOBSEN, J. P., 1908: Der Sauerstoffgehalt des Meereswassers in den Dänischen Gewässern innerhalb Skagens. Bidrag til de Danske Farvandes Hydrografi. Medd. Komm. Havunders., Ser. Hydrogr., **1**: 12, 23 pp (in German).

JACOBSEN, T. S., 1994: Blandingsenergi fra vind og strøm i Storebælt. Miljøstyrelsen, 49 pp (in Danish with English summary). - Havforskning fra Miljøstyrelsen, nr. 31.

JACOBSEN, T. S., 1980: Sea Water Exchange of the Baltic. Measurements and Methods. The National Agency of Environmental Protection, Copenhagen, Denmark, 106 pp.

JACOBSEN, T. S. AND N.-E. O. HANSEN, 1985: Oxygen depletion in the Kattegat. Nordic Hydrology, **16**: 237 - 256.

JAKOBSEN, F., G. ÆRTEBJERG, C. T. AGGER, N. HØJERSLEV, N. HOLT, J. HEILMANN AND K. RICHARDSON, 1994: Hydrografisk og biologisk beskrivelse af Skagerrak-fronten Havforskning fra Miljøstyrelsen, nr. 49, 112 pp (in Danish with English summary)

JENSEN, J. C. , 1937: Fluctuations in the hydrography of the transition area during 50 years. Rapport et Procés-Verbaux, **CII.**

KNUDSEN, M., 1899: De hydrografiske Forhold i de danske Farvande inden for Skagen. Beretning fra Commissionen for videnskabelig Undersøgelse af de danske Farvande. Andet Bind, andet Hefte, Copenhagen (in Danish).

KNUDSEN, M., 1900: Ein hydrographischer Lehrsatz. Annalen der Hydrographie und Maritimen Meteorologie, 316 - 320 (in German).

KNUDSEN, M., 1905: Havets Naturlære. Hydrografi med særligt Hensyn til de danske Farvande. G. E. G. Gad, Copenhagen (in Danish).

KRUSE, B. AND B. RASMUSSEN, 1995: The occurrence of a subsurface oxygen minimum layer over a small length scale in a stratified coastal water in spring. Marine Ecology Progress Series. **125**: 293 - 303.

MATTHÄUS, W. AND H. FRANK, 1992: Characteristics of major Baltic inflow - a statistical analysis. Continental Shelf Research, **12**: 1375 - 1400.

MØLLER, J. S., 1980: Østersøens Hydrografi. En model med henblik p vurdering af ferskvandstilstrømningens betydning. Internal Report. Institute of Hydrodynamics and Hydraulic Engineering, Technical University of Denmark. 126 pp. Master Thesis (in Danish).

PETERSEN, E. L., I. TROEN, S. FRANDSEN AND K. HEDEGAARD, 1981: Windatlas for Denmark. A Rational Method of Wind Energy Siting. Risø National Laboratory, DK-4000 Roskilde, 229 pp.

PHILLIPS, O. M., 1969: The Dynamics of the Upper Ocean. Cambridge University Press, Cambridge, 261 pp.

POULSEN, O., 1991: The hydrography of Skagerrak and Kattegat. The dynamics of the Skagerrak front. Series Paper 54. Institute of Hydrodynamics and Hydraulic Engineering, Technical University of Denmark. 164 pp. Ph.D.-Thesis.

RASMUSSEN, B., 1995a: Stratification and wind-mixing in the southern Kattegat.

Ophelia **42**: 319 - 334.

RASMUSSEN, B., 1995b: Stratification in Kattegat. National Environmental Research Institute. Department of Marine Ecology and Microbiology, Denmark, 145 pp. Ph.D.-thesis.

SPARRE, A., 1984: The Climate of Denmark, Summaries of Observations from Light Vessels (IV), Salinity A, Means, Extremes and Frequency. Danish Meteorological Institute, Climatological Papers, no 11. Copenhagen, Denmark, 232 pp.

STIGEBRANDT, A., 1983: A model for the exchange of water and salt between the Baltic and the Skagerrak. Journal of Physical Oceanography, **13**: 411 - 427.

Svansson, A., 1975: Physical and Chemical Oceanography of the Skagerrak and the Kattegat. Fishery Board of Sweden. Institute of Marine Research, Report No. 1, 44 pp.

TURNER, J. S., 1986: Turbulent entrainment: the development of the entrainment assumption, and its application to geophysical flows. Journal of Fluid Mechanics, **173**: 431 - 471.

Meereswissenschaftliche Berichte

MARINE SCIENCE REPORTS

---

1 (1990) Postel, Lutz:
Die Reaktion des Mesozooplanktons, speziell der Biomasse, auf küstennahen Auftrieb vor Westafrika (The mesozooplankton response to coastal upwelling off West Africa with particular regard to biomass)

2 (1990) Nehring, Dietwart:
Die hydrographisch-chemischen Bedingungen in der westlichen und zentralen Ostsee von 1979 bis 1988 – ein Vergleich (Hydrographic and chemical conditions in the western and central Baltic Sea from 1979 to 1988 – a comparison)
Nehring, Dietwart; Matthäus, Wolfgang:
Aktuelle Trends hydrographischer und chemischer Parameter in der Ostsee, 1958 – 1989 (Topical trends of hydrographic and chemical parameters in the Baltic Sea, 1958 – 1989)

3 (1990) Zahn, Wolfgang:
Zur numerischen Vorticityanalyse mesoskaler Strom- und Massenfelder im Ozean (On numerical vorticity analysis of mesoscale current and mass fields in the ocean)

4 (1992) Lemke, Wolfram; Lange, Dieter; Endler, Rudolf (Eds.):
Proceedings of the Second Marine Geological Conference – The Baltic, held in Rostock from October 21 to October 26, 1991

5 (1993) Endler, Rudolf; Lackschewitz, Klas (Eds.):
Cruise Report RV "Sonne" Cruise SO82, 1992

6 (1993) Kulik, Dmitri A.; Harff, Jan:
Physicochemical modeling of the Baltic Sea water-sediment column: I. Reference ion association models of normative seawater and of Baltic brackish waters at salinities 1–40 ‰, 1 bar total pressure and 0 to 30°C temperature
(system Na-Mg-Ca-K-Sr-Li-Rb-Cl-S-C-Br-F-B-N-Si-P-H-O)

7 (1994) Nehring, Dietwart; Matthäus, Wolfgang; Lass, Hans-Ulrich; Nausch, Günther:
Hydrographisch-chemische Zustandseinschätzung der Ostsee 1993

8 (1995) Hagen, Eberhard; John, Hans-Christian:
Hydrographische Schnitte im Ostrandstromsystem vor Portugal und Marokko 1991 - 1992

9 (1995) Nehring, Dietwart; Matthäus,Wolfgang; Lass, Hans Ulrich; Nausch, Günther; Nagel, Klaus:
Hydrographisch-chemische Zustandseinschätzung der Ostsee 1994
Seifert, Torsten; Kayser, Bernd:
A high resolution spherical grid topography of the Baltic Sea

10 (1995) Schmidt, Martin:
Analytical theory and numerical experiments to the forcing of flow at isolated topographic features

11 (1995) Kaiser, Wolfgang; Nehring, Dietwart; Breuel, Günter; Wasmund, Norbert; Siegel, Herbert; Witt, Gesine; Kerstan, Eberhard; Sadkowiak, Birgit:
Zeitreihen hydrographischer, chemischer und biologischer Variablen an der Küstenstation Warnemünde (westliche Ostsee)
Schneider, Bernd; Pohl, Christa:
Spurenmetallkonzentrationen vor der Küste Mecklenburg-Vorpommerns

12 (1996) Schinke, Holger:
Zu den Ursachen von Salzwassereinbrüchen in die Ostsee

13 (1996) Meyer-Harms, Bettina:
Ernährungsstrategie calanoider Copepoden in zwei unterschiedlich trophierten Seegebieten der Ostsee (Pommernbucht, Gotlandsee)

14 (1996) Reckermann, Marcus:
Ultraphytoplankton and protozoan communities and their interactions in different marine pelagic ecosystems (Arabian Sea and Baltic Sea)

15 (1996) Kerstan, Eberhard:
Untersuchung der Verteilungsmuster von Kohlenhydraten in der Ostsee unter Berücksichtigung produktionsbiologischer Meßgrößen

16 (1996) Nehring, Dietwart; Matthäus, Wolfgang; Lass, Hans Ulrich; Nausch, Günther; Nagel, Klaus:
Hydrographisch-chemische Zustandseinschätzung der Ostsee 1995

17 (1996) Brosin, Hans-Jürgen:
Zur Geschichte der Meeresforschung in der DDR

18 (1996) Kube, Jan:
The ecology of macrozoobenthos and sea ducks in the Pomeranian Bay

19 (1996) Hagen, Eberhard (Editor):
GOBEX - Summary Report